ESCUELA DE DOCTORADO DE LA UNIVERSIDAD DE CANTABRIA

Advanced methodology for LPS capture from biofluids

Metodología avanzada para la captura de LPS en biofluidos

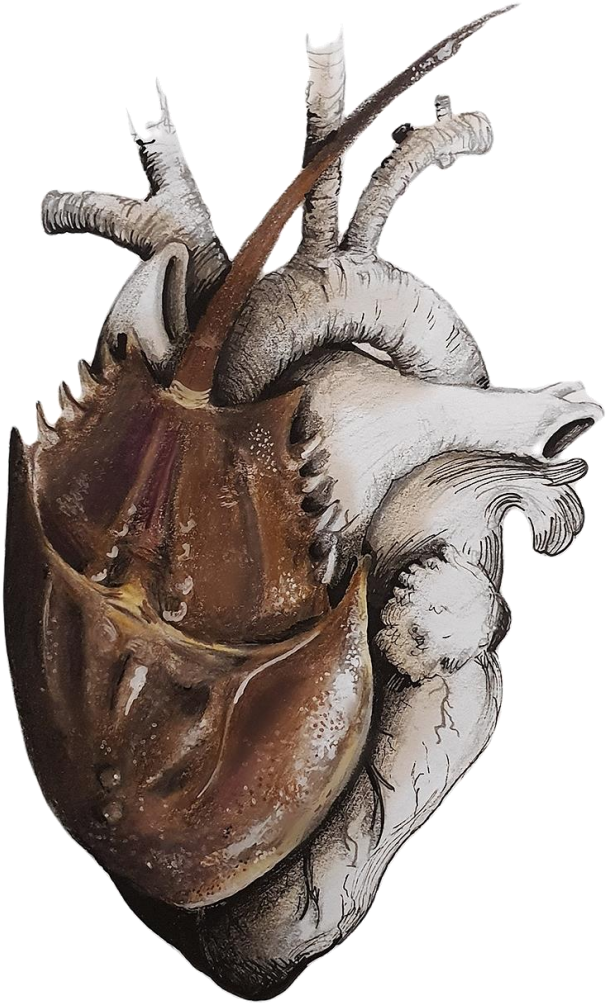

Arantza Basauri Penagos

Dirigida por:

Prof. Dra. Inmaculada Ortiz Uribe

Dr. Marcos Fallanza Torices

Santander, 2021

UNIVERSIDAD DE CANTABRIA

ESCUELA DE DOCTORADO DE LA UNIVERSIDAD DE CANTABRIA

DOCTORADO EN INGENERÍA QUÍMICA, DE LA ENERGÍA Y DE PROCESOS

Advanced methodology for LPS capture from biofluids

Metodología avanzada para la captura de LPS en biofluidos

Memoria de Tesis Doctoral presentada para optar al título de Doctor por la Universidad de Cantabria

Arantza Basauri Penagos

Dirigida por:

Prof. Dr. Inmaculada Ortiz Uribe

Dr. Marcos Fallanza Torices

Santander, 2021

The research described in this dissertation was conducted at the Advanced Separation Processes research group of the Department of Chemical and Biomolecular Engineering at the University of Cantabria. The research was financially supported by the Ministry of Economy and Competitiveness of the Spanish Government through the R&D project RTI2018-093310-B-I00 (MINECO / FEDER, UE).

Arantza Basauri acknowledges the Ministry of Economy and Competitiveness of the Spanish Government for the financial support through the research fellowship BES-2016-077206.

Arantza Basauri also thanks BioRender.com online software as this science illustration tool has allowed to create some of the figures of this work.

A mis padres,
por la vida que nos habéis ofrecido
y que seguimos disfrutando

Agradecimientos

Estos años han supuesto un aprendizaje continuo. Gracias a todas las personas que me he cruzado durante el camino y que han contribuido a llegar a la meta.

Gracias en primer lugar a la Prof. Inmaculada Ortiz, por darme esta oportunidad y confiar en mí para afrontar este reto. Tu trato, comprensión, orientación y apoyo han sido claves durante el proceso.

Me gustaría también agradecer al Dr. Marcos Fallanza su esfuerzo, dedicación y, sobre todo, la libertad con la que me ha permitido trabajar.

A su vez, no me puedo olvidar de la Dr. Laura Giner y el Dr. Gabriel Moncalián por aceptarme en vuestro laboratorio, enseñarme tanto y responder a una infinidad de preguntas sin perder la paciencia y con la mayor predisposición. Gran parte del trabajo recogido en esta tesis es gracias a vosotros.

Del mismo modo, me gustaría agradecer al Dr. Ernesto Osorio su tutela y orientación durante la estancia en la FU Berlin. Siempre fuiste atento, amable y optimista, gracias de corazón por tu inmejorable trato. A su vez, acordarme de Obi, todo un descubrimiento en tierras alemanas y en gran parte, principal partícipe de que esos meses fuesen sin saberlo, mi última gran aventura pre-covid.

Mil gracias a todos los compañeros del departamento que, durante estos años, no han sido pocos. Resaltar a Bea, quien siempre estuvo para echar una mano y con la que comparto el recuerdo de viajes no exentos de sobresaltos y aventuras varias. A Gema, la joya del departamento, siempre diligente y dispuesta a solucionar todos los problemas con una sonrisa y un buen humor envidiable. A Fer, porque siempre tiene una buena palabra además de una paciencia infinita cada vez que aparezco en

el despacho pidiendo sopitas. A Lucía y Prince, quienes seguro no se olvidarán de mí después de la semana de pre depósito que les he hecho pasar. Muchísimas gracias por vuestra ayuda, vuestras correcciones incisivas y por todos los buenos ratos que hemos compartido durante este tiempo.

También, mi sincero agradecimiento para Adri, mi compi de laboratorio en el IBBTEC durante estos los últimos meses. Trabajar contigo ha sido muy enriquecedor y un gustazo. Me has dado unas clases magistrales de biología molecular que me han ayudado enormemente a redactar partes de esta Tesis. Agradezco inmensamente tu buen talante y carisma.

No puedo olvidarme de mis mejores e incomparables amigos, a los que además de quereros, os admiro profundamente. Sois un ejemplo de resiliencia, superación y optimismo, maestros en relativizar y unos grandes triunfadores. Gracias por todo lo que he aprendido a vuestro lado; todos estáis presentes en los mejores recuerdos de mi vida. Aitor, Luis, Ane, Pacha y Lucía: no sois conscientes de hasta qué punto hoy soy esta Aran gracias a vosotros.

Mención especial para mis padres, siempre comprensivos y generosos y quienes nos han permitido vivir nuestra vida con total libertad y confianza. Vuestra educación ha sido de 10. Mil gracias por vuestro apoyo y amor.

Summary

Lipopolysaccharide (LPS), also called endotoxins, is the major component of the outer membrane of Gram-negative bacteria and is constituted of three regions; the O-specific chain, the core region and the lipid A, which is the responsible segment of toxicity. Lipid A presence often poses a serious risk not only when delivered in the bloodstream but also in several industrial fields.

As described in chapter 1, endotoxin contamination has been reported in different industries and environments as for example, in water and sewage treatment plants and in the cotton, food and pharmaceutical industry. Also, endotoxins have also been detected in house-dust, in bioaerosols, soil, water, air conditioners and waste treatment plants where organic-water solvent extraction systems, ultrafiltration processes and chromatographic techniques have been employed to avoid contamination in both processes and products.

Besides, LPS is highly toxic when is present in human blood, and causes fever, physical discomfort, leukocyte alterations and respiratory affections. In the worst scenario it can lead to sepsis, an exaggerated response to LPS that triggers immune suppression, organ dysfunction or even death. Despite the advances in knowledge on sepsis pathophysiology, several observational studies and clinical trials have failed to identify effective adjuvant therapies that could modify the course of the disease.

In the search of alternative methods of contaminant removal, blood cleansing procedures for the extracorporeal endotoxin separation have received increased attention. In this context, various strategies for LPS separation from contaminated fluids have been developed such as organic solvent extraction, the use of detergents such as Triton X-100 or

antibiotics (polymyxin B) immobilized on polystyrene fibers and packed into columns ready for direct perfusion of the biofluids. Unfortunately, in spite of these efforts, most of these systems have drawbacks that make endotoxin detection/removal a crucial challenge to achieve safe and effective detoxification processes.

In this regard, progress and capabilities of magnetofluidic devices deserves special attention. Magnetofluidic devices entail two main stages taking part in the whole process; the initial entrapment of LPS in conveniently functionalized magnetic nanoparticles (MNPs) and, the removal of the loaded MNPs from the biofluid. Whereas the second stage has received the attention of a great number of researchers, the LPS capture, where functionalized beads selectively bind to the target pathogen needs further research.

Consequently, this dissertation reports the methodology to advance in the design of the LPS sequestration stage to promote its separation from biofluids. To this end, first, chapter 2 reports the procedure for an antilipopolysaccharides protein from *Limulus polyphemus* (LALF) synthesis based on genetic engineering techniques where the first step was to assembly a plasmid, a small, circular, double-stranded DNA molecule consisting of a gene encoding the protein of interest in a specialized vehicle called vector. Subsequently, the circular DNA was transformed into cells capable of expressing the protein, which, in a final stage was successfully purified.

Afterwards, chapter 3 addresses the binding strength of the LALF protein to LPS quantification through a newly approach that consisted of a functionalization stage where the protein was supported on the surface of agarose beads and then, a capture stage where the decorated particles were contacted to fluorescent LPS solution. Moreover, variables affecting the beads-LALF-LPS complex formation such as binding and capture temperature, the optimum bead: protein and protein:LPS ratios, were experimentally studied to accurately determine the LALF activity.

Once LALF:LPS complexation equilibrium was determined, it was necessary to develop an application to carry out the continuous LPS capture aimed at fluid detoxification based on the use of flow-through microdevices. Because of the novelty of this approach, an in-depth methodology has been developed and described in chapter 3, making use of chemical systems with known equilibrium and kinetics and maintaining the fluid-dynamic similarity. Thus, the design of microdevices for the homogeneous and L-L heterogeneous separation of aqueous anions (chromate) has been developed, setting the grounds to continue with the microfluific design of L-S separation and finally its application to LPS capture.

ANSYS FLUENT software was used to develop a flexible model that solves under dynamic conditions both Navier-Stokes and species balance equations; the model also implements the surface tension between the liquid phases that had been experimentally determined, and the fluid-wall interaction through the measurement of the contact angle.

Last, experimental and simulated results were compared in order to validate the model and apply it to the subsequent analysis of the reactive L-S systems and, finally perform the capture of LPS.

Resumen

El lipopolisacárido (LPS), o endotoxina, es el principal componente de la membrana externa de las bacterias Gram negativas y está constituido por tres regiones: la cadena específica O, la región del núcleo y el lípido A, que es el segmento responsable de su toxicidad. La presencia del lípido A suele suponer un grave riesgo no sólo cuando llega al torrente sanguíneo, sino también en varios ámbitos industriales.

El capítulo 1 explica la problemática asociada a la contaminación por endotoxinas registrada en diferentes industrias y entornos, como, por ejemplo, en las plantas de tratamiento de agua y aguas residuales y en la industria del algodón, la alimentaria y la farmacéutica. También se han detectado endotoxinas en el polvo doméstico, en los bioaerosoles, en el suelo, en el agua, en los aires acondicionados y en las plantas de tratamiento de residuos, donde se han empleado sistemas de extracción con disolventes orgánico-acuosos, procesos de ultrafiltración y técnicas cromatográficas para evitar la contaminación tanto en procesos como en productos.

Además, el LPS es altamente tóxico cuando está presente en la sangre humana, y provoca fiebre, malestar físico, alteraciones leucocitarias y afecciones respiratorias. En el peor de los casos, puede conducir a la sepsis, una respuesta exagerada al LPS que desencadena una supresión inmunitaria, una disfunción orgánica o incluso la muerte. A pesar de los avances en el conocimiento de la fisiopatología de la sepsis, estudios y ensayos clínicos no han logrado identificar terapias adyuvantes eficaces que puedan modificar el curso de la enfermedad.

En la búsqueda de métodos alternativos para la eliminación de contaminantes, los procedimientos de detoxificación de la sangre para la

eliminación de endotoxinas han recibido gran atención. En este contexto, se han desarrollado diversas estrategias para promover la separación del LPS de fluidos contaminados tales como la extracción con disolventes orgánicos, el uso de detergentes como Triton X-100 o de antibióticos (polimixina B) inmovilizados en fibras de poliestireno y empaquetados en columnas a través de las que se puede realizar la perfusión directa del fluido contaminado. Lamentablemente, a pesar de estos esfuerzos, la mayoría de estos sistemas extracorpóreos presentan inconvenientes que hacen que la detección/eliminación de endotoxinas sea un reto crucial para lograr procesos de detoxificación seguros y eficaces.

En este sentido, los avances y las capacidades de los dispositivos magnetofluídicos merecen especial atención e implican dos etapas principales; el secuestro de LPS en nanopartículas magnéticas (MNPs) convenientemente funcionalizadas y, la eliminación del complejo MNPs-LPS del fluido biológico. Mientras que la segunda etapa ha sido ampliamente abordada, la captura de LPS en la que las partículas funcionalizadas se unen selectivamente al patógeno objetivo necesita más estudios al respecto.

En consecuencia, esta disertación aporta una metodología integrada para avanzar en el diseño de la etapa de secuestro de LPS para promover su separación de los biofluidos. Para ello, el capítulo 2 describe la síntesis de una proteína antilipopolisacáridos (LALF) procedente de la especie *Limulus polyphemus* mediante técnicas de ingeniería genética. Inicialmente, se construyó un plásmido, una pequeña molécula de ADN circular de doble cadena, compuesta por un gen que codifica la proteína de interés en un vehículo especializado denominado vector. Posteriormente, el plásmido fue transformado en células capaces de expresar la proteína que, finalmente fue purificada con éxito.

Posteriormente, el capítulo 3 aborda la cuantificación de la fuerza de unión de la proteína LALF al LPS mediante un nuevo enfoque que consiste en una etapa de funcionalización en la que la proteína es adherida en la superficie de las partículas de agarosa y, a continuación, una etapa de captura en la que las partículas decoradas se ponen en contacto con una

disolución de LPS fluorescente. Además, se estudiaron experimentalmente las variables que afectan a la formación del complejo partícula-LALF-LPS, como la temperatura de unión y captura, y las proporciones óptimas partícula: proteína y proteína:LPS, para determinar la actividad de LALF.

Una vez detallado el equilibrio de complejación LALF: LPS, fue necesario desarrollar una aplicación para llevar a cabo la captura de LPS en continuo para a la detoxificación de fluidos. Debido a la novedad de este enfoque, el capítulo 4 recoge una metodología desarrollada en la que se ha empleado un sistema químico cuyo equilibrio y cinética son conocidos y con similitud fluido-dinámica. Por tanto, se ha desarrollado el diseño de microdispositivos para la separación homogénea y heterogénea L-L de aniones acuosos (cromato), sentando las bases para continuar con el diseño microfluidico para la separación L-S y finalmente, su aplicación a la captura de LPS.

Además, utilizando el software ANSYS FLUENT se desarrolló un modelo flexible que resuelve, en condiciones dinámicas, tanto las ecuaciones de Navier-Stokes como las del balance de especies. En el modelo también se han implementado la tensión superficial entre fases determinada experimentalmente y la interacción fluido-pared mediante la medición del ángulo de contacto.

Por último, los resultados experimentales y simulados fueron comparados para validad el modelo y aplicarlo al posterior análisis de sistemas reactivos L-S y a la captura de LPS.

Contents

1

Introduction

Abstract

This thesis reports an integrated methodology to advance in the design of the LPS sequestration stage to promote its separation from biofluids. The methodology combines protein and separation fundamentals and starts with the synthesis of an anti LPS factor protein (ALF), followed by the quantitative determination techniques of its binding strength to LPS. For this analysis ALF was supported on agarose beads and the variables affecting the functionalization and subsequent LPS binding, as binding and capture temperature, the optimum bead:protein and protein:LPS ratios, have been experimentally studied. The methodology and results here reported constitute the information needed to advance the knowledge for the design of LPS separation devices.

1.1. Gram negative bacteria and LPS structure

Prokaryotic cells comprise bacteria and archaea, both characterized by the absence of nucleus and membrane bound organelles. Focusing on bacteria, these single-celled microorganisms are found everywhere on the planet and show diverse shapes and structures. About 5,000 different bacteria have been identified living in Earth ecosystems, including our body [1,2].

Bacteria are classified into two large groups: gram-positive (GPB) and gram-negative (GNB) since, in 1884, Hans Christian Gram developed a method to distinguish between them by using a crystal violet-iodine complex and a safranin counter stain. While gram-positive bacteria turned violet or purple, gram-negative bacteria did not retain the complex and stained pink. This different behavior is explained due to the composition or the morphology of the cell wall in each bacterial type [3] as depicted in **Figure 1.1.**

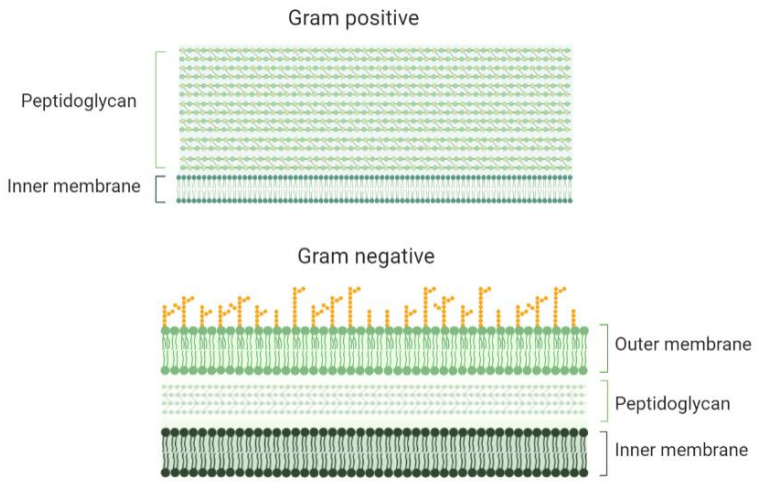

Figure 1.1. Gram-positive and gram-negative bacteria structural differences.

Gram-negative bacteria are characterized by an envelope that consists of the inner and the outer membrane separated by an aqueous cellular compartment termed the periplasm that contains a peptidoglycan cell wall which provides the cell from their specific shape [4] as shown in **Figure 1.2.** The inner membrane (IM), which surrounds cytoplasmic components, is a phospholipid bilayer that is responsible for structure, transport, and biosynthetic functions [5]. The outer membrane (OM) is the main feature that distinguishes GNB from GPB. This outer layer separates the cell from the environment and constitutes the first defense line against potential threats. It is a highly asymmetric bilayer that contains phospholipids in the inner leaflet and lipopolysaccharide (LPS) molecules in the outer leaflet [6].

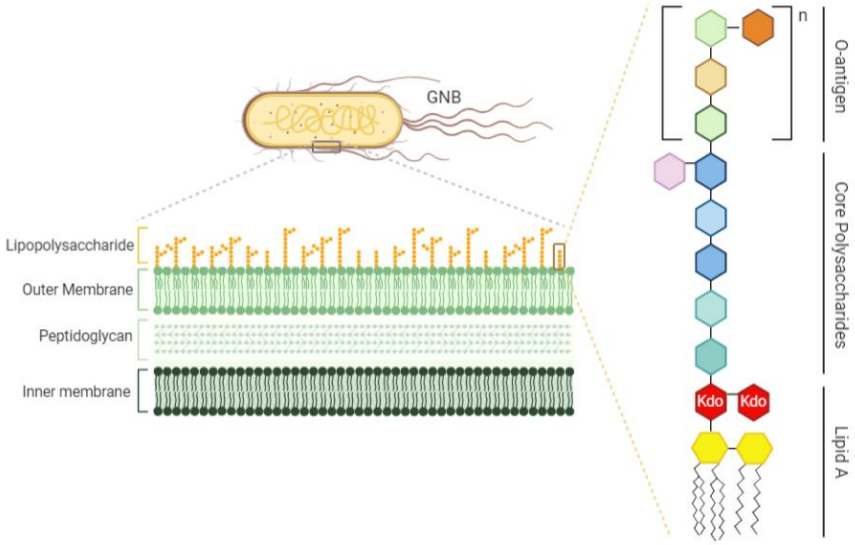

Figure 1.2. LPS structural regions on GMB outer membrane.

LPS, also called endotoxins, is recognized as the major structural component of the OM. These LPS molecules have the ability to transform the OM into an effective permeability barrier against small, hydrophobic molecules that can otherwise cross phospholipid bilayers, making GNB resistant to antimicrobial compounds [7,8].

LPS is a large glycolipid whose chemical structure consists of three structural domains: O-antigen, outer and inner core and Lipid A [9]. The O-antigen is an extended polysaccharide composed of a repeating oligosaccharide made of two to eight sugars that is attached to the core oligosaccharide with hydrophilic nature [10,11]. The core is a partially phosphorylated heteropolysaccharide composed of a non-repeating oligosaccharide linked to the glucosamines of lipid A [12,13] and usually contains 3-deoxy-D-manno-oct-2-ulosonic acid (Kdo) residues, heptoses, and various hexoses [14,15] and structurally is more uniform than the O-antigen. Finally, the lipid A region that forms the outer leaflet of the OM is responsible for biological activity and toxicity. Lipid A is the hydrophobic portion of the molecule commonly composed of two glucosamine units, each containing a phosphate group, with attached fatty acids. The phosphorylated glucosamines, together with the KDO-containing inner core portion, represent the most conserved region of LPS in structural terms. Lipid A is thus an amphiphilic glycolipid that has the ability to adopt different physical structures under different temperature or pH conditions [16,17]. Due to the toxic effects, LPS presence causes relevant contamination problems that must be addressed as it affects to diverse fields.

1.2. LPS in industrial environments and removal techniques

Endotoxin contamination has been reported in different industries and environments as for example, in wastewater treatment plants. Endotoxins in public drinking water supplies pose a potential concern where the removal involves traditional treatment processes as coagulation, sedimentation and filtration as well as granular activated carbon (GAC) adsorption chlorination [18,19]. Moreover, sewage treatment plants have also involved exposure to different types of microorganisms, viruses and chemicals, mainly gram-negative bacteria

which are of particular interest as the acute effects of endotoxins are well documented in several inhalation experiments in humans [20,21].

In fact, LPS has also been detected in other industrial environments, such as the cotton industry, from which chronic dust inhalation could involve byssinosis due to an inadequately ventilated working environment during exposition to cotton [22]. Food industry has also been affected by endotoxin presence in milk and dairy products, where process hygienic levels must be guaranteed [23]. In addition, undercooked beef burgers, raw milk, cold sandwiches, vegetables and even water have been considered potential sources of outbreaks and therefore, reliable detection methods are needed to screen high-risk foods [24].

Furthermore, potential risk of engineered nanoparticles is of particular importance in nanomedicine since endotoxins can mask the toxic effects of nanoparticles. Endotoxin presence in nanomaterials can distort the evaluation of the possible toxic and inflammatory effects of the nanomaterials as several studies both, in vivo and in vitro, have demonstrated, suggesting a potential risk for human health [25]. Also, endotoxin has also been detected in house-dust, in bioaerosols, soil, water, air conditioners and waste treatment plants, where organic dusts are present and negative health effects have been described as a consequence of handling waste and biofuels [26].

Among all the different fields affected by LPS contamination, endotoxins pose a high risk to pharmaceutical industries due to the employment of Gram-negative bacteria in biopharma manufacturing to produce recombinant DNA products like proteins and peptides. In this context, contamination by toxins or pyrogens involve high batch rejection rates of biopharmaceuticals as these bioproducts are rigorously controlled to avoid serious issues and work safety infractions. In fact, this industry is adhered to regulations and strict international quality standards regulated by different organisms as the Federal Drug Administration and the Occupational Health and Safety Administration in the United States or

the European Agency for Safety and Health Work in Europe, that ensures the contamination control [27].

When unfortunately, endotoxin presence is detected on a bioproduct, there are two difficulties to face in order to proceed with the removal. The first one is to make sure that the applied procedure must not alter the product during the endotoxin clearance. The second one is related to the low endotoxin concentration in the product and the difficulty in removing bound endotoxin. In this regard, different removal techniques based on endotoxins structure and composition have been developed to address its removal [28].

As an alternative to organic-water solvent extraction systems, the use of aqueous systems has become popular as it favours milder conditions that do not harm or denature labile biomolecules. In addition, *aqueous*- two-phase partitioning systems serve effectively for endotoxin removal thanks to their hydrophobic nature. Moreover, these systems offer flexibility in the face of altering factors like polymer mass, pH, ionic strength and concentration of the phase component or through the addition of affinity ligands [29]. Although endotoxins tend to form micelles or vesicles in aqueous solutions, ultrafiltration techniques work by excluding endotoxins through molecular weight using an ultrafine filter that blocks molecules greater to 10 kDa and often, this process is coupled with 0.1 µm filters for bioburden control. Despite ultrafiltration has shown effectiveness for water decontamination, little effect on endotoxin levels has been reported [30,31]. Besides, for many applications of endotoxin clearance, the negative chromatographic technique is the preferred method as it acts to bind endotoxin through binding affinity.

In contrast, ion exchange chromatography uses positive charges that non-selectively attract the negatively charged endotoxin allowing the elution step. Variables as the pH range, temperature, flow rate and the amount of electrolytes in the solution directly affect both processes and some modifications of the technique include large bead hydrogel-based methods as the inside-out ligand attachment technique [32,33].

Furthermore, size exclusion chromatography, in spite of the dependence of the biomolecules size, can also be considered [34,35].

Additionally, but not so widely used, electrophoresis has been reported to separate LPS from biomolecules and washing steps with non-ionic surfactants can favour endotoxin dissociation from protein solutions. However, the aforementioned techniques for endotoxin clearance can lead to some loss of product yield and are not suitable for many processes as sometimes, the contamination risk is not completely eliminated [36–38]. Therefore, the implementation of routine endotoxin tests could minimize the undesired consequences of LPS contamination.

Conventional LPS detection methods are the rabbit pyrogen test (RPT) and the Limulus amoebocyte lysate assay (LAL). The principle of detection of the RPT, which came out in the 1920s, consists on the injection of pharmaceutical drugs into rabbits and the observation of the response in terms of temperature rise or fever [39]. In 1997, the US Food and Drug Administration approved the use of the LAL test in replacement of RPT as a method for endotoxin detection. The LAL assay uses blood extract from horseshoe crab (*Limulus Polyphemus*) and is based on clot formation when the blood extract is contacted with LPS. An improvement of the LAL detection method was implemented with the discovery of zymogen factor C, the major endotoxin-mediated cascade component with high LPS detection capacity, which switches to its active form under LPS presence [40]. Despite its high sensitivity and specificity for G(-) bacterial walls, crab over-fishing is threatening the species and therefore, the European Directorate for the Quality of Medicines and Healthcare (EDQM) revised its using guidelines [41–43] which rises the importance of the design and development of sustainable and affordable new LPS capture or detection systems.

1.3. LPS in human body and removal techniques

LPS is highly toxic when is present in human blood, and causes fever, physical discomfort, leukocyte alterations and respiratory affections. In the worst scenario it can lead to sepsis, an exaggerated response to LPS that triggers immune suppression, organ dysfunction or even death [44,45]. Just to contextualize, 49 million cases of sepsis (41% of all global sepsis cases in 2017 affected to children under 5 years of age) and 11 million sepsis-related deaths occurred worldwide in 2017, accounting for approximately 20% of all-cause deaths. Mortality is estimated to be 42% in intensive care patients treated for sepsis and, among sepsis survivors, one in three died within a year and one in six experienced significant, long term mortality. Consequently, the economic burden of this disease is tremendous; for example, the annual cost in the USA is estimated at $16.7 billion and the median of the mean hospital-wide cost of sepsis per patient was $32,421 [46,47].

1.3.1. Immune response

Several studies have been carried out to deeply describe the immune mechanism triggered by the LPS presence in the human body. When LPS presence activates the immune system response, it starts a “cascade mechanism” involving membrane proteins as toll like receptors (TLR) and CD14, [48–50] as illustrated in **Figure 1.3**.

LPS interacts with different cell types, inducing the activation of macrophages whose cell surface contains many pattern recognition receptors for different microorganisms. Among these receptors, toll-like receptors (TLR) are transmembrane proteins enriched in leucine in the ectodomain that selectively recognize LPS [51]. TLR4 is predominantly expressed in phagocytes and, its signaling task needs the co-expression of an adaptor protein called MD-2. MD-2 is a lymphocyte antigen present in most cells of the human body and it has been identified as an accompanying receptor of TLR4 in LPS sensing stages. This means that both MD-2 and TLR4 are co-expressed and form an heterodimer prior to

LPS binding on the MD-2 positively charged region, [52–55]. Five of the six lipid chains of LPS are bound to MD-2 and the remaining chain interacts with TLR4 of a second MD-2-TLR4 complex inducing the formation of a TLR4–MD-2–LPS dimer [56] which triggers an intracellular signal that leads to pro-inflammatory cytokines and chemokines [57]. TLR ligands induce co-stimulating molecules as CD14 [58–60], which is both a phospholipid and an LPS transporter [61,62]. LPS released by bacteria is previously complexed with the lipid binding protein (LBP), a plasma protein which is mainly produced by hepatocytes and is by far the most extensively studied soluble protein with LPS-binding capacity [63,64]. LBP is an elongated molecule formed by two domains (N-terminal and C-terminal) [65]. Each N- and C- terminal domain contains a hydrophobic pocket able to bind phospholipids. The basic mechanism involving LPS and LBP starts when LPS aggregates are dissociated by the LPS-binding protein (LBP) to form LPS-LBP complexes [66,67]; the LPS-LBP complexes are transferred to CD14 representing the early step in cell activation by LPS. Thus, the rate of either process will determine the response of the host to LPS [58].

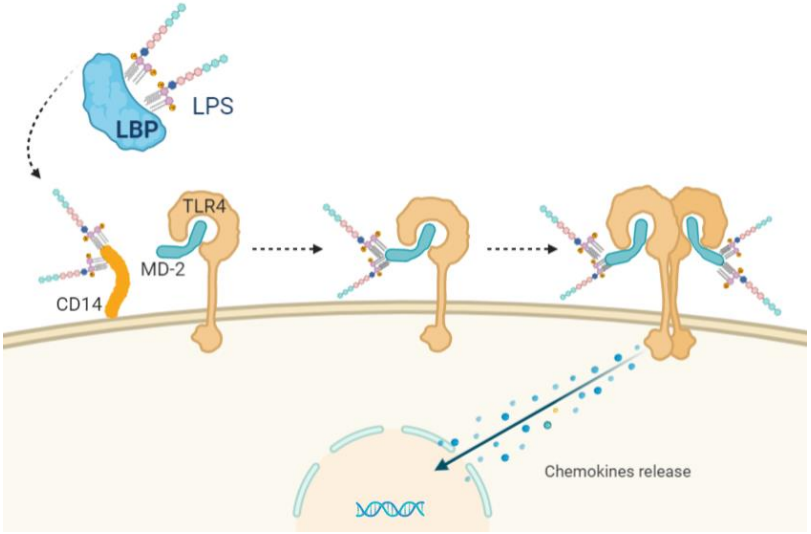

Figure 1.3. Human immune cascade triggered by LPS presence.

1.3.2. LPS removal techniques in poisoned blood

Sepsis is a medical emergency and life-threatening condition due to a dysregulated host response to infection but, despite the advances in knowledge on sepsis pathophysiology, several observational studies and clinical trials have failed to identify effective adjuvant therapies that could modify the course of the disease [68,69]. In the absence of any specific sepsis treatment, it is crucial to treat sepsis as a medical emergency, to seek for the early control of infection and organ support [70–72]. Since time is paramount in the prognosis of sepsis, the 2016 Surviving Sepsis Campaign (SCC) guidelines advocate for intravenous broad-spectrum antibiotics that must be a priority, ideally within the first hour of diagnosis [72,73].

In the search of alternative methods of contaminant removal, blood cleansing procedures for the extracorporeal endotoxin separation has received increased attention. Various extracorporeal strategies have been developed, such as organic solvent extraction, the use of detergents such as Triton X-100 or antibiotics (polymyxin B) immobilized on polystyrene fibers and packed into columns for direct blood perfusion [74–78].

Endotoxin removal cartridges (Toraymyxyn, PMX-F) were developed as medical devices via hemoperfusion employed for the treatment of patients with endotoxic septic shock who are unresponsive to conventional therapies. These cartridges consist on polymyxin B (PMB) covalently immobilized in polystyrene fibers as PMB has been demonstrated as an LPS-neutralizer thanks to its antibacterial and antiendotoxin capabilities [79]. Removal efficiencies up to 90% have been reported [80] but the use of these cartridges is restricted to 12 countries worldwide and side effects have been reported [81].

In spite of these efforts, most of these extracorporeal systems have drawbacks that make endotoxin detection/removal a crucial challenge to achieve safe and effective detoxification processes.

Alternatively, the progress and capabilities of magnetofluidic devices deserves special attention. These continuous blood-cleansing devices for LPS removal comprise a first LPS sequestration step followed by the separation of the LPS loaded particles stage via magnetophoretic-microfluidic techniques as depicted in **Figure 1.4.**

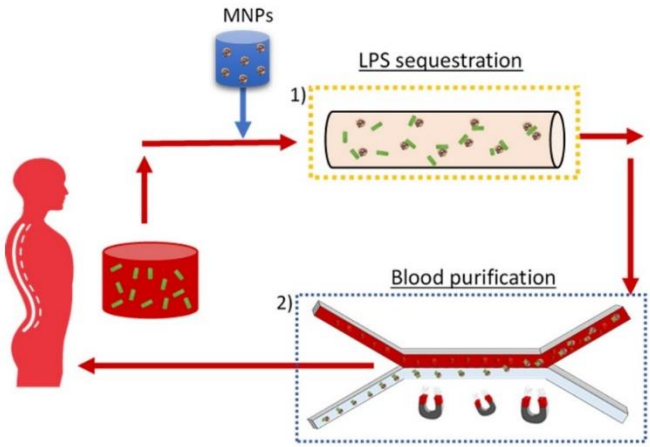

Figure 1.4. Schematic illustration of micro-magnetophoretic extracorporeal blood cleansing process for LPS separation.

Firstly, the functionalized magnetic beads are mixed with the patient´s blood and selectively bind to target pathogens forming an LPS-MNPs complex. For that to occur, it is necessary the presence of a binding molecule decorating the MNPs surface, with LPS affinity and biocompatible with blood to avoid side effects when the blood is returned to the patient. Moreover, selective LPS capture should take place and the initial LPS concentration in blood should significantly decrease to accomplish with the desired capture efficiency (>90%). Once the LPS adsorption on the beads surface is completed, blood is flowed into a Y-Y microfluidic device where the toxin-bead complex is magnetically deflected and collected in a co-flowing buffer in the continuous-flow separator. Afterwards, the resulting toxin-free blood solution is returned to the patient's circulatory system.

Recently, the continuous-flow magnetophoretic system has been analyzed by our group through a computational fluid dynamic (CFD) model to characterize the trajectory of the beads under the external magnetic force and to predict the overall performance of the two-phase liquid-liquid separation with the Y-Y flow configuration and where critical details of the separation process were also studied [82–86]. Since the MNPs separation has been already addressed, synthesis of LPS active binding molecules and their coupling on quantitative LPS removal systems are key factors necessary to improve for the endotoxin separation systems success.

1.4. Thesis scope and outline

This thesis reports an integrated methodology to advance in the design of the LPS sequestration stage to promote its separation from biofluids. The methodology combines protein engineering and separation fundamentals and starts with the synthesis of an anti LPS factor protein (ALF), followed by the quantitative determination of its binding strength to LPS. For this analysis ALF was supported on agarose beads and the variables affecting LPS binding, as binding and capture temperature, the optimum bead:protein and protein:LPS ratios, were experimentally studied. The methodology and results here reported constitute the information needed to advance the knowledge for the correct design of LPS separation devices.

Chapter 2 reports information about the potential binding molecules that have exhibited some affinity towards LPS such as organic solvents, polymers, antibiotics and proteins. In order to contribute to the capture stage of micro-magnetophoretic cleansing systems, a biologically active molecule has been produced. As peptide-based structures typically produced by living organisms present higher affinities towards endotoxins and at the same time high LPS-binding specificity, an anti LPS factor protein (ALF) has been designed and synthesized through protein engineering. Different protein sequences, genetic vectors and hosting

cells have been tested to get a soluble protein with LPS entrapping capabilities.

Chapter 3 describes the functionalization of a solid matrix with the obtained ALF protein to form a bead-protein complex. Initial experiments were carried out to select the variables that provided the best LPS separation performance; specifically, the influence of bead/protein ratio and process temperature was experimentally addressed. Afterwards, the active particles were contacted to a FITC-LPS solution to test the affinity of the LPS capture and the influence of the temperature on LPS removal was studied. Protein:endotoxin optimal ratio (ϕ) was determined to achieve removal rates greater than 90% and finally, an apparent association constant is reported.

Chapter 4 is focused on the preliminary design of microfluidic devices for fluids separation. The methodology has been developed starting with the analysis of Y-Y geometry with the separation of aqueous Cr (VI) as system model. Two different scenarios have been considered: (a) two homogeneous phases, where water is the receptor phase, and (b) a heterogeneous system where the solute moves from the feed solution to a receptor phase composed of Shellsol D-70 and Alamine 336 as the selective extractant. A rigorous and flexible model has been constructed through Computational Fluid Dynamics (CFD) seeking to provide a useful tool for the design of micro separation processes by predicting the technical performance for numerous applications at micro scale.

Finally, Chapter 5 collects the general conclusions of this thesis and an overview of the challenges and prospects for future research.

1.5. References

[1] D. Murat, M. Byrne, A. Komeili, Cell biology of prokaryotic organelles., Cold Spring Harb. Perspect. Biol. 2 (2010) 1–18. https://doi.org/10.1101/cshperspect.a000422.

[2] T. Vellail, G. Vida, Origin Eukaryotes : Prokaryotic and the Difference Cells Eukaryotic, 266 (2010) 1571–1577. doi: 10.1098/rspb.1999.0817.

[3] R.B. Moyes, J. Reynolds, D.P. Breakwell, Differential staining of bacteria: Gram stain, Curr. Protoc. Microbiol. (2009) 1–8. https://doi.org/10.1002/9780471729259.mca03cs15.

[4] B. Bertani, N. Ruiz, Function and Biogenesis of Lipopolysaccharides, EcoSal Plus. 8 (2018) 1–33. https://doi.org/10.1128/ecosalplus.esp-0001-2018.

[5] P.R. Murray, K.S. Rosenthal, M.A. Pfaller, Medical Microbiology, Ninth Edit, Elsevier, 2020.

[6] Y. Kamio, H. Nikaido, Outer Membrane of Salmonella Typhimurium: Accessibility of Phospholipid Head Groups to Phospholipase C and Cyanogen Bromide Activated Dextran in the External Medium, Biochemistry. 15 (1976) 2561–2570. https://doi.org/10.1021/bi00657a012.

[7] S.M. Galloway, C.R.H. Raetz, A mutant of Escherichia coli defective in the first step of endotoxin biosynthesis, J. Biol. Chem. 265 (1990) 6394–6402. doi.org/10.1016/S0021-9258(19)39339-1.

[8] H. Nikaido, M. Vaara, Molecular basis of bacterial outer membrane permeability, Microbiol. Rev. 49 (1985) 1–32. https://doi.org/10.1128/mmbr.49.1.1-32.1985.

[9] Y. Zhang, N. Takagi, B. Yuan, Y. Zhou, N. Si, H. Wang, J. Yang, X. Wei, H. Zhao, B. Bian, The protection of indolealkylamines from LPS-induced inflammation in zebrafish, J. Ethnopharmacol. 243 (2019) 112122. https://doi.org/10.1016/j.jep.2019.112122.

[10] L. Wang, Q. Wang, P.R. Reeves, The variation of O antigens in gram-negative bacteria, Subcell. Biochem. 53 (2010) 123–152.

https://doi.org/10.1007/978-90-481-9078-2_6.

[11] Y. Hong, M.A. Liu, P.R. Reeves, Progress in our understanding of Wzx flippase for translocation of bacterial membrane lipid-linked oligosaccharide, J. Bacteriol. 200 (2018) 1–14. https://doi.org/10.1128/JB.00154-17.

[12] C.R.H. Raetz, C. Whitfield, Lipopolysaccharide Endotoxins, Annu. Rev. Biochem. 71 (2002) 635–700. https://doi.org/10.1146/annurev.biochem.71.110601.135414.Lipopolysaccharide.

[13] D.E. Heinrichs, J.A. Yethon, C. Whitfield, Molecular basis for structural diversity in the core regions of the lipopolysaccharides of Escherichia coli and Salmonella enterica, Mol. Microbiol. 30 (1998) 221–232. https://doi.org/10.1046/j.1365-2958.1998.01063.x.

[14] C. Whitfield, N. Kaniuk, E. Frirdich, Molecular insights into the assembly and diversity of the outer core oligosaccharide in lipopolysaccharides from Escherichia coli and Salmonella, J. Endotoxin Res. 9 (2003) 244–249. https://doi.org/10.1179/096805103225001440.

[15] G. Klein, S. Raina, Regulated control of the assembly and diversity of lps by noncoding sRNAs, Biomed Res. Int. 2015 (2015). https://doi.org/10.1155/2015/153561.

[16] K. Palkovicova, R. Ihnatko, P. Vadovic, E. Betinova, L. Skultety, D. Frangoulidis, R. Toman, A monoclonal antibody specific for a unique biomarker, virenose, in a lipopolysaccharide of Coxiella burnetii, Clin. Microbiol. Infect. 15 (2009) 183–184. https://doi.org/10.1111/j.1469-0691.2008.02218.x.

[17] D.M. Livermore, Current Epidemiology and Growing Resistace of Gram-negative Pathogens, Korean J. Intern. Med. 27 (2012) 128–142. https://doi.org/10.11261/iryo1946.60.637.

[18] W.B. Anderson, R.M. Slawson, C.I. Mayfield, A review of drinking-water-associated endotoxin, including potential routes of human exposure., Can. J. Microbiol. 48 (2002) 567–587.

https://doi.org/10.1139/w02-061.

[19] Z. Can, L. Wenjun, S. Wen, Z. Minglu, Q. Lingjia, L. Cuiping, T. Fang, Endotoxin contamination and control in surface water sources and a drinking water treatment plant in Beijing , China, Water Res. 47 (2013) 3591–3599. https://doi.org/10.1016/j.watres.2013.04.009.

[20] J. Thorn, L. Beijer, T. Jonsson, Measurement Strategies for the Determination of Airborne Bacterial Endotoxin in Sewage Treatment, 46 (2002) 549–554. https://doi.org/10.1093/annhyg/mef068.

[21] O. Michel, M. Dentener, F. Corazza, W. Buurman, R. Rylander, Healthy subjects express differences in clinical responses to inhaled lipopolysaccharide that are related with inflammation and with atopy, J. Allergy Clin. Immunol. 107 (2001) 797–804. https://doi.org/10.1067/mai.2001.114249.

[22] S.R. Lane, P.J. Nicholls, R.D.E. Sewell, The Measurement and Health Impact of Endotoxin Contamination in Organic Dusts from Multiple Sources: Focus on the Cotton Industry, Inhal. Toxicol. 16 (2004) 217–229. https://doi.org/10.1080/08958370490277164.

[23] K. Hansen, T. Mikkelsenf, A. M0Ller-Madsen, Use of the Limulus test to determine the hygienic status of milk products as characterized by levels of Gram-negative bacterial lipopolysaccharide present, J. Dairy Res. 49 (1982) 323–328. https://doi.org/10.1017/S0022029900022421.

[24] C. Vernozy-Rozand, S. Ray-Gueniot, C. Ragot, C. Bavai, C. Mazuy, M.P. Montet, J. Bouvet, Y. Richard, Prevalence of Escherichia coli O157:H7 in industrial minced beef, Lett. Appl. Microbiol. 35 (2002) 7–11. https://doi.org/10.1046/j.1472-765X.2002.01116.x.

[25] Y. Li, D. Boraschi, Endotoxin contamination: A key element in the interpretation of nanosafety studies, Nanomedicine. 11 (2016) 739. https://doi.org/10.2217/nnm.16.29.

[26] R. Rylander, Endotoxin in the environment – exposure and effects, J. Endotoxin Res. 8 (2002) 241–252. https://doi.org/10.1179/096805102125000452.

[27] V. Salema, L. Saxena, P. Pattnaik, Removing endotoxin from biopharmaceutical solutions, Pharm. Technol. Eur. 21 (2009) 36.

[28] P.O. Magalhães, A.M. Lopes, G. Priscila, C. Rangel-Yagui, T.C. Penna, A. Pessoa Jr, Methods of Endotoxin Removal from Biological Preparations : a Review, J. Pharm. Pharm. Sci. 10 (2007) 388–404.

[29] A.M. Lopes, P.O. Magalhães, P.G. Mazzola, C.O. Rangel-Yagui, J.C.M. De Carvalho, T.C.V. Penna, A. Pessoa, LPS removal from an E. coli fermentation broth using aqueous two-phase micellar system, Biotechnol. Prog. 26 (2010) 1644–1653. https://doi.org/10.1002/btpr.463.

[30] F.B. Anspach, Endotoxin removal by affinity sorbents, J. Biochem. Biophys. Methods. 49 (2001) 665–681. https://doi.org/10.1016/S0165-022X(01)00228-7.

[31] H. Jang, K.-Y. Yu, J.-S. Kim, Y.-J. Jeong, B.-S. Kim, H.-Z. Youn, Y.-R. Lee, H.-S. Kim, S.-H. Lee, B.-K. Lee, S.-C. Moon, Effects of protein concentration and detergent on endotoxin reduction by ultrafiltration, BMB Rep. 42 (2011) 462–466. https://doi.org/10.5483/bmbrep.2009.42.7.462.

[32] M.F. Lin, C. Williams, M. V. Murray, P.A. Ropp, Removal of lipopolysaccharides from protein-lipopolysaccharide complexes by nonflammable solvents, J. Chromatogr. B Anal. Technol. Biomed. Life Sci. 816 (2005) 167–174. https://doi.org/10.1016/j.jchromb.2004.11.029.

[33] T. Maciołek, Preparative Purification of Recombinant Protein: Current Status and Future Trends, BioMed Res. Res. Int. 89 (2013) 12–16. https://doi.org/10.1155/2013/312709

[34] D. Petsch, F.B. Anspach, Endotoxin removal from protein solutions, J. Biotechnol. 76 (2000) 97–119. https://doi.org/10.1016/S0168-1656(99)00185-6.

[35] M.M. Diogo, J.A. Queiroz, D.M.F. Prazeres, Chromatography of plasmid DNA, J. Chromatogr. A. 1069 (2005) 3–22. https://doi.org/10.1016/j.chroma.2004.09.050.

[36] B. JANN, K. RESKE, K. JANN, Heterogeneity of Lipopolysaccharides. Analysis of Polysaccharide Chain Lengths by Sodium Dodecylsulfate-Polyacrylamide Gel Electrophoresis, Eur. J. Biochem. 60 (1975) 239–246. https://doi.org/10.1111/j.1432-1033.1975.tb20996.x.

[37] P. Reichelt, C. Schwarz, M. Donzeau, Single step protocol to purify recombinant proteins with low endotoxin contents, Protein Expr. Purif. 46 (2006) 483–488. https://doi.org/10.1016/j.pep.2005.09.027.

[38] O. Adam, A. Vercellone, F. Paul, P. F. Monsan, G. Puzo, A Nondegradable Route for the Removal of Endotoxin from Exopolysaccharides, Anal. Biochem. 225 (1995) 321–327. doi: 10.1006/abio.1995.1161.

[39] B. Akbar John, B.Y. Kamaruzzaman, K.C.A. Jalal, K. Zaleha, TAL - a source of bacterial endotoxin detector in liquid biological samples, Int. Food Res. J. 19 (2012) 423–425. doi: 10.3791/958

[40] T. Muta, T. Miyata, Y. Misumi, F. Tokunaga, T. Nakamura, Y. Toh, Y. Ikehara, S. Iwanaga, Limulus factor C: An endotoxin-sensitive serine protease zymogen with a mosaic structure of complement-like, epidermal growth factor-like, and lectin-like domains, J. Biol. Chem. 266 (1991) 6554–6561.

[41] R. Santos-Oliveira, Comparison of limulus amebocyte lysates with the United States pharmacopeial pyrogen test and the portable test system for radiopharmaceuticals, J. AOAC Int. 93 (2010) 1458–1461. https://doi.org/10.1093/jaoac/93.5.1458

[42] C.Y. Park, S.H. Jung, J.P. Bak, S.S. Lee, D.K. Rhee, Comparison of the rabbit pyrogen test and Limulus amoebocyte lysate (LAL) assay for endotoxin in hepatitis B vaccines and the effect of aluminum hydroxide, Biologicals. 33 (2005) 145–151. https://doi.org/10.1016/j.biologicals.2005.04.002.

[43] R. Blechová, D. Pivodová, Limulus amoebocyte lysate (LAL) test - an alternative method for detection of bacterial endotoxins, Acta Vet. Brno. 70 (2001) 291–296. https://doi.org/10.2754/avb200170030291.

[44] V. Espinosa, A. Rivera, First line of defense: Innate cell-mediated control of pulmonary Aspergillosis, Front. Microbiol. 7 (2016) 1–12. https://doi.org/10.3389/fmicb.2016.00272.

[45] J. Gómez-Pastora, E. Bringas, M. Lázaro-Díez, J. Ramos-Vivas, I. Ortiz, The reverse of controlled release: Controlled sequestration of species and biotoxins into nanoparticles (NPs), Drug Deliv. Syst. (2017) 207–244. https://doi.org/10.1142/9789813201057_0006.

[46] L.R. França, R. Launois, K. Le Lay, P. Aegerter, M. Bouhassira, P. Meshaka, B. Guidet, Cost-effectiveness of drotrecogin alfa (activated) in the treatment of severe sepsis with multiple organ failure, Int. J. Technol. Assess. Health Care. 22 (2006) 101–108. https://doi.org/10.1017/S0266462306050896.

[47] Global report on the epidemiology and burden of sepsis: current evidence, identifying gaps and future directions, Geneva, 2020.

[48] E. Hailman, J.J. Albers, G. Wolfbauer, A.Y. Tu, S.D. Wright, Neutralization and transfer of lipopolysaccharide by phospholipid transfer protein, J. Biol. Chem. 271 (1996) 12172–12178. https://doi.org/10.1074/jbc.271.21.12172.

[49] C.J. Vesy, R.L. Kitchens, G. Wolfbauer, J.J. Albers, R.S. Munford, Lipopolysaccharide-binding protein and phospholipid transfer protein release lipopolysaccharides from gram-negative bacterial membranes, Infect. Immun. 68 (2000) 2410–2417. https://doi.org/10.1128/IAI.68.5.2410-2417.2000.

[50] [1] R.R. Schumann, S.R. Leong, G.W. Flaggs, P.W. Gray, S.D. Wright, J.C. Mathison, P.S. Tobias, R.J. Ulevitcht, Structure and function of lipopolysaccharide binding protein, 35533 (1990) 1429–1432. https://doi.org/doi: 10.1126/science.2402637.

[51] K. Anderson V, Toll signaling pathways in the innate inmune response, Development. 129 (2000) 5635–5645. https://doi.org/10.1242/dev.00161.

[52] D. Artner, A. Oblak, S. Ittig, J.A. Garate, S. Horvat, C. Arrieumerlou, A. Hofinger, C. Oostenbrink, R. Jerala, P. Kosma, A. Zamyatina, Conformationally constrained lipid a mimetics for exploration of

structural basis of TLR4/MD-2 activation by lipopolysaccharide, ACS Chem. Biol. 8 (2013) 2423–2432. https://doi.org/10.1021/cb4003199.

[53] J.A. Garate, C. Oostenbrink, Lipid a from lipopolysaccharide recognition: Structure, dynamics and cooperativity by molecular dynamics simulations, Proteins Struct. Funct. Bioinforma. 81 (2013) 658–674. https://doi.org/10.1002/prot.24223.

[54] J.A. Garate, J. Stöckl, M. Del Carmen Fernández-Alonso, D. Artner, M. Haegman, C. Oostenbrink, J. Jiménez-Barbero, R. Beyaert, H. Heine, P. Kosma, A. Zamyatina, Anti-endotoxic activity and structural basis for human MD-2·TLR4 antagonism of tetraacylated lipid A mimetics based on ßGlcN(1-1)αGlcN scaffold, Innate Immun. 21 (2015) 490–503. https://doi.org/10.1177/1753425914550426.

[55] J. Gao, J.-X. Wang, X.-W. Wang, MD-2 Homologue Recognizes the White Spot Syndrome Virus Lipid Component and Induces Antiviral Molecule Expression in Shrimp, J. Immunol. 203 (2019) 1131–1141. https://doi.org/10.4049/jimmunol.1900268.

[56] B.S. Park, D.H. Song, H.M. Kim, B.S. Choi, H. Lee, J.O. Lee, The structural basis of lipopolysaccharide recognition by the TLR4-MD-2 complex, Nature. 458 (2009) 1191–1195. https://doi.org/10.1038/nature07830.

[57] F. Cochet, F.A. Facchini, L. Zaffaroni, J.M. Billod, H. Coelho, A. Holgado, H. Braun, R. Beyaert, R. Jerala, J. Jimenez-Barbero, S. Martin-Santamaria, F. Peri, Novel carboxylate-based glycolipids: TLR4 antagonism, MD-2 binding and self-assembly properties, Sci. Rep. 9 (2019) 1–13. https://doi.org/10.1038/s41598-018-37421-w.

[58] E. Hailman, H. Lichenstein, M. Wurfel, D. Miller, D. Johnson, M. Kelley, L. Busse, M. Zukowski, S. Wright, Lipopolysaccharide (LPS)-binding protein accelerates the binding of LPS to CD14., J. Exp. Med. 179 (1994) 269–77. http://www.pubmedcentral.nih.gov/articlerender.fcgi?artid=2191344&tool=pmcentrez&rendertype=abstract%5Cnhttp://jem.rupress.org/content/179/1/269.abstract.

[59] T.N. Kirkland, F. Finley, D. Leturcq, A. Moriarty, J.D. Lee, R.J. Ulevitch, P.S. Tobias, Analysis of lipopolysaccharide binding by CD14, J. Biol. Chem. 268 (1993) 24818–24823.

[60] D. Heumann, R. Lauener, B. Ryffel, The dual role of LBP and CD14 in response to Gram-negative bacteria or Gram-negative compounds, J. Endotoxin Res. 9 (2003) 381–384. https://doi.org/10.1179/096805103225003312.

[61] M.O. Labeta, J. -J Durieux, N. Fernandez, R. Herrmann, P. Ferrara, Release from a human monocyte-like cell line of two different soluble forms of the lipopolysaccharide receptor, CD14, Eur. J. Immunol. 23 (1993) 2144–2151. https://doi.org/10.1002/eji.1830230915.

[62] R.I. Tapping, P.S. Tobias, Cellular binding of soluble CD14 requires lipopolysaccharide (LPS) and LPS-binding protein, J. Biol. Chem. 272 (1997) 23157–23164. https://doi.org/10.1074/jbc.272.37.23157.

[63] G. Ramadori, K.-H.M. zum Buschenfelde, T. P.S, M. J.C, U. R.J, Biosynthesis of Lipopolysaccharide-Binding protein in rabbit hepatocytes, Pathobiology. 58 (1990) 89–94. doi.org/10.1016/S0021-9258(19)74538-4

[64] M. Müller, O. Scheel, B. Lindner, T. Gutsmann, U. Seydel, The role of membrane-bound LBP, endotoxin aggregates, and the MaxiK channel in LPS-induced cell activation, J. Endotoxin Res. 9 (2003) 181–186. https://doi.org/10.1179/096805103125001595.

[65] J.K. Eckert, Y.J. Kim, J.I. Kim, K. Gürtler, D.Y. Oh, S. Sur, L. Lundvall, L. Hamann, A. vanderPloeg, P. Pickkers, E. Giamarellos-Bourboulis, A. V. Kubarenko, A.N. Weber, M. Kabesch, O. Kumpf, H.J. An, J.O. Lee, R.R. Schumann, The crystal structure of lipopolysaccharide binding protein reveals the location of a frequent mutation that impairs innate immunity, Immunity. 39 (2013) 647–660. https://doi.org/10.1016/j.immuni.2013.09.005.

[66] K. Brandenburg, G. Jürgens, J. Andrä, B. Lindner, M.H.J. Koch, A. Blume, P. Garidel, Biophysical characterization of the interaction of high-density lipoprotein (HDL) with endotoxins, Eur. J. Biochem.

269 (2002) 5972–5981. https://doi.org/10.1046/j.1432-1033.2002.03333.x.

[67] B. Yu, S.D. Wright, Catalytic Properties of Lipopolysaccharide (LPS) Binding Protein, J. Biol. Chem. 271 (2002) 4100–4105. https://doi.org/10.1074/jbc.271.8.4100.

[68] M. Chen, M. Ji, X. Si, The effects of statin therapy on mortality in patients with sepsis: A meta-analysis of randomized trials, Med. (United States). 97 (2018). https://doi.org/10.1097/MD.0000000000011578.

[69] A.A. Fowler, J.D. Truwit, R.D. Hite, P.E. Morris, C. Dewilde, A. Priday, B. Fisher, L.R. Thacker, R. Natarajan, D.F. Brophy, R. Sculthorpe, R. Nanchal, A. Syed, J. Sturgill, G.S. Martin, J. Sevransky, M. Kashiouris, S. Hamman, K.F. Egan, A. Hastings, W. Spencer, S. Tench, O. Mehkri, J. Bindas, A. Duggal, J. Graf, S. Zellner, L. Yanny, C. McPolin, T. Hollrith, D. Kramer, C. Ojielo, T. Damm, E. Cassity, A. Wieliczko, M. Halquist, Effect of Vitamin C Infusion on Organ Failure and Biomarkers of Inflammation and Vascular Injury in Patients with Sepsis and Severe Acute Respiratory Failure: The CITRIS-ALI Randomized Clinical Trial, JAMA - J. Am. Med. Assoc. 322 (2019) 1261–1270. https://doi.org/10.1001/jama.2019.11825.

[70] E.P. Plata-Menchaca, R. Ferrer, Life-support tools for improving performance of the Surviving Sepsis Campaign Hour-1 bundle, Med. Intensiva. 42 (2018) 547–550. https://doi.org/10.1016/j.medin.2018.07.008.

[71] H. Il Kim, S. Park, Sepsis: Early recognition and optimized treatment, Tuberc. Respir. Dis. (Seoul). 82 (2019) 6–14. https://doi.org/10.4046/trd.2018.0041.

[72] A. Rhodes, L.E. Evans, W. Alhazzani, M.M. Levy, M. Antonelli, R. Ferrer, A. Kumar, J.E. Sevransky, C.L. Sprung, M.E. Nunnally, B. Rochwerg, G.D. Rubenfeld, D.C. Angus, D. Annane, R.J. Beale, G.J. Bellinghan, G.R. Bernard, J.D. Chiche, C. Coopersmith, D.P. De Backer, C.J. French, S. Fujishima, H. Gerlach, J.L. Hidalgo, S.M. Hollenberg, A.E. Jones, D.R. Karnad, R.M. Kleinpell, Y. Koh, T.C. Lisboa, F.R. Machado, J.J. Marini, J.C. Marshall, J.E. Mazuski, L.A.

McIntyre, A.S. McLean, S. Mehta, R.P. Moreno, J. Myburgh, P. Navalesi, O. Nishida, T.M. Osborn, A. Perner, C.M. Plunkett, M. Ranieri, C.A. Schorr, M.A. Seckel, C.W. Seymour, L. Shieh, K.A. Shukri, S.Q. Simpson, M. Singer, B.T. Thompson, S.R. Townsend, T. Van der Poll, J.L. Vincent, W.J. Wiersinga, J.L. Zimmerman, R.P. Dellinger, Surviving Sepsis Campaign: International Guidelines for Management of Sepsis and Septic Shock: 2016, Springer Berlin Heidelberg, 2017. https://doi.org/10.1007/s00134-017-4683-6.

[73] G. Husabø, R.M. Nilsen, H. Flaatten, E. Solligård, J.C. Frich, G.T. Bondevik, G.S. Braut, K. Walshe, S. Harthug, E. Hovlid, Early diagnosis of sepsis in emergency departments, time to treatment, and association with mortality: An observational study, PLoS One. 15 (2020) 1–15. https://doi.org/10.1371/journal.pone.0227652.

[74] E.C. Dullah, C.M. Ongkudon, Current trends in endotoxin detection and analysis of endotoxin–protein interactions, Crit. Rev. Biotechnol. 37 (2017) 251–261. https://doi.org/10.3109/07388551.2016.1141393.

[75] A. Serdakowski London, B. Kerins, W.R. Tschantz, K. Mackay, Endotoxin removal and prevention for pre-clinical biologics production, Biotechnol. J. 7 (2012) 1509–1516. https://doi.org/10.1002/biot.201200220.

[76] B. Szermer-Olearnik, J. Boratyński, Removal of endotoxins from bacteriophage preparations by extraction with organic solvents, PLoS One. 10 (2015) 1–10. https://doi.org/10.1371/journal.pone.0122672.

[77] K. Hanasawa, T. Tani, T. Oka, T. Yoshioka, Y. Endo, M. Horisawa, Y. Nakane, M. Kodama, K. Teramoto, S. Nishiumi, A new treatment for endotoxemia with direct hemoperfusion by polymyxin immobilized fiber, Ther. Apher. 4 (2000) 142–145. https://doi.org/10.1046/j.1526-0968.2000.004002142.x.

[78] A.F. Grootendorst, The Potential Role of Hemofiltration in the Treatment of Patients With Septic Shock and Multiple Organ Dysfunction Syndrome, Adv. Ren. Replace. Ther. 1 (1994) 176–184. https://doi.org/10.1016/S1073-4449(12)80049-5.

[79] K. Teramoto, Y. Nakamoto, T. Kunitomo, H. Shoji, T. Tani, K. Hanazawa, M. Kodama, Removal of endotoxin in blood by polymyxin B immobilized polystyrene-derivative fiber, Ther. Apher. 6 (2002) 103–108.

[80] A.D. Romaschin, C. V. Obiezu-Forster, H. Shoji, D.J. Klein, Novel Insights into the Direct Removal of Endotoxin by Polymyxin B Hemoperfusion, Blood Purif. 44 (2017) 193–197. https://doi.org/10.1159/000475982.

[81] T. Shimizu, T. Miyake, M. Tani, History and current status of polymyxin B-immobilized fiber column for treatment of severe sepsis and septic shock, Ann. Gastroenterol. Surg. 1 (2017) 105–113. https://doi.org/10.1002/ags3.12015.

[82] J. Gómez-Pastora, I. Karampelas, E. Bringas, E.P. Furlani, I. Ortiz, Computational Analysis of a Two-Phase Continuous-Flow Magnetophoretic Microsystem for Particle Separation from Biological Fluids, Elsevier Masson SAS, 2017. https://doi.org/10.1016/B978-0-444-63965-3.50199-9.

[83] J. Gómez-Pastora, C. González-Fernández, E. Real, A. Iles, E. Bringas, E.P. Furlani, I. Ortiz, Computational modeling and fluorescence microscopy characterization of a two-phase magnetophoretic microsystem for continuous-flow blood detoxification, Lab Chip. 18 (2018) 1593–1606. https://doi.org/10.1039/c8lc00396c.

[84] J. Gómez-Pastora, I.H. Karampelas, X. Xue, E. Bringas, E.P. Furlani, I. Ortiz, Magnetic Bead Separation from Flowing Blood in a Two-Phase Continuous-Flow Magnetophoretic Microdevice: Theoretical Analysis through Computational Fluid Dynamics Simulation, J. Phys. Chem. C. 121 (2017) 7466–7477. https://doi.org/10.1021/acs.jpcc.6b12835.

[85] J. Gómez-Pastora, I.H. Karampelas, E. Bringas, E.P. Furlani, I. Ortiz, Numerical Analysis of Bead Magnetophoresis from Flowing Blood in a Continuous-Flow Microchannel: Implications to the Bead-Fluid Interactions, Sci. Rep. 9 (2019) 1–13. https://doi.org/10.1038/s41598-019-43827-x.

[86] J. Gómez-Pastora, X. Xue, I.H. Karampelas, E. Bringas, E.P. Furlani, I. Ortiz, Analysis of separators for magnetic beads recovery: From large systems to multifunctional microdevices, Sep. Purif. Technol. 172 (2017) 16–31. https://doi.org/10.1016/j.seppur.2016.07.050.

2

LPS binding molecules

Abstract

This chapter pursues the synthesis of an active molecule to selectively bind LPS. For that purpose, first, a thorough revision of the state-of-art of binding molecules that have shown anti-LPS activity has been accomplished. Among all the potential candidates, two main proteins were selected to be obtained by the rational method of protein design: human lipid binding protein (LBP) and Anti LPS factor protein from *Limulus polyphemus* (LALF). These peptides were attempted to obtain using the recombinant DNA technology. Recombinant proteins were achieved by expressing a cloned gene in both *Escherichia coli* bacteria and yeast, specifically *Pichia Pastoris*. During the protein expression process, solubilization issues arose and the protein of interest was located in the insoluble fraction of the cells. Finally, after constructing a Fusion protein formed by maltose binding protein (MBP) and LALF (MBP_LALF) and finding the appropriate strain, Arctic express, which allows expression at lower temperatures (18˚C), a soluble heterologous protein was obtained.

2.1. Introduction

The interaction between lipid A and different molecules has been studied in order to clarify the binding mechanisms and to develop new diagnosis methodologies and advanced therapies for sepsis control.

There is a large number of molecules that interact with LPS (**see Appendix A**). In brief, it has been proved that some organic solvents such as octanol and butanol [1,2] and polymers like polyamide and polysulfone [3,4] present some affinity towards LPS and therefore, they could be useful for certain applications.

However, the most important molecules that selectively bind LPS are peptide-based structures that are usually produced by living organisms. There is a variety of structures and biological functions, but generally, peptides present higher affinities towards endotoxins and at the same time high LPS-binding specificity.

Within anti-LPS potential peptides, two main groups can be distinguished; peptides produced in humans and in other living organisms as bacteria, responsible for FhuA, OmpT and MsbA, membrane proteins located in their outer membrane [5–7], and invertebrates, which are also capable of synthesizing antimicrobial peptides such as LALF and TALF (ALF from *Tachypleus tridentatus*) [8,9].

Regarding the human peptides, proteins with potential activity against LPS like HDL [10–12], hemoglobin [13–15], lactoferrin [16,17] or BPI (bactericidal permeability-increasing protein) have been reported [18–20].

But, undoubtedly, the most studied proteins as potential ligands to LPS are the ones involved in the human response where the most in-depth reviewed are CD14 [21–23], LBP [24–26], TLR4 [27–29] and MD-2 [30,31].

Among all the molecules that have exhibited activity against LPS, two of them are particularly interesting for application in a capture system such

as the one proposed in this work: LBP and LALF (ALF protein from *Limulus polyphemus*) protein.

LBP (58 kDa) is by far the most extensively studied soluble protein with LPS-binding capacity as its presence plays a key role in the human immune cascade [24,25]. On the other side, LALF, a 11.8 kDa protein from the Atlantic horseshoe crab, has been found to inhibit the endotoxin mediated activation of its coagulation system so that its neutralizing capacity renders this molecule attractive for LPS sequestration systems [32–34].

Currently, both proteins are commercially available but their acquisition price is so high that their implementation would make the process economically unsustainable. In addition, regarding LALF protein, the conventional obtaining method is based on the bleeding of live horseshoe crabs which has been reported as an ecologically unsustainable practice for the marine species [35].

This highlights the need to find an alternative for obtaining the aforementioned proteins. Fortunately, in recent decades, thanks to the application of genetic engineering techniques that allow the manipulation of DNA, it has been possible to produce recombinant proteins which were proposed for the first time by Peter Lobban who, for the first time, described the successful production and intracellular replication of recombinant DNA between 1972 and 1973 [36–38].

To obtain these recombinant proteins, a gene encoding the protein of interest and a specialized vehicle called a vector are required. In a typical DNA cloning procedure, the DNA fragment is inserted in the vector resulting in a plasmid, which is a small, circular, double-stranded DNA molecule that replicates independently from the host chromosomal DNA (**Figure 2.1**). They are mainly found in bacteria, but also exist naturally in archaea and eukaryotes such as yeast and plants [38,39].

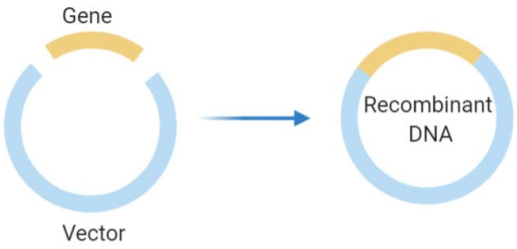

Figure 2.1. DNA cloning illustration.

Lab-created plasmids have an origin of replication (which controls the host range and copy number of the plasmid), selection marker and cloning site **(Figure 2.2)**. The easiness of modifying plasmids and the ability of plasmids to self-replicate within a cell make them attractive tools for the life scientist or bioengineer [40].

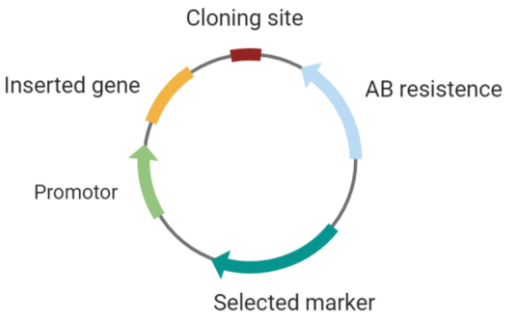

Figure 2.2. Schematic representation of a plasmid.

The constructed plasmids or recombinant DNA are then introduced into host cells and grown in LB agar plates. As plasmids develop antibiotic resistance, organisms that take up the plasmid will survive and reproduce while the ones without the plasmid will die [41–43]. **Figure 2.3** details the transformation process using bacteria as host cells.

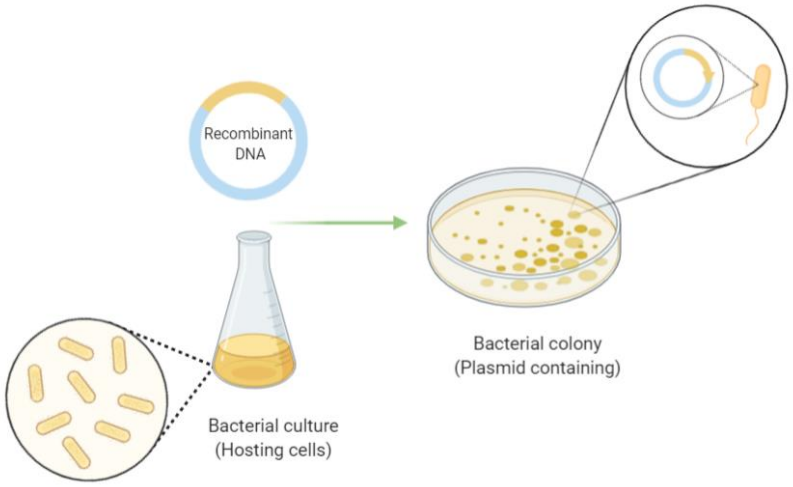

Figure 2.3. Transformation process illustration. Recombinant DNA is introduced in hosting cells (bacteria) which grow in a petri dish when the cells satisfactorily contain the recombinant DNA.

Systems used to express recombinant DNA include both prokaryotic and eukaryotic systems. Often this choice is based on the type of protein, functional activity, as well as the required yield needed.

Expression in *E.coli* bacteria is one of the most widely used, due to its ease of handling and high yield. However, since it is a prokaryotic expression system, recombinant proteins from eukariotic origin cannot be expressed in prokariotic systems, which lack the molecular machinery needed to generate the correct native structure of some proteins. To solve this problem, more complex eukaryotic expression systems are used, such as yeast, insect cells, mammalian cells or plants [44,45].

Regardless of the host cell chosen, when they reproduce, replicate the plasmid and pass it on to their offspring that contain copies of the DNA template. Afterwards, cells containing the DNA template are larger cultured so that they can be induced to transcribe and translate the protein of interest. Finally, these cells are lysed or ruptured to release the protein together with other proteins and macromolecules (**Figure 2.4**). Because of this, the target protein is subject to purification methods to

remove residual cells. Eventually, the purified protein can then be used in the experimental runs.

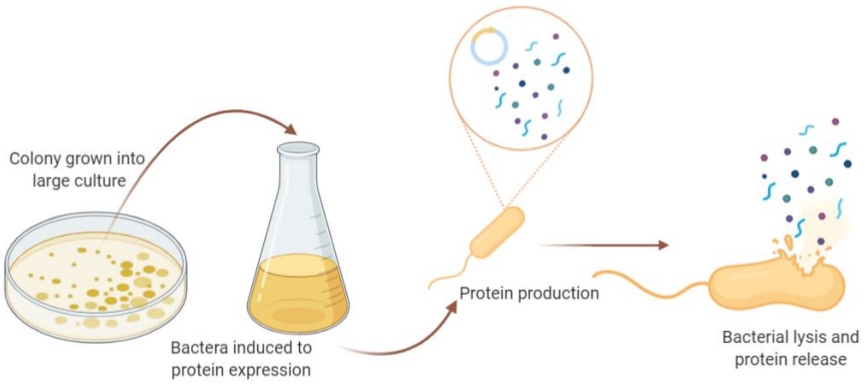

Figure 2.4. Schematics of the protein production process.

This protein obtaining alternative procedure where the recombinant protein technology is used have reported 90% reduction in reagents consumption and can lead to both lower production costs and to contribute to horseshoe crab conservation [35,46,47]. Consequently, this work reports the strategy designed to obtain biologically active proteins: LBP, LBD (LBS binding domain from human LBP), and two ALF proteins, LALF and GALF (antilipopolysaccharides protein from *Penaeus monodon*).

2.2. Materials

2.2.1. Gene sequences

Gene sequences employed in this work have been codon optimized for the specific host to Integrated DNA Technologies (IDT) and are described in **table 2.1.**

Table 2.1. Gene sequences employed in this work.

Gene	ID	Length	Origin	Reference
GALF	A5A3I5	377	Penaeus monodon	[48]
LALF	1307201A	342	Limulus Polyphemus	[7]
LBP	AAH22256.1	1434	Homo sapiens	[26]
LBD	4767724	636	Homo sapiens (LBP binding domain)	[49]

2.2.2. Major microbial strains

Bacterial strains employed for this work are described in **Appendix B (Table B.1).** All of them were gently provided from the collection of the Institute of Biomedicine and Biotechnology of Cantabria (IBBTEC).

2.2.3. Expression vectors

Expression vectors employed during this work have been obtained from the IBBTEC collection and are detailed in **Table 2.2**.

Table 2.2.Expression vectors used in this thesis.

Plasmid	Phenotype	Size (Kb)
pET29c	Kn^R	5.4
pET3a	Ap^R	2.6
pPICZ	Zn^R	3.3

2.2.4. Plasmids construction

Plasmids constructed during this work through enzyme restriction (RE) or isothermal assembly (EI).

Table 2.3.Plasmids used in this work.

Plasmid	Insert	Vector	Stability Tag	Size (Kb)
pABP1	LBP	pPICZ	-	4.9
pABP2	GALF	pPICZ	-	3.7
pABP3	LALF	pPICZ	-	3.7
pABP4	LALF	pPICZ	α Factor	4.5
pABP5	LBD	pPICZ	-	4.0
pABP6	LBP	pET29c	-	7.0
pABP7	LALF	pET29c	-	5.8
pABP8	LBD	pET29c	-	6.1
pABP9	LBD	pET3a	TRX	5.3
pABP10	ALF	pET29c	MBP	6.2
pABP11	ALF	pET29c	SUMO	5.9
pABP12	ALF	pET29c	TRX	6.0
pABP13	ALF	pET29c	GST	6.1

2.2.5. Oligonucleotides

Oligonucleotides were designed and optimized for the different DNA fragments and expression vectors and were purchased to IDT. **Appendix B** collects the sequences employed for *E.coli* constructions (**Table B.2**), Primers employed for *E.coli* plasmids construction (**Table B.3**) and Oligonucleotides employed for PCR and Sanger sequencing (**Table B.4**).

2.2.6. Chemical reagents

Required antibiotics were purchased to Apollo Scientific, Isopropyl ß-D-1-thiogalactopyranoside (IPTG) to Thermo Scientific, and phenylmethylsulfonyl fluoride (PMSF) and Lysozyme from chicken egg white to Sigma Aldrich. Dithiothreitol (DTT) and 20% SDS were obtained from Fisher Scientific. Trizma base, glycine, Tris-HCl, NaCl, LB medium and LB Agar medium were acquired from Scharlab, S.L. His Trap HP columns were purchased to GE Healthcare and the required solutions were made up with MiliQ® water.

2.2.7. Buffers and solutions

Buffers and solutions employed in this work are described in **Table 2.4.**

Table 2.4. Buffers and solutions employed during this work.

Lysis Buffer	100 mM Tris-HCl, 500 mM NaCl, 1% Triton X-100, 5 mM DTT, pH 7.5. Supplemented when used with 100 µg/mL Lysozyme, PMSF
Buffer A	100 mM Tris-HCl, 500 mM NaCl, 500 mM Imidazole, pH 7.5
Buffer B	100 mM Tris-HCl, 500 mM NaCl, 500 mM Imidazole, pH 7.5
Buffer C	50 mM Tris-HCl, 150 mM NaCl, pH 7.5
dNTPs	10 mM dGTP, dCTP, dATP, dTTP
0.5x TBE	45 mM Tris-HCl, 45 mM boric acid, 0.5mM EDTA, pH 8.2
DNA Sample Loading Buffer 6x	0.25% (w/v) bromophenol blue, 30% (v/v) glycerol in 0.5xTBE
SDS Sample Loading Buffer 2x	50 mM Tris-HCl pH=6.8, 2% SDS, 10% glycerol, 0.1% bromophenol, 100mM β- mercaptoethanol
1x SDS-PAGE Buffer	25 mM Tris-HCl, 192mM Glycine, 1% SDS, pH=8.4
Assembly Mixture Buffer (6 mL)	3 mL 1M Tris-HCl pH 7.5, 150 µL 2M $MgCl_2$, 60 µL 100 mM dGTP, 60 µL 100mM dATP, 60 µL 100 mM dTTP, 60 µL 100 mM dCTP, 300 µL 1M DTT, 1.5g PEG-800, 300 µL 100 mM NAD.
Master Mix (80 aliquots)	320 µL 5x Isothermal reaction buffer, 0.64 µL 10 U µL-1 T5 exonuclease, 20 µL 2 U µL-1 Phusion DNA polymerase, 160 µL 40 U µL-1 Taq DNA ligase, water up to 1.2 mL.

2.3. Experimental procedure

2.3.1. Molecular cloning

Gene insertion

Obtaining plasmids implies the union of the chosen vector and the desired insert. This process was carried out following two strategies: restriction enzymes digestion and isothermal assembly.

Restriction enzyme digestion is the traditional cloning process based on recombinant DNA methods that begins with the preparation of a vector to receive the insertion DNA by digesting each (insert and vector) separately with the appropriate restriction enzymes. The digested fragments were then joined at the cohesive ends by the T4 DNA ligase (Thermo) to form a plasmid capable of expressing the gene of interest **(Figure 2.5)**.

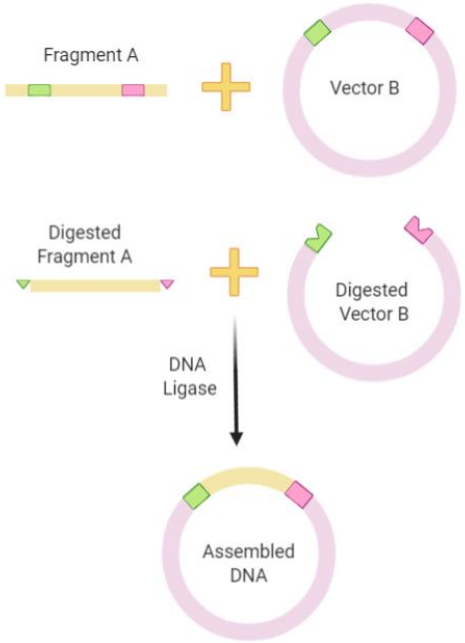

Figure 2.5. Gene cloning procedure by Enzyme Restriction.

Digested vector and DNA were purified from the agarose gels with the GeneJet Gel Extraction Kit (Thermo Fisher) and DNA ligation was performed using a molar ratio of vector: insert DNA of 1:3 and 1U of T4 DNA ligase (Thermo Fisher) in a final volume of 20 µL for overnight incubation at room temperature. The final concentration was measured through spectrophotometry (Nanodrop 200c) and electroporation was performed on DH5α cells.

On the other hand, isothermal assembly (Gibson Assembly), the modern approach for plasmids construction, was also employed. This method combines several overlapping DNA fragments to produce a ligated plasmid ready for transformation in a single reaction as explained in **Figure 2.6** [56].

Polymerase chain reaction (PCR) is carried out under isothermal conditions using three enzymatic steps: a 5' exonuclease generates long overhangs, Phusion High-Fidelity DNA polymerase fills in the gaps of the annealed single strand regions, and a DNA ligase seals the nicks of the annealed and filled-in gaps (**see appendix C**).

Frozen 15µl assembly mixture aliquots were thawed and then kept on ice until ready to be used. Five microliters of the DNA to be assembled were added to the master mixture in equimolar amounts. Between 10 and 100 ng of each ~6 kb DNA fragment were added. For larger DNA segments, proportional amounts of DNA were added. Incubation was performed at 50 °C for 15 to 60 min (60 min was optimal).

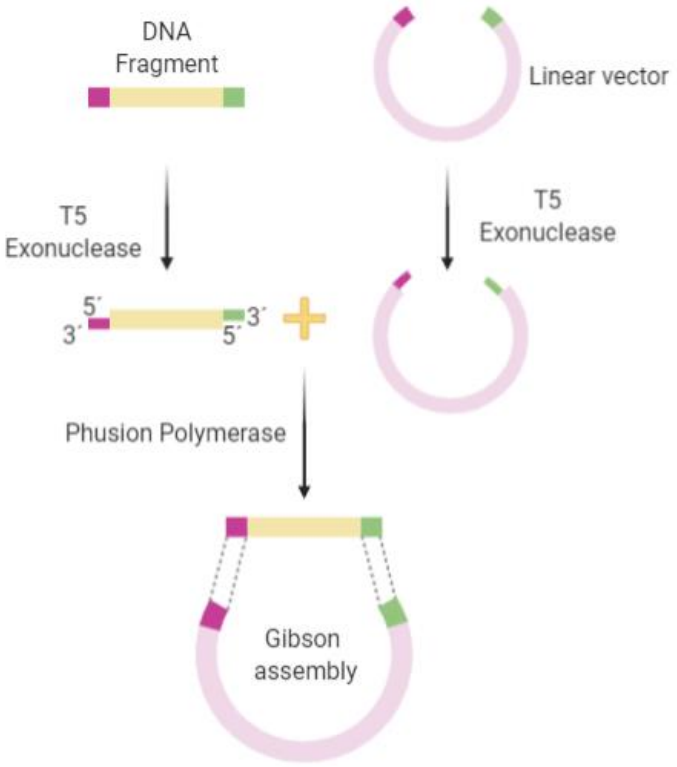

Figure 2.6. Gibson assembly cloning procedure.

DNA electrophoresis in agarose gels

In order to observe the presence and DNA band size obtaining either by PCR or enzymatic digestion, DNA fragments were separated via 1% (w/v) agarose gel prepared in 0.5x TBE buffer. To visualize the DNA, 5 µL of intercalating agent SafeView Classic (ABM) were added to the 100 mL (1%) agarose solution. Usually, 20 µL of sample solution were mixed with 4 µL of DNA sample-loading buffer and loaded into wells (indentations) at one end. For sizing and approximate DNA kb quantification, Generuler 1Kb DNA ladder plus (Thermofisher) was used.

Horizontal cells were employed for the electrophoresis with 0.5x TBE buffer and an electrical field of 120V was applied for 45 minutes to move the negatively charged DNA through the agarose gel matrix towards the positive electrode (**Figure 2.7**). Finally, agarose gels were visualized in a transilluminator UV Gel Doc 2000 (BioRad) and images were analyzed with Quantity One program (BioRad).

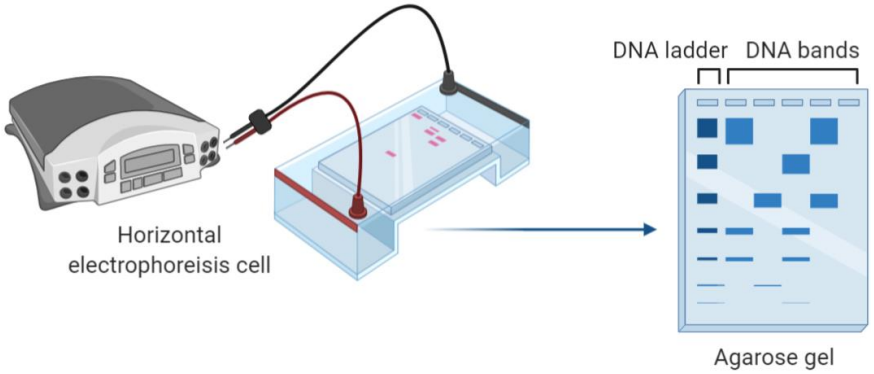

Figure 2.7. DNA electrophoresis schematic illustration.

DNA extraction

Plasmid DNA from cultures was extracted using the GeneJET plasmid miniprep kit **(Fisher Scientific)** following the manufacture's protocol.
In addition, DNA purification from agarose gel was performed cutting bands from the electrophoresis gel. After that, it was employed a GeneJET gel extraction kit, following the manufacturer´s guide.

Nucleic acids quantification

DNA concentration was measured by spectrophotometer techniques at a wavelength of 260 nm with a Nanodrop 2000c (Thermo Scientific) with 2 µL of each sample. Purity of the extracted DNA was checked taking into account the 260/280 nm ratio which should be 1.8.

Sanger sequencing

Every constructed or modified plasmid was verified through DNA sequencing by using the "YouTube It" service offered by StabVida company. Samples (DNA + primer) were prepared according to their recommendations.

2.3.2. Protein expression

Culture medium

For *E.coli* cultures it was employed Luria Bertani (LB) growth medium composed of 10 g/L tryptone, 5 g/L yeast extract, and 5 g/L NaCl (Pronadisa) supplemented with 1.5% (w/v) of plate agar, 50 µg/mL Kanamycin (kn) (Apollo) sterilized by filtration (0.22um) was used as antibiotic.

For *Pichia pastoris* cultures, Yeast Extract-Peptone-Dextrose (YPD) medium was used. YPD consists of 10 g/L Yeast extract, 20 g/L Peptone and 20 g/L dextrose. The antibiotic resistance for this case was 50 µg/mL zeocin (Zn). Microbial strains were preserved frozen at -20˚C in 50% (v/v) glycerol peptone from the pellets in stationary phase.

Pichia cells were expressed in Buffered Glycerol-complex Medium (BMGY) and Buffered Methanol-complex Medium (BMMY) was employed for protein induction. Growing medium was prepared with 8 g Yeast extract (Pronadisa) and 16 g Peptone in 560 mL water. The mixture was autoclaved for 20 minutes on liquid cycle. Once the solution was cooled down to room temperature (RT) 80 mL of 1 M Potassium Phosphate Buffer of pH=6 and 80 mL 10x YNB (13.4% Yest Nitrogen Based with Ammonium Sulfate without amino acids, Pronadisa) were added. For BMGY 0.16mL of 0.02% Biotin solution were added and BMMY was finally prepared with 80mL of 10% Glycerol solution.

Bacterial growth measures

Cultures growth was measured through optical density (OD) at a wavelength of 600 nm using a Nanodrop 2000c spectrophotometer (Thermo Scientific) with 1 mL sample volume.

DNA transformation

E.coli and *Pichia Pastoris* strains transformations were carried out by electroporation due to the high efficiency of the method which consists of the application of an electrical current from an external source on any competent cell which becomes more permeable allowing DNA to enter it [57].

Four different types of competent cells were employed to perform this stage; DH5α provided by the support service of the IBBTEC, BL21, Arctic Express, and *Pichia Pastoris* obtained through the following protocols.

Primary cultures of *E.coli* electrocompetent cells were grown in 10 mL LB supplemented if required with the appropriate antibiotic at 37˚C for 12-18 h in a shaking incubator. Then, 2.5 mL were inoculated into a 50 mL LB culture until reaching an OD_{600} of 0.5-0-7. After approximately 1.5 h, the flask was placed in cold storage to stop cell growth. Then, the culture was poured into a previously cooled falcon tube and centrifuged at 4˚C for 15-20 minutes. The supernatant was discarded and the pellet was resuspended in the following order of washing: two washes with 50 mL of cold distilled water and, finally, one wash with 50 mL of 10% cold sterile glycerol. The supernatant of the last rinsing was discarded and the pellet was finally resuspended in 150 µL-200 µL glycerol resuspension. As a final step, the electrocompetent cells were aliquoted in 100µL Eppendorf tubes (80 µL/tube) which could be directly used or frozen utilizing dry ice and ethanol for a fast freezing and then, preserved at -80˚C.

Pichia Pastoris competent cells preparation started with a primary culture in YPD medium incubated overnight at 30˚C with 1:1000 Zeocin. Then, 2.5 mL were inoculated in 50 mL of fresh medium and left growing overnight

until an OD_{600} around 1.3 or 1.5. Once reached the desired OD, the culture was centrifuged at 1500 rpm during 5 minutes at 4˚C.The pellet was resuspended with ice-cold sterile water twice; a first rinse with 50 mL and the second one with 25 mL. For the final wash 20 mL of ice-cold 1M Sorbitol were employed, as well as for the last resuspension in 200 µL. Electrocompetent cells were used in the same day, never stored.

Before stating the transformation process in *Pichia* cells, 15 ng of plasmid DNA was linearized by restriction enzyme digestion with SacI and using the Fast Digest Value Pack (ThermoFisher). The transformation process (**Figure 2.8**) for both, yeast and bacteria, was performed by mixing an aliquot of 50 µL electrocompetent cells and 2 µL of the desired plasmid DNA in a 2 mm electroporation cell (Molecular BioProducts) previously cooled in ice. An electric pulse (2.5 kV/cm, 25 uF capacitance and 200Ω) was applied using a MicroPulser electroporator (BioRad). The mixture was finally resuspended in 1 mL YPD sterile and preheated to 30˚C and then transferred to a 1.5 mL Eppendorf tube which was also incubated at 30˚C under agitation for 1-2 h. Finally, 200 µL of the culture were plated in a Petri dish with LB agar (*E.coli*) or YPD (*Pichia*) supplemented with the appropriate antibiotics to select the transformed cells.

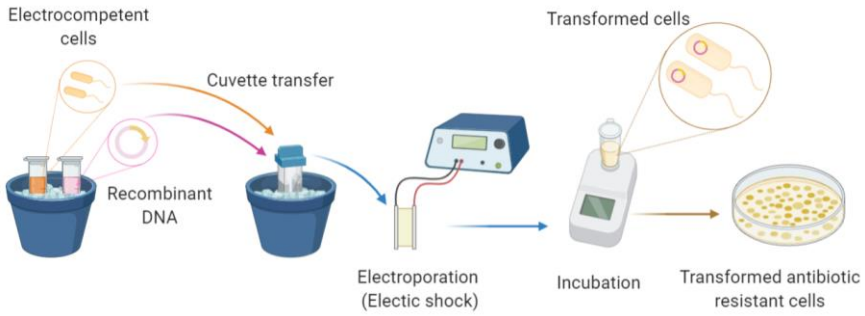

Figure 2.8. Recombinant DNA transformation process.

Overexpression and cells lysate

Bacterial colonies from transformation were incubated in 50 mL medium with the required antibiotics at 37˚C overnight until an OD_{600} around 0.4-0.6 was reached. Then, 50 mL culture were transferred into a 37˚C preheated 1L medium flask. When the OD_{600} reached a value of 1-1.5, the culture was cooled down to 18˚C. After 30 minutes, protein expression was induced with 1 mM IPTG and the culture remained at 18˚C overnight. For *Pichia*, colonies were grown at 30˚C during 72 h in BMGY and induced with methanol (BMMY).

The cells were then harvested by centrifugation at 4000 rpm at 4˚C for 15 minutes and the cellular pellet was flash frozen at -80 ˚C. After defrosting at room temperature, cells were resuspended in lysis buffer, supplemented with 10 µg/mL of lysozyme and 1:1000 PMSF as proteases inhibitor, incubated at 4˚C for 30 min and sonicated 3 times (1 min ON/ 1 min OFF) for cells disruption (**Figure 2.9**).

In order to verify the protein expression and once centrifuged, both samples from the supernatant and pellet were taken and the obtained protein was observed by electrophoresis under denaturalizing conditions.

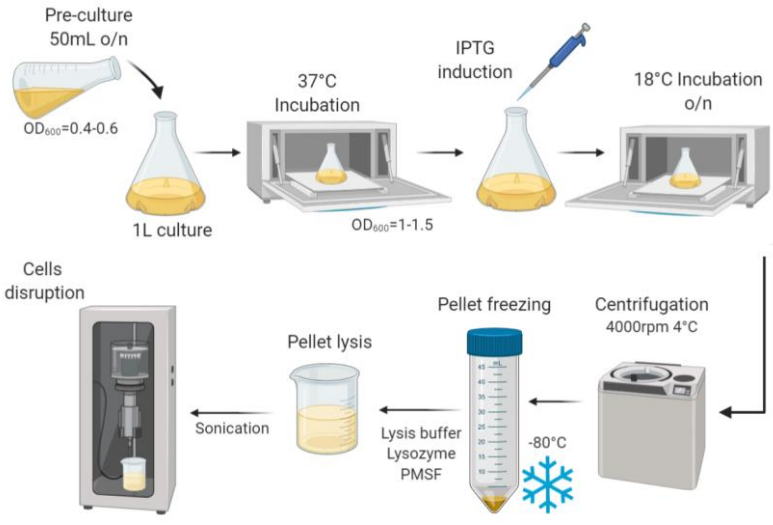

Figure 2.9. Overexpression and cells lysate procedure illustration.

Protein electrophoresis under denaturalizing conditions.

Protein expression was analyzed through electrophoresis with polyacrylamide gels in sodium dodecyl sulphate buffer (SDS-PAGE). Due to the size of the target protein, 15% polyacrylamide gels were used and prepared with 0.1% SDS (Sigma Aldrich) and acrylamide: Bis-acrylamide (29:1) (BioRad).

Pellet samples were resuspended in 200 µL of 2x loading buffer while 50 µL of supernatant ones were mixed with 50 µL of the same loading buffer. Both types of samples were incubated during 5 minutes at 100˚C and 10 or 15µL of each were loaded into acrylamide gel wells. Page Ruler Plus Prestained Protein Ladder (Thermofisher) was used as molecular weight marker.

Electrophoresis took place in a Mini-protean system (BioRad) at 180V during 50 minutes in 1x SDS-PAGE buffer (25 mM Tris-HCl, 192 mM Glycine, 1% (w/v) DS, pH=8.4). Subsequently, eluted protein fractions in acrylamide gels were visualized using BlueSafe protein stain (Nzytech) to determine the fractions containing the tagged protein (**Figure 2.10**).

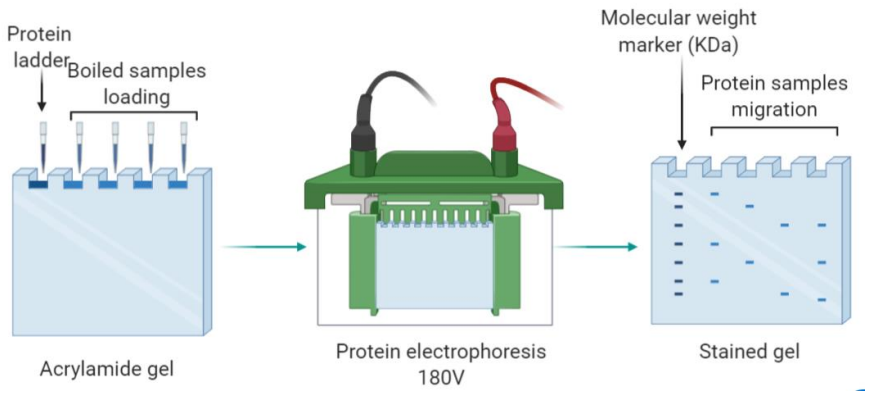

Figure 2.10. Protein electrophoresis and visualization procedure.

2.3.3. Protein purification

Fast protein liquid chromatography (FPLC) purification

Previous lysate was ultra-centrifuged at 40000 rpm at 4 °C for 20 min and the supernatant, containing the soluble protein, was loaded into a HisTrap HP histidine-tagged protein purification column (GE Healthcare). These columns are packed with Ni-Agarose resins because the nickel present on them binds to the 6x histidine tag added to the protein sequences during the cloning stage.

The column was initially washed with 5 column volumes (CV) of filtered and sterile Mili-Q water using a MiniPlus 3 peristaltic pump bomb (Gilson) with an adequate flow rate following the manufacturers' indications. Then, 5 CV of buffer A were passed through. Afterwards, the protein sample was loaded, the flow through) was saved and as a final step, the column was equilibrated with 5 CV Buffer A before connecting it to the FPLC system ÄKTA type (GE, Healthcare). This system eluted the protein through a buffer B gradient with the following program: initial wash with 5 mL Buffer A, 0-100% buffer B gradient in 15 fractions of 2.5 mL, 15 mL buffer B rinsing and final wash with 15 mL buffer A. The overall purification process is described in **Figure 2.11**.

Every buffer employed during this purification stage was previously filtered using Membrane MF-Millipore, 0.45 µm (Merck Millipore) for removing bubbles and suspension particles susceptible to damaging the matrix of the columns.

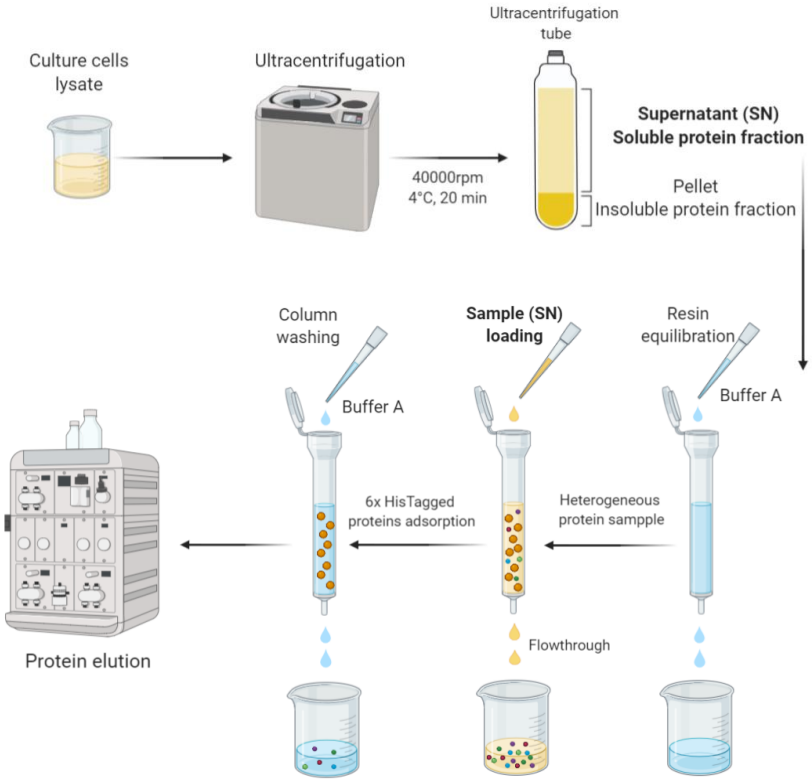

Figure 2.11. Protein purification process; from lysate cells to protein elution.

Determination of protein concentration

Final concentration of the obtained protein was determined by absorbance measurements at 280 nm wavelength using a Nanodrop 200c (Thermo scientific) spectrophotometer and using the molar extension coefficient for greater precision.

Protein concentration and buffer exchange

Protein solutions obtained after the purification method are quite diluted and also contain high salt concentration. With the objective of protein concentration and decrease of the salts content (NaCl, imidazole), 30 kDa Centricon ® centrifugal filters were used (Amicon Ultra, Millipore). This pore size filtration systems retain the proteins while allowing the passage of smaller molecules. For this purpose, samples were centrifuged with a Centrifuge 5810R (Eppendorf) with A-4-62 rotor at 4200rpm at 4˚C and diluted 1/5 in buffer C until reaching the desired concentration for the subsequent experiments (**Figure 2.12**).

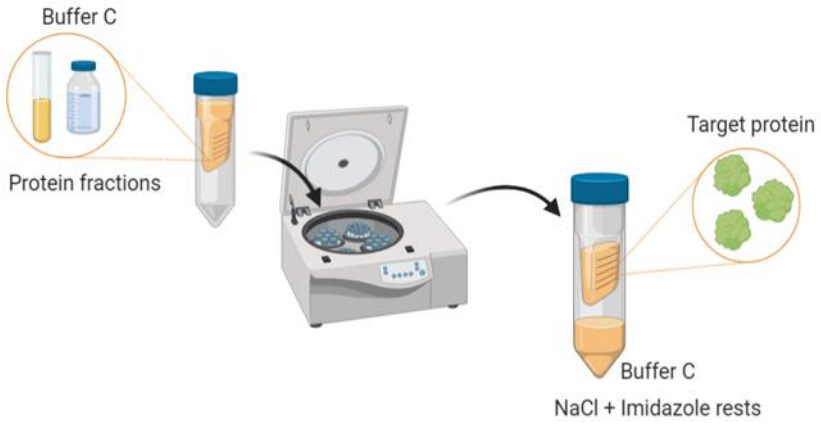

Figure 2.12. Protein concentration and buffer exchange graphical representation.

Protein Identification

Protein identification was performed by mass spectrophotometry Matrix-Assisted Laser Desorption/Ionization with Time of Light detector (MALDI-TOF) thanks to the proteomic service of the UPV/EHU University. Molecular mass and peptides sequences of the proteins were determined by MALDI-TOF from band cuts of acrylamide gels. Peptides were identified by confronting the MASCOT software search engine against the Swissprot database.

2.4. Results

2.4.1. Molecular cloning

Every genetic construction carried out in this work was optimized containing a 6x Histidines tag for its later purification with HisTrap columns.

Moreover, plasmids construction was performed via isothermal assembly (IA) or enzyme restriction (ER). In this regard, **Table 2.5** summarizes each of the plasmids used in this thesis according to the employed strategy and details whether or not they were verified by sanger sequencing.

The same procedure was carried out with each plasmid independently of the cloning strategy. As an example, the process and verification of the first construction of the table (pET29c_LALF) is explained.

Table 2.5. Summary of plasmids constructed by ER or IA and sanger sequencing results.

Gene	Vector	Fusion protein	Host	Cloning strategy	Sanger sequencing
LALF	pET29c	-	*E. coli*	ER	Yes
	pET29c	TRX	*E. coli*	IA	Yes
	pET29c	GST	*E. coli*	IA	Yes
	pET29c	MBP	*E. coli*	IA	Yes
	pET29c	SUMO	*E. coli*	IA	Yes
	pPICZ	-	P. pastoris	IA	Yes
	pPICZ- α Factor	-	P. pastoris	ER	Yes
GALF	pET29c	-	*E. coli*	IA	No
LBP	pPICZ	-	P. pastoris	ER	No
	pPICZ- α Factor	-	P. pastoris	ER	No
LBD	pET3a	TRX	*E. coli*	ER	Yes

Initially, pET29c_LALF construction was approached via isothermal assembly. Since amplification was unsuccessful, the strategy was modified and finally tested using restriction enzymes employing XhoI and NdeI oligonucleotides. Samples were stained with loading buffer and 5 µL Safeview was added to visualize the gel. Besides, GeneRuler plus DNA ladder (1kb for pET29c and 100bp for LALF) was loaded in an agarose well to visualize each band and verify the correct digestion of each vector (**Figure 2.13a**) and fragment (**Figure 2.13b**).

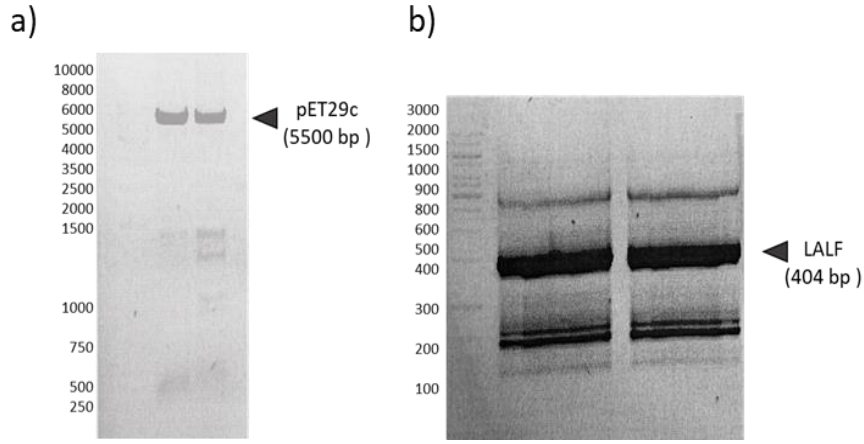

Figure 2.13. DNA electrophoresis verification of a) pET29c vector and b) LALF fragment.

Afterwards, recombinant DNA was transformed into DH5α electrocompetent cells and seeded on LB agar plates with their corresponding antibiotic. Several colonies were randomly selected, DNA was extracted and sent for verification by sanger sequencing to STABVIDA (Portugal). This procedure verified that the extracted DNA coincided with the target sequence.

2.4.2. Protein overexpression

As shown in **Table 2.6**, many of the gene constructions performed were not satisfactory in terms of protein production despite being overexpressed in different strains of *E.coli* and also in yeasts (**more information available in appendix D**).

In general terms, none of the proteins that were attempted to be overexpressed were finally obtained. Thus, it was decided to address fewer variables and, taking into account the experience acquired so far, it was decided to work only with the LALF protein.

Table 2.6. Protein expression results based on each constructed plasmid.

Gene	Vector	Fusion protein	Host	Size (kDa)	Protein production	Conditions
LALF	pET29c	-	*E. coli*	13	No	18°C,37°C BL21,Arctic express
	pET29c	TRX	*E. coli*	27	Yes	
	pET29c	GST	*E. coli*	42	Yes	
	pET29c	MBP	*E. coli*	58	Yes	
	pET29c	SUMO	*E. coli*	24	No	
	pPICZ	-	P.pastoris	13	No	
	pPICZ-α Factor	-	P.pastoris	22	No	
GALF	pET29c	-	*E. coli*	13	No	
LBP	pPICZ	-	P.pastoris	54	No	
	pPICZ-α Factor	-	P.pastoris	63	No	
LBD	pET3a	TRX	*E. coli*	18	No	

Since LALF protein production was not observed despite employing different hosting cells, we proceeded to construct fusion proteins using 3 stability tags for *E.coli* strains: TRX (Thioredoxin), GST (Glutathione S-

transferase), MBP (Maltose Binding Protein), and SUMO (Small Ubiquitin-like Modifier) and α Factor secretion signal for *P. pastoris*.

The efforts made for protein obtention in yeast even with the addition of the α-factor secretion signal were unsuccessful. Therefore, it was decided to continue the process focusing on *E.coli* expression of LALF gene.

Initially, fusion vectors were introduced in BL21 strain derived from *E.coli* and overexpression for each protein was performed at both 30˚C and 18˚C as shown in **Figure 2.14,** where it is marked with a star on the gel and with an arrow on the right side, the height at which the band corresponding to each fusion protein should appear when cultures samples were loaded. As appreciable, the expression of SUMO_ALF did not occur either at 30˚C or at 18˚C. On the contrary, GST_ALF (42kDa) expression seemed to work better at 18˚C than at 37˚C as the protein band is better visualized under that condition. On the other side, MBP_ALF worked for the two tested conditions and the protein band corresponding to 58 kDa is appreciable under the two temperatures. (Expression tests with TRX_LALF and other constructions carried out during this thesis are detailed in **appendix D**).

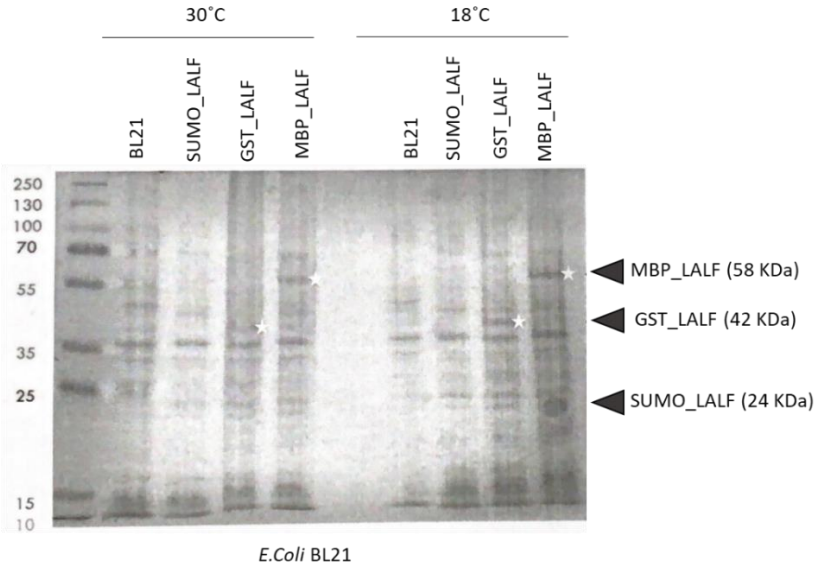

Figure 2.14. LALF fusion proteins expressed at 30˚C and 18˚C in BL21 strain.

So far, the most promising expression corresponded to MBP_LALF in BL21. Furthermore, cells were lysed by sonication and samples were centrifuged to separate the soluble proteins present in the supernatant (SN) from the insoluble proteins or inclusion bodies located in the pellet (P). Supernatant and pellet fractions were loaded separately on an SDS-PAGE gel; MBP_LALF was observed mainly in the pellet fraction which indicated that the protein was in the insoluble fraction of the cell culture. (data not shown)

In cases where proteins are located in the insoluble fraction, denaturation and renaturation protocols using urea have been described [58]. Nonetheless, this process possesses high risk as protein denaturation may result in total loss of activity. Alternatively, it was decided to introduce a new *E.coli* strain called Arctic Express for new over-expressions.

E.coli is a mesophilic bacterium, whose growth range is between 20˚C and 42˚C, being 37˚C the optimum temperature. Below 20 ˚C, *E.coli* presents a slow in growth rate, probably due to a reduction in the activity of chaperonins GroEl and GroES, proteins that assist in the protein folding process [59].

In order to compensate for the lack of chaperonin activity at low temperatures, Ferrer et al. 2003 [54], expressed in *E.coli* the genes Cpn60 and Cpn10 from the psychrophilic bacterium Oleispira antarctica, two chaperonins analogous to GroEl and GroES whose folding activity range is between 4˚C and 18˚C. This modification demonstrated that the expression of Cpn10 and Cpn60 improved the protein folding capacity of *E.coli* at low temperatures.

Up to this point, it was decided to express the MBP_LALF protein at 18˚C and compare the yield of Arctic express and BL21 strains.

Both cell cultures were lysed and centrifuged to separate the cell debris from the soluble fraction. Both fractions were analyzed by SDS-PAGE. As detailed in **Figure 2.15**, obtained MBP_LALF protein in BL21 was insoluble and present in the pellet while when it was expressed in Arctic Express, the protein was observed in the supernatant and therefore, in the soluble fraction.

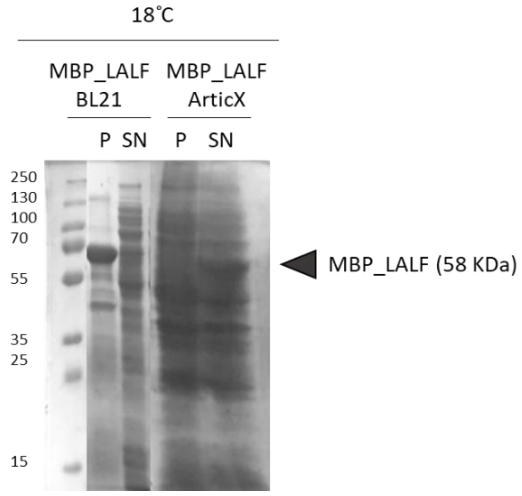

Figure 2.15. Pellet and supernatant samples of MBP_LALF protein expression in BL21 and Arctic express at 18˚C.

2.4.3. Protein Purification

MBP_LALF in Arctic express cultures were prepared, induced and incubated overnight at 18˚C. Afterwards, the cells were then harvested by centrifugation at 4000 rpm at 4 ˚C for 15 minutes and the cellular pellet was flash frozen at -80 ˚C. After defrosting at room temperature, cells were resuspended in buffer A, incubated at 4 ˚C for 30 min and sonicated on ice 3 times (1 min ON/ 1 min OFF). The lysate was then ultra-centrifuged at 40000 rpm at 4 °C for 20 min and the supernatant was separated from the pellet. The supernatant was loaded directly onto a HisTrap HP histidine-tagged protein 5 mL purification column (GE Healthcare) previously equilibrated in buffer A. (This procedure is previously detailed in **Figure 2.11**).

These columns are prepacked with Ni Sepharose® High Performance, which consists of 34 µm highly cross-linked agarose beads with an immobilized chelating group as Ni^{2+} ions are present in the medium. Proteins with 6-histidine labels, such as MBP_LALF, increase the affinity

for Ni^{2+} ions and are the strongest binder among other proteins in the sample, therefore these are the preferred columns for recombinant histidine-tagged proteins purification [60].

Protein purification was then performed through FPLC and the MBP_LALF protein was eluted by an imidazole concentration gradient of buffer B (from 20 mM to 500 mM) as shown in **Figure 2.16,** which depicts the chromatogram obtained during the process.

Since proteins absorb UV radiation at 280 nm, while purifying a 6x His Tagged protein, the elution profile shows an absorbance increase allowing identifying the target protein fractions. In this case, it can be observed that fractions between 7 and 11 apparently contained the MBP_LALF protein.

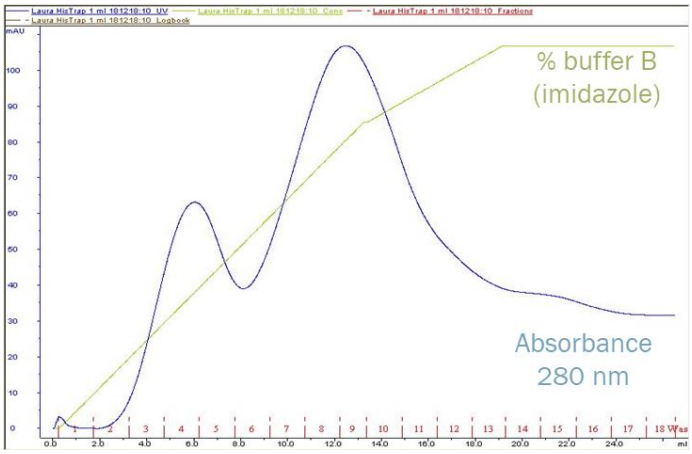

Figure 2.16. FPLC chromatogram of the protein elution process.

Once the protein elution was finished, the system was rinsed with buffer A, MiliQ water and ethanol to remove imidazole and salts residues from the system. Subsequently, fractions obtained during the purification were mixed with SDS Sample Loading Buffer and loaded onto an SDS-PAGE acrylamide gel to verify the presence of MBP_LALF. As appreciable in **Figure 2.17** and accordingly to the absorbance peaks of the chromatogram, fractions from 7^{th} to 11^{th} contain MBP_LALF protein as the

intensity of those gel bands is stronger than others whose protein content is almost negligible.

These fractions where concentrated and buffer exchanged to Buffer C to remove salt and imidazole residuals that could interfere in subsequent assays using a Amicon Ultra 30k Centrifugal filters.

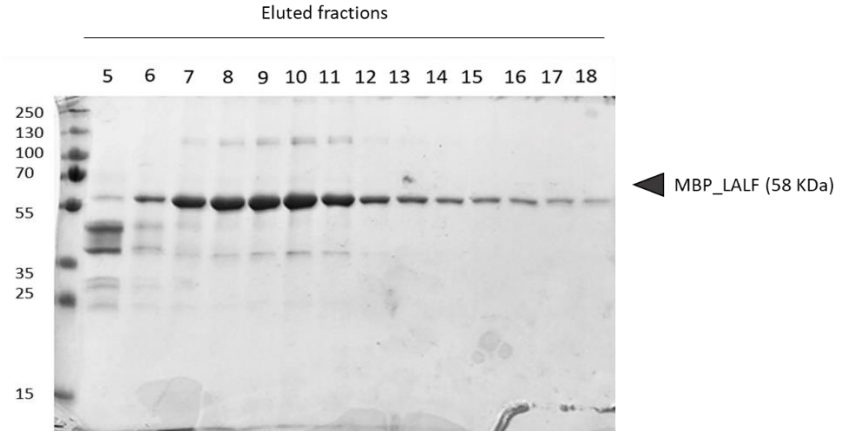

Figure 2.17. Eluted protein fractions where MBP_LALF is mostly present from 7th to 11th.

Finally, it was proceeded to identify whether the observed band corresponded to the theoretical protein by MALDI-TOF mass spectrometry. The majority products corresponded to the expected LALF protein and both the first and the last peptides were identified (bold typed amino acids) in order to confirm the complete fusion protein configuration as depicted in **Figure 2.18** so that the results obtained concluded that the protein was unequivocally MBP_LALF.

```
  1 MSYYHHHHHH DYMIEEGKLV IWINGDKGYN GLAEVGKKFE KDTGIKVTVE
 51 HPDKLEEKFP QVAATGDGPD IIFWAHDRFG GYAQSGLLAE ITPDKAFQDK
101 LYPFTWDAVR YNGKLIAYPI AVEALSLIYN KDLLPNPPKT WEEIPALDKE
151 LKAKGKSALM FNLQEPYFTW PLIAADGGYA FKYENGKYDI KDVGVDNAGA
201 KAGLTFLVDL IKNKHMNADT DYSIAEAAFN KGETAMTING PWAWSNIDTS
251 KVNYGVTVLP TFKGQPSKPF VGVLSAGINA ASPNKELAKE FLENYLLTDE
301 GLEAVNKDKP LGAVALKSYE EELAKDPRIA ATMENAQKGE IMPNIPQMSA
351 FWYAVRTAVI NAASGRQTVD EALKDAQTNS SSNNNNNNNN NNLGDIPTTE
401 NLYFQGMDGI WTQLIFTLVN NLATLWQSGD FQFLDHECHY RIKPTFRRLK
451 WKYKGKFWCP SWTSITGRAT KSSRSGAVEH SVRNFVGQAK SSGLITQRQA
501 EQFISQYNLE HHHHHH
```

Figure 2.18. MBP_LALF protein identification through MALDI-TOFF mass spectrometry.

2.5. Conclusions

With the aim of contributing to an extracorporeal detoxification system, specifically to the LPS sequestration stage, a thorough review of the molecules with activity against LPS has been carried out. Among all the molecules studied, two in particular are highlighted due to their LPS high affinity previously reported: human lipid binding protein (LBP) and LALF protein. Since acquiring any of them for their implementation in the desired capture system is unfeasible due to their high price and due to the ecologically unsustainable practice to obtain the LALF protein from the live bleeding horseshoe crab, it was decided to address their production through the rational method of protein design.

This procedure entails three main stages: molecular cloning, overexpression and protein purification. Several plasmids consisting of genes coding for different proteins (LBP, LALF and LBD, the binding domain of LBP), a tag of 6x His and diverse vectors (pET29c, pET3a from *E.coli* and pPICZ derived from *Pichia pastoris*) were constructed, transformed in DH5α electrocompetent cells and satisfactorily validated via Sanger sequencing. Subsequently, all plasmids were transformed and overexpressed even in different *E.coli* strains but, unfortunately, in the cases where protein was obtained, it was located in the insoluble fraction

of the cells and therefore, it was not viable for further purification and final use. In an attempt to obtain soluble protein, it was proceeded to construct fusion proteins using 3 stability tags for *E.coli* strains: TRX (Thioredoxin), GST (Glutathione S-transferase), MBP (Maltose Binding Protein), and SUMO (Small Ubiquitin-like Modifier).

Two of the fusion constructs showed good expression at low temperature, however the protein was found in the insoluble fraction when analyzed by SDS-PAGE. Thus it was decided to express these constructs in Arctic express, a variant of *E.coli* that allows the expression at low temperatures (18˚C). In this case, the MBP_LALF protein was present in the soluble fraction or supernatant and was therefore loaded into a HisTrap HP histidine-tagged protein purification column. The target protein was eluted through FPLC with an imidazole gradient (20 mM-500mM). Fractions were analyzed and protein was identified between 7^{th} to 11^{th} fractionation steps which, then, were washed with buffer C and concentrated, and the final protein concentration was determined by spectrophotometry.

Finally, the identity of the protein was verified by MALDI-TOF, as the majority of the peptides identified corresponded to the expected LALF protein and both the first and the last peptides were identified so that, the results obtained concluded that the protein was unequivocally MBP_LALF.

2.6. References

[1] B. Szermer-Olearnik, J. Boratyński, Removal of endotoxins from bacteriophage preparations by extraction with organic solvents, PLoS One. 10 (2015) 1–10. https://doi.org/10.1371/journal.pone.0122672.

[2] J.D. Van Belleghem, M. Merabishvili, B. Vergauwen, R. Lavigne, M. Vaneechoutte, A comparative study of different strategies for removal of endotoxins from bacteriophage preparations, J. Microbiol. Methods. 132 (2017) 153–159. https://doi.org/10.1016/j.mimet.2016.11.020.

[3] U.B. Bommer J , Becker KP , Urbaschek R , Ritz E, No evidence for endotoxin transfer across high flux polysulfone membranes, Clin. Nephrol. 27 (1987) 278–282. https://doi.org/10.1111/lam.12667.

[4] G. Lonnemann, T.C. Behme, B. Lenzner, J. Floege, M. Schulze, C.K. Colton, K.M. Koch, S. Shaldon, Permeability of dialyzer membranes to TNFα-inducing substances derived from water bacteria, Kidney Int. 42 (1992) 61–68. https://doi.org/10.1038/ki.1992.261.

[5] Z. Zhou, K.A. White, A. Polissi, C. Georgopoulos, C.R.H. Raetz, Function of Escherichia coli MsbA, an essential ABC family transporter, in lipid A and phospholipid biosynthesis, J. Biol. Chem. 273 (1998) 12466–12475. https://doi.org/10.1074/jbc.273.20.12466.

[6] S. Stumpe, R. Schmid, D.L. Stephens, G. Georgiou, E.P. Bakker, Identification of OmpT as the Protease That Hydrolyzes the\rAntimicrobial Peptide Protamine before It Enters, J. Bacteriol. 180 (1998) 4002–4006. https://doi.org/10.1007/s00520-014-2245-9.

[7] L. Vandeputte-Rutten, R.A. Kramer, J. Kroon, N. Dekker, M.R. Egmond, P. Gros, Crystal structure of the outer membrane protease Ompt from Escherichia coli suggests a novel catalytic site, EMBO J. 20 (2001) 5033–5039. https://doi.org/10.1093/emboj/20.18.5033.

[8] A. Hoess, S. Watson1, G.R. Siber2, R. Liddington4, E. Schulz, Crystal structure of an endotoxin-neutralizing protein fromothe horseshoe crab, Limulus anti-LPS factor, at 1.5 A resolution Munchen, Germany 4Corresponding author Communicated by G, EMBO J. 12 (1993) 3351–3356. https://www.ncbi.nlm.nih.gov/pmc/articles/PMC413608/pdf/emboj00081-0013.pdf.

[9] M. Kloczewiak, K.M. Black, P. Loiselle, J. Cavaillon, H.S. Warren, N. Wainwright, Synthetic Peptides that Mimic the Binding Site of Horseshoe Crab Factor Antilipopolysaccharide, Culture. 170 (2010) 1490–1497. doi: 10.1093/infdis/170.6.1490.

[10] K. Brandenburg, G. Jürgens, J. Andrä, B. Lindner, M.H.J. Koch, A. Blume, P. Garidel, Biophysical characterization of the interaction of high-density lipoprotein (HDL) with endotoxins, Eur. J. Biochem. 269 (2002) 5972–5981. https://doi.org/10.1046/j.1432-1033.2002.03333.x.

[11] B. Yu, S.D. Wright, Catalytic Properties of Lipopolysaccharide (LPS) Binding Protein, J. Biol. Chem. 271 (2002) 4100–4105. https://doi.org/10.1074/jbc.271.8.4100.

[12] S. Tanaka, D. Diallo, S. Delbosc, C. Genève, N. Zappella, J. Yong-Sang, J. Patche, A. Harrois, S. Hamada, E. Denamur, P. Montravers, J. Duranteau, O. Meilhac, High-density lipoprotein (HDL) particle size and concentration changes in septic shock patients, Ann. Intensive Care. 9 (2019) 1–9. https://doi.org/10.1186/s13613-019-0541-8.

[13] W. Kaca, R.I. Roth, J. Levin, Hemoglobin, a newly recognized lipopolysaccharide (LPS)-binding protein that enhances LPS biological activity, J. Biol. Chem. 269 (1994) 25078–25084. https://doi.org/10.1016/S0021-9258(17)31501-6.

[14] G. Jürgens, M. Müller, M.H.J. Koch, K. Brandenburg, Interaction of hemoglobin with enterobacterial lipopolysaccharide and lipid A, Eur. J. Biochem. 268 (2003) 4233–4242. https://doi.org/10.1046/j.1432-1327.2001.02338.x.

[15] C. Liepke, S. Baxmann, C. Heine, N. Breithaupt, L. Ständker, W.G. Forssmann, Human hemoglobin-derived peptides exhibit antimicrobial activity: A class of host defense peptides, J. Chromatogr. B Anal. Technol. Biomed. Life Sci. 791 (2003) 345–356. https://doi.org/10.1016/S1570-0232(03)00245-9.

[16] P. Berkel, M. Geerts, H. Veen, M. Mericskay, H. Boer, J. Nuijens, N-terminal stretch Arg 2 , Arg 3 , Arg 4 and Arg 5 of human lactoferrin is essential for binding to heparin, bacterial lipopolysaccharide, human lysozyme and DNA, Biochem. J. 328 (1997) 145–151. doi: 10.1042/bj3280145.

[17] B.E. Britigan, T.S. Lewis, M. Waldschmidt, M.L. McCormick, A.M. Krieg, Lactoferrin Binds CpG-Containing Oligonucleotides and Inhibits Their Immunostimulatory Effects on Human B Cells, J. Immunol. 167 (2014) 2921–2928. https://doi.org/10.4049/jimmunol.167.5.2921.

[18] M. Gough, R.E.W. Hancock, N.M. Kelly, Antiendotoxin activity of cationic peptide antimicrobial agents, Infect. Immun. 64 (1996) 4922–4927. doi: 10.1128/IAI.64.12.4922-4927.1996.

[19] O. Levy, G. Canny, C.N. Serhan, S.P. Colgan, Expression of BPI (bactericidal/permeability-increasing protein) in human mucosal epithelia., Biochem. Soc. Trans. 31 (2003) 795–800. https://doi.org/10.1042/.

[20] R.G. Little, D.N. Kelner, E. Lim, D.J. Burke, P.J. Conlon, Functional domains of recombinant bactericidal/permeability increasing protein (rBPI 23), J. Biol. Chem. 269 (1994) 1865–1872. https://doi.org/10.1016/S0021-9258(17)42107-7.

[21] E. Hailman, H. Lichenstein, M. Wurfel, D. Miller, D. Johnson, M. Kelley, L. Busse, M. Zukowski, S. Wright, Lipopolysaccharide (LPS)-binding protein accelerates the binding of LPS to CD14., J. Exp. Med. 179 (1994) 269–77. http://www.pubmedcentral.nih.gov/articlerender.fcgi?artid=2191344&tool=pmcentrez&rendertype=abstract%5Cnhttp://jem.rupress.org/content/179/1/269.abstract.

[22] T.N. Kirkland, F. Finley, D. Leturcq, A. Moriarty, J.D. Lee, R.J. Ulevitch, P.S. Tobias, Analysis of lipopolysaccharide binding by CD14, J. Biol. Chem. 268 (1993) 24818–24823. https://doi.org/10.1016/S0021-9258(19)74538-4..

[23] D. Heumann, R. Lauener, B. Ryffel, The dual role of LBP and CD14 in response to Gram-negative bacteria or Gram-negative compounds, J. Endotoxin Res. 9 (2003) 381–384. https://doi.org/10.1179/096805103225003312.

[24] G. Ramadori, K.-H.M. zum Buschenfelde, T. P.S, M. J.C, U. R.J, Biosynthesis of Lipopolysaccharide-Binding protein in rabbit hepatocytes, Pathobiology. 58 (1990) 89–94. DOI: 10.1159/000163569..

[25] M. Müller, O. Scheel, B. Lindner, T. Gutsmann, U. Seydel, The role of membrane-bound LBP, endotoxin aggregates, and the MaxiK channel in LPS-induced cell activation, J. Endotoxin Res. 9 (2003) 181–186. https://doi.org/10.1179/096805103125001595.

[26] J.K. Eckert, Y.J. Kim, J.I. Kim, K. Gürtler, D.Y. Oh, S. Sur, L. Lundvall, L. Hamann, A. vanderPloeg, P. Pickkers, E. Giamarellos-Bourboulis, A. V. Kubarenko, A.N. Weber, M. Kabesch, O. Kumpf, H.J. An, J.O. Lee, R.R. Schumann, The crystal structure of lipopolysaccharide binding protein reveals the location of a frequent mutation that impairs innate immunity, Immunity. 39 (2013) 647–660. https://doi.org/10.1016/j.immuni.2013.09.005.

[27] D. Artner, A. Oblak, S. Ittig, J.A. Garate, S. Horvat, C. Arrieumerlou, A. Hofinger, C. Oostenbrink, R. Jerala, P. Kosma, A. Zamyatina, Conformationally constrained lipid a mimetics for exploration of structural basis of TLR4/MD-2 activation by lipopolysaccharide, ACS Chem. Biol. 8 (2013) 2423–2432. https://doi.org/10.1021/cb4003199.

[28] J.A. Garate, J. Stöckl, M. Del Carmen Fernández-Alonso, D. Artner, M. Haegman, C. Oostenbrink, J. Jiménez-Barbero, R. Beyaert, H. Heine, P. Kosma, A. Zamyatina, Anti-endotoxic activity and structural basis for human MD-2·TLR4 antagonism of tetraacylated lipid A mimetics based on ßGlcN(1-1)αGlcN scaffold, Innate Immun. 21 (2015) 490–503.

https://doi.org/10.1177/1753425914550426.

[29] N. Inohara, G. Nuez, ML - A conserved domain involved in innate immunity and lipid metabolism, Trends Biochem. Sci. 27 (2002) 219–221. https://doi.org/10.1016/S0968-0004(02)02084-4.

[30] F. Cochet, F.A. Facchini, L. Zaffaroni, J.M. Billod, H. Coelho, A. Holgado, H. Braun, R. Beyaert, R. Jerala, J. Jimenez-Barbero, S. Martin-Santamaria, F. Peri, Novel carboxylate-based glycolipids: TLR4 antagonism, MD-2 binding and self-assembly properties, Sci. Rep. 9 (2019) 1–13. https://doi.org/10.1038/s41598-018-37421-w.

[31] J. Gao, J.-X. Wang, X.-W. Wang, MD-2 Homologue Recognizes the White Spot Syndrome Virus Lipid Component and Induces Antiviral Molecule Expression in Shrimp, J. Immunol. 203 (2019) 1131–1141. https://doi.org/10.4049/jimmunol.1900268.

[32] G. Alpert, G. Baldwin, C. Thompson, N. Wainwright, T.J. Novitsky, Z. Gillis, J. Parsonnet, G.R. Fleisher, G.R. Siber, Limulus Antilipopolysaccharide Factor Protects Rabbits from Meningococcal Endotoxin Shock, J. Infect. Dis. 165 (1992) 494–500. https://doi.org/10.1093/infdis/165.3.494.

[33] J. Aketagawa, T. Miyata, S. Ohtsubo, T. Nakamura, T. Morita, H. Hayashida, T. Miyata, S. Iwanaga, T. Takao, Y. Shimonishi, Primary structure of limulus anticoagulant anti-lipopolysaccharide factor, J. Biol. Chem. 261 (1986) 7357–7365. https://doi.org/10.1016/S0021-9258(17)38399-0.

[34] R.D. Rosa, A. Vergnes, J. de Lorgeril, P. Goncalves, L.M. Perazzolo, L. Sauné, B. Romestand, J. Fievet, Y. Gueguen, E. Bachère, D. Destoumieux-Garzón, Functional Divergence in Shrimp Anti-Lipopolysaccharide Factors (ALFs): From Recognition of Cell Wall Components to Antimicrobial Activity, PLoS One. 8 (2013) 17–19. https://doi.org/10.1371/journal.pone.0067937.

[35] J. Krisfalusi-Gannon, W. Ali, K. Dellinger, L. Robertson, T.E. Brady, M.K.M. Goddard, R. Tinker-Kulberg, C.L. Kepley, A.L. Dellinger, The role of horseshoe crabs in the biomedical industry and recent trends impacting species sustainability, Front. Mar. Sci. 5 (2018) 1–

13. https://doi.org/10.3389/fmars.2018.00185.

[36] P.E. Lobban, A.D. Kaiser, Enzymatic end-to-end joining of DNA molecules, J. Mol. Biol. 78 (1973) 453–471. https://doi.org/10.1016/0022-2836(73)90468-3.

[37] W.S. Klug, M.R. Cummings, C.A. Spenser, Concepts of Genetics, 8th ed., Pearson Education, Inc, New Jersey, 2006. https://doi.org/10.1136/mp.48.4.m220-b.

[38] S. Khan, M.W. Ullah, R. Siddique, G. Nabi, S. Manan, M. Yousaf, H. Hou, Role of recombinant DNA technology to improve life, Int. J. Genomics. 2016 (2016). https://doi.org/10.1155/2016/2405954.

[39] R.C. Clowes, Molecular structure of bacterial plasmids., Bacteriol. Rev. 36 (1972) 361–405. https://doi.org/10.1128/br.36.3.361-405.1972.

[40] L.K. Nyberg, S. Quaderi, G. Emilsson, N. Karami, E. Lagerstedt, V. Müller, C. Noble, S. Hammarberg, A.N. Nilsson, F. Sjöberg, J. Fritzsche, E. Kristiansson, L. Sandegren, T. Ambjörnsson, F. Westerlund, Rapid identification of intact bacterial resistance plasmids via optical mapping of single DNA molecules, Sci. Rep. 6 (2016) 1–11. https://doi.org/10.1038/srep30410.

[41] J.C. Mell, R.J. Redfield, Natural competence and the evolution of DNA uptake specificity, J. Bacteriol. 196 (2014) 1471–1483. https://doi.org/10.1128/JB.01293-13.

[42] S.J. Karcher, Getting DNA into a Cell: A Survey of Transformation Methods, Am. Biol. Teach. 56 (1994) 197–197. https://doi.org/10.2307/4449794.

[43] M. Kostylev, A.E. Otwell, R.E. Richardson, Y. Suzuki, Cloning should be simple: Escherichia coli DH5α-mediated assembly of multiple DNA fragments with short end homologies, PLoS One. 10 (2015) 1–15. https://doi.org/10.1371/journal.pone.0137466.

[44] G.L. Rosano, E.A. Ceccarelli, Recombinant protein expression in Escherichia coli: Advances and challenges, Front. Microbiol. 5 (2014) 1–17. https://doi.org/10.3389/fmicb.2014.00172.

[45] S. Gavanji, M. Doostmohammadi, An Introduction to Recombinant Proteins-A Review, SMU Med. J. 1 (2014).

[46] J. Puetz, F.M. Wurm, Recombinant Proteins for Industrial versus Pharmaceutical Purposes: A Review of Process and Pricing, Processes. 7 (2019) 476. https://doi.org/10.3390/pr7080476.

[47] T. Maloney, R. Phelan, N. Simmons, Saving the horseshoe crab: A synthetic alternative to horseshoe crab blood for endotoxin detection, PLoS Biol. 16 (2018) 1–10. https://doi.org/10.1371/journal.pbio.2006607.

[48] Y. Yang, H. Boze, P. Chemardin, A. Padilla, G. Moulin, A. Tassanakajon, M. Pugnière, F. Roquet, D. Destoumieux-Garzón, Y. Gueguen, E. Bachère, A. Aumelas, NMR structure of rALF-Pm3, an anti-lipopolysaccharide factor from shrimp: Model of the possible lipid A-binding site, Biopolymers. 91 (2009) 207–220. https://doi.org/10.1002/bip.21119.

[49] J. Kohara, N. Tsuneyoshi, J.F. Gauchat, M. Kimoto, K. Fukudome, Preparation and characterization of truncated human lipopolysaccharide-binding protein in Escherichia coli, Protein Expr. Purif. 49 (2006) 276–283. https://doi.org/10.1016/j.pep.2006.05.015.

[50] D.G. Gibson, L. Young, R.Y. Chuang, J.C. Venter, C.A. Hutchison, H.O. Smith, Enzymatic assembly of DNA molecules up to several hundred kilobases, Nat. Methods. 6 (2009) 343–345. https://doi.org/10.1038/nmeth.1318.

[51] W. J. Dower, J. F.Miller, C. W.Ragsdale, High efficiency transformation of E.coli by high voltage electroporation, Nucleic Acids Res. 16 (1988) 6127–6145. doi: 10.1093/nar/16.13.6127.

[52] H. Yang, S. Li, F. Li, X. Lv, J. Xiang, Recombinant expression and functional analysis of an isoform of anti-lipopolysaccharide factors (FcALF5) from Chinese shrimp Fenneropenaeus chinensis, Dev. Comp. Immunol. (2015). https://doi.org/10.1016/j.dci.2015.06.015.

[53] M. Strocchi, M. Ferrer, K.N. Timmis, P.N. Golyshin, Low temperature-induced systems failure in Escherichia coli: Insights

from rescue by cold-adapted chaperones, Proteomics. 6 (2006) 193–206. https://doi.org/10.1002/pmic.200500031.

[54] M. Ferrer, T. N. Cherikova, M. M. Yakimov, P. N. Golyshin, K. N. Timmis, Chaperonins govern growth of Escherichia coli at low temperatures, Nat. Biotechnol. 21 (2003) 1266–1267. doi: 10.1038/nbt1103-1266.

[55] GE Healthcare, HisTrap affinity columns intructions, 2009. http://webhome.auburn.edu/~duinedu/manuals/HisTrapHP.pdf.

3

Experimental LPS capture

Abstract

The purpose of this chapter is to experimentally determine the binding strength of the synthesized LALF protein to LPS. Initially, a thorough review of the literature concerning affinity parameters, kinetics and the employed measuring techniques for the main ligand-LPS interactions was carried out. Besides, LALF affinity was analyzed by supporting it on agarose beads selected as particle model system and the variables affecting the beads-LALF-LPS complex formation as binding and capture temperature, the optimum bead:protein and protein:LPS ratios, were experimentally studied. In addition, magnetic nanogels were synthesized and characterized as a potential alternative to be implemented on the biofluids cleansing system; this information is included in the **Appendix G** to this chapter. The methodology and results here reported constitute the information needed to advance the knowledge for the correct design of LPS separation devices.

3.1. Introduction

Affinity of the ligand-LPS complex formation is a key point to develop detection and control protocols. Although multiple molecules have reported activity against endotoxins, only a few potential ligands have been deeply studied to determine their binding capacity to LPS.

The characteristic parameters of the main ligand-LPS binding complexes have been quantitatively described through the use of techniques such as surface plasmon resonance (SPR), isothermal titration calorimetry (ITC) and fluorescence resonance energy transfer (FRET) (**see Appendix E for techniques explanation**) and have been thoroughly reviewed (**see Appendix F**). Briefly, **Table 3.1** summarizes the state of the art referred to the association constants of the main complexes which primarily imply the proteins involved in the human immune response and polymyxin (PMB), a cyclic amphipathic peptide antibiotic. Association constants are defined as $K_A=k_1/k_{-1}$ and the values ranged from 10^4 M^{-1} to 10^8 M^{-1}, for the analyzed groups of LPS ligand molecules.

Table 3.1. Association constants of the LPS-biomolecule interactions.

	LPS-receptor molecule	**K_A (M^{-1})**	**Ref**
Proteins extracted from G(+) bacteria	LPS-PMB	$3\ 10^5$ -$2.1\ 10^6$	[1,2]
Human proteins involved in the immune system response	LPS-CD14	$<10^6$ - $5.00\ 10^8$	[3–6]
	LPS-TLR4	$7.1\ 10^4$ - $3.30\ 10^8$	[6,7]
	LPS-MD-2	$4.29\ 10^5$ – $1.54\ 10^7$	[6,8]
	LPS-LBP	$1.40\ 10^8$ - $2.88\ 10^8$	[3,5]

Most of the interactions studied report association constants K_A higher than 10^7 M^{-1} reflecting a very favorable affinity towards LPS binding. With

regard to the types of molecules, first, PMB, that is a polypeptide bactericidal antibiotic, has been widely studied with values of the affinity constant K_A in the range of 3 10^5 – 2.1 10^6 M^{-1}. The highest value of the association constant corresponds to polymyxin nonapeptide (PMBN) which exhibited the strongest binding capacity to LPS [1,2]. In overall terms, PMB exhibits fast kinetics and good affinity to lipopolysaccharides but, despite its nephrotoxic and neurotoxic properties when released in the bloodstream, its use is limited to extracorporeal cartridges Toraymyxin PMX-F) [9–11] thus, the design of less toxic analogues is a challenge in defining more effective LPS binding molecules.

The second type of molecules collected in **Table 3.1** refers to biomolecules related to the human cascade mechanism implicated in LPS recognition. The lipopolysaccharides receptor CD14, whose interaction to LPS , yielded association constant values ranging from 1 10^6 M^{-1} to 5 10^8 M^{-1} obtained by Viriyakosol et al. [4] who developed different CD14 mutants. Both, the lowest and the highest association values obtained for this interaction correspond to DPRQY and DDED/PQPD double delection respectively.

It is worth noting that, the same authors also studied the binding capacity of LPS- CD14 wild type, whose K_A was 1.35 10^7 M^{-1}, two orders of magnitude higher than the one previously reported by Shin et al. [6], a fact that may be explained because of the peptide synthesis carried out [6] entailed CD14 fusion proteins which could imply steric impediments in the LPS binding.

TLR4, is a transmembrane protein responsible of LPS recognition whose interaction to LPS has been quantitatively determined in the range of K_A= 7.1 10^4 - 3.30 10^8 M^{-1}. The remarkable difference in the association values lies in the studied interaction because, while LPS-TRL4 interaction reported the lowest K_A value, when MD-2 is added to the complex formation, its binding activity is enhanced. This ternary complex binds with higher affinity than LPS-MD-2, suggesting that TLR4 could directly

bind to LPS or even it could mediate in the interaction between LPS and MD-2 [7].

MD-2, an adaptive protein that plays an important role in the inflammatory response, reported association values for the LPS-MD-2 interaction that varied from 4.29 10^5 M^{-1} to 1.54 10^7 M^{-1} [8]. Once again, the differences between the two studies and the quantified values of K_A for the same interaction of LPS-MD-2 could rely on the peptide synthesis stage as Shin et al. [6] developed a MD-2 fusion protein.

Finally, LBP, is a soluble acute-phase protein that binds to LPS and has shown the highest LPS binding capacity among all the studied molecules. In fact, three different quantification methods were employed to quantify the activity of the LPS-LBP complex and all reported K_A values ranging from 1.40 10^8 M^{-1} to 2.88 10^8 M^{-1} , which highlights the importance of the LBP presence in the LPS recognition dynamics [3,5].

Affinity constant values could be well considered as the baseline to make a step forward in the development of new LPS detection and/or sequestration techniques but it also highlights the necessity of further research to expand the studies on the affinity and selectivity of already known ligand molecules as well as synthesizing new antimicrobial peptides capable to interact to LPS with affinity constant values sufficiently high to bind and remove LPS from different environments.

However, the interaction kinetics needed for the use of these promising peptides in advanced blood-cleansing devices is still lacking. In this regard, we describe a new methodology to quantitatively determine the binding strength of the previously obtained LALF protein to LPS. For this analysis, LALF was supported on agarose beads employed as a particle model system and afterwards, the functionalized beads were contacted to LPS solutions to analyze the interaction between the lipid A and the binding molecule.

Once the activity of the protein has been determined, the next step consists on the development of a continuous blood-cleansing device for

LPS removal which entails two main stages taking part in the whole process, i) entrapment of LPS in conveniently functionalized particles and, ii) removal of the loaded beads from the biofluid [12–20].

For the removal stage to be successful, a solid and magnetic substrate is required. In this sense, and as a potential alternative to agarose particles, magnetic nanogels (MNGs) were synthesized and characterized to contribute to the advancement of these LPS separation processes. MNGs are three-dimensional materials with dimensions in the nanoscale; they are formed by cross-linked, swellable polymeric networks and embedded magnetic nanoparticles (MNPs) that have a high water-holding capacity, without dissolving in the aqueous medium. In addition, they have shown high biocompatibility and biodegradation capacity that make them nontoxic carriers with a great potential for biomedical applications [21–24].

Despite the existent theoretical and experimental studies have clarified the binding mechanism of different ligands-LPS complexes, our newly approach for the experimental determination of the kinetic parameters opens the way for further improvement and advances on the state-of-the art of LPS separation processes, thus, playing an important role in the design and optimization of treatment devices.

3.2. Materials

Escherichia Coli O111:B4 with FITC conjugate was purchased from Merck. HisTrap HP histidine-tagged protein purification columns (5 mL) were purchased from GE Healthcare as well as the agarose beads (Ni Sepharose® 6Fast Flow). Employed lysozyme was obtained from sigma (Lysozyme from chicken egg White, Sigma) as well as Trizma base, glycine, Tris HCl, NaCl, $FeCl_3.6H_2O$, $FeCl_2.4H_2O$, NH_4OH, HNO_3, EtOH, 3-(methacryloyloxy) propyl trimethoxysilane (MEMO), diethylenglycol methacrylate (DEGMA), oligoethylenglycol methacrylate (OEGMA), 2-Hydroxyethyl metacrylate (HEMA), dodecyl sulfate (SDS), ammonium

persulfate (APS), N,N,N',N'-Tetramethylethylenediamine (TEMED), N,N-Dimethylformamide, Nα,Nα-Bis(carboxymethyl)-L-lysine hydrate, N-Ethyl-N'-(3-dimethylaminopropyl)carbodiimide (EDC), 1-Hydroxy-2,5-pyrrolidinedione, (NHS), NiCl. MNPs and MNGs were synthesized using an Omni-Ruptor 400 or Bandelin UW 2070 sonicator.

LB medium and LB Agar medium were purchased by Scharlab, S.L, SDS 20% from Fischer Scientific and kanamycin and gentamicin from Apollo Scientific, Ltd. Protein concentration measurements were performed using a Thermo Scientific™ NanoDrop 2000c and the LPS-FITC supernatant measurements were carried out with the Thermo Scientific Multiskan® Spectrum microplate spectrophotometer. MiliQ® water was employed for the required solutions.

3.3. Experimental procedure

This experimental procedure for LPS sequestration consisted of two different steps i) particles functionalization with the synthesized LALF protein and ii) LPS binding.

Agarose beads were employed as model particle system for functionalization and subsequent proof of concept for LPS uptake. As an alternative to be implemented in the micro-magnetophoretic system, magnetic nanogels (MNGs) have been synthesized and characterized as described in **Appendix G** as an initial approach in the search for a magnetic and biocompatible substrate.

3.3.1. Agarose beads functionalization

Initially, as agarose beads are suspended in ethanol, they were centrifuged to remove the alcohol, rinsed for 3 times and re-suspended in 50 mM Tris-HCl and 150 mM NaCl buffer. Afterwards, the beads were contacted to the LALF protein in order to achieve the particles coverage

due to the ability of the histidine tail to coordinate metals such as the nickel present on the surface of the selected beads.

The procedure started measuring the initial concentration of the protein (no beads presence) and then, it was contacted to the beads under gentle shaking in order to study the change of the concentration with time by Ultraviolet Spectrophotometry (280 nm) measurements of the supernatant (protein size 57.9 kDa and molar extinction coefficient; ε=104.5 mol L^{-1}). We assume that the difference between the initial and the last measured concentration of the protein corresponds to the amount of protein on the beads surface.

Besides, after every bead:protein contact, once the equilibrium was achieved and the beads capture ability was saturated, the unbound protein in the sample was removed as particles were washed 3 times and resuspended in the same buffer as before. Ultraviolet Spectrophotometry measurements were performed for the washing solution to verify the protein absence and to confirm its presence on the beads surface. The detected protein concentration in the washing buffer was around 0.1 and 0.2 mg/mL for every bead:protein contact. To proceed with a rigorous study of this step, firstly, it was analyzed the protein uptake working with different bead:protein ratios as described in **Table 3.2**.

Table 3.2. Experimental design to study the bead-protein ratio influence on the protein uptake.

Bead-protein ratio (v)	µL Beads	Time (min)	Objective
0.5:1	100	1500	Effect of the beads-protein ratio on the protein uptake
1:1	200	1500	
2:1	400	1500	
5:1	1000	1500	
10:1	2000	1500	

Then, the influence of the temperature on the beads-protein binding was also analyzed as described in **Table 3.3**.

Table 3.3.Experimental design to determine the Influence of the temperature on the bead-protein contact stage

Bead-protein ratio (v)	Temperature (˚C)	Time (min)	Objective
2:1	4	1500	Study the temperature effect on the bead-protein contact
2:1	20	1500	
2:1	37	1500	

3.3.2. LPS capture assay

The washed and functionalized beads were contacted to a FITC-LPS solution to proceed to the endotoxin sequestration stage. The concentration of the FITC-LPS stock solution was 1 mg/mL but, after contacting the same volume of LPS and the functionalized beads solution, the initial concentration of LPS was 500 µg/mL. After a certain time, the functionalized beads-LPS solution was centrifuged and the supernatant was placed in a 96 well plate. As LPS contained fluorescent conjugates, variations of endotoxin supernatant concentration were analyzed by fluorometric techniques at constant excitation/emission wavelengths of 495 nm and 525 nm respectively. Then, the supernatant was contacted again with the protein covered beads and the process was repeated until the protein-lipid A system was saturated to determine the LPS percentage able to be trapped by the covered beads. Moreover, all these experiments were contrasted to a negative control consisting of the same experimental conditions but in absence of the protein, to discard unspecific unions between the beads and the lipopolysaccharides. In a first approach, the influence of the temperature on the LPS capture was studied as detailed in **Table 3.4**.

Table 3.4.Experimental design to study the influence of the temperature on the LPS sequestration stage.

[LPS] (mg/mL)	Bead:protein ratio (v)	Temperature (˚C)	Time (min)	Objective
1	2:1	4	120	Study the temperature effect on LPS sequestration stage
1	2:1	20	120	
1	2:1	37	120	

Once the temperature effect was examined during the LPS sequestration stage, experiments with different protein-LPS ratios were carried out to determine the best ratio in order to achieve the desired removal as depicted in **Table 3.5**.

Table 3.5.Experimental design to evaluate the optimum protein-LPS ratio.

[LPS] (mg/mL)	LPS-protein ratio (ϕ)	Temperature (˚C)	Time (min)	Objective
1	35	20	120	Effect of the LPS-protein ratio on the LPS removal
1	50	20	120	
1	100	20	120	
1	400	20	120	

3.4. Results

3.4.1. Analysis of the protein support on agarose beads

Once the protein was synthesized, the next step was to analyze if the histidine tail coordinated adequately to the nickel present on the agarose beads surface and to determine the optimum bead/protein ratio for the contact. The studied bead: protein volume ratios were 0.5:1, 1:1, 2:1, 5:1 and 10:1 and the experiments proceeded by triplicate with an error, calculated as standard deviation, between 0.034 and 0.002.

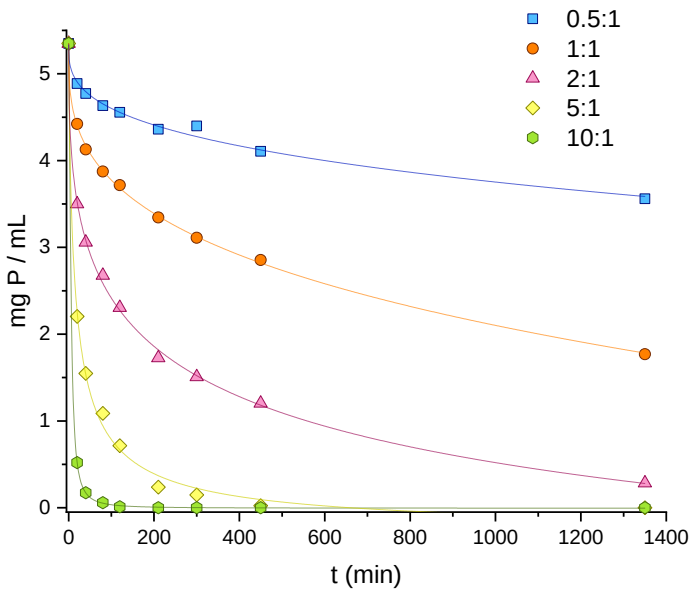

Figure 3.1. Supernatant protein concentration during the functionalization stage.

The initial protein concentration contacted to beads was 5.35 mg/mL and, in **Figure 3.1**, it can be appreciated the decrease on the protein concentration in the supernatant with time as it was captured on the beads for the different tested ratios. For the smallest ratio (0.5:1), the protein adsorption was 34% whereas at 1:1 ratio, the uptake increased to

67%, approximately twice the previous value, but not enough int terms of protein use. On the contrary, the highest bead-protein ratios achieved 94.6% (2:1) and 100% (5:1, 10:1) protein capture so that, the protein concentration in the equilibrium was similar for the three cases.

In order to select the most convenient experimental condition, it was important to analyze the functionalization degree of the beads by calculating the mg of protein per mg of beads; **Figure 3.2** depicts the kinetics of protein uptake on the agarose beads.

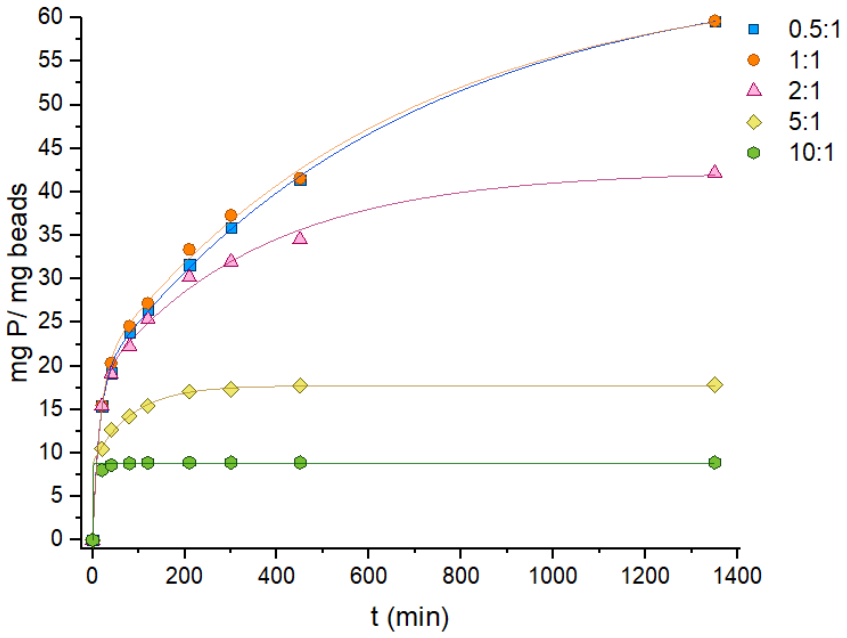

Figure 3.2. Protein uptake (mg) per mg of beads during the bead-protein stage.

The higher beads concentration in the sample (5:1 and 10:1 ratios), the less functionalization degree, 17.8 mg P/ mg beads and 8.9 mg P/ mg beads respectively. On the contrary, the lowest ratio achieved the same concentration of protein per mg of beads, 59.6 mg protein/mg beads corresponding to 0.5:1 and 1:1 ratio. In addition, the 2:1 ratio revealed a value of 42 mg of protein captured per mg of beads; thus, this ratio was

selected for further experiments as it required an adequate number of beads covered by the protein with a reasonable protein uptake time, contributing to a cost-effective stage and to an improved utilization of the protein.

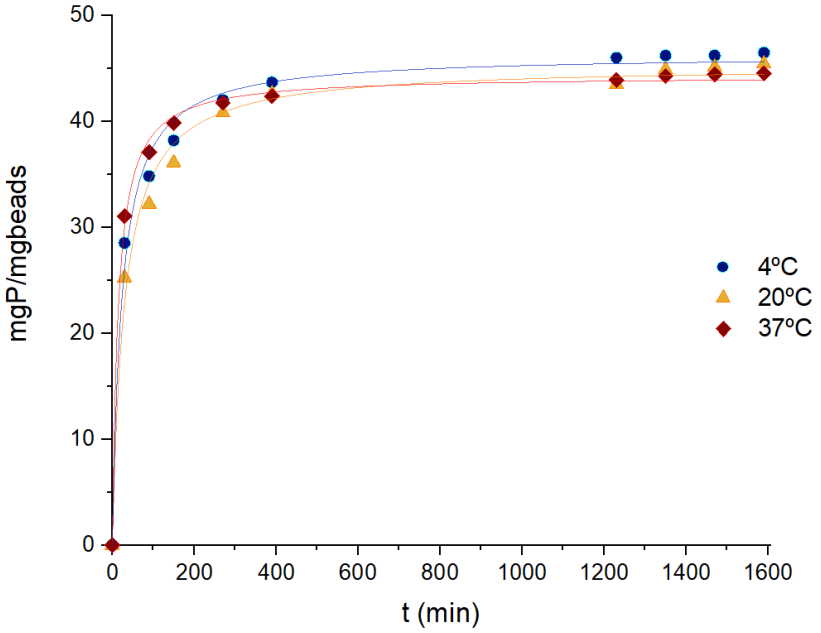

Figure 3.3. Influence of the temperature on the bead:protein interaction.

Protein expression was performed at 18˚C. Thus, the influence of the temperature on the beads capture ability was studied. Bead-protein contacts were carried out by triplicate and the error between the different runs, calculated as standard deviation, ranged from 0.001 to 0.014. **Figure 3.3** gathers the behavior of the protein adsorption kinetics expressed in terms of mg of protein adsorbed per mg of beads with time at three different temperatures, 37˚C, 20˚C and 4˚C.

Consequently, temperature for the bead-protein contact did not reveal influence in the range from 4˚C to 37˚C; 50% of the equilibrium was achieved at 30 minutes, 75% at 90 minutes and complete protein uptake

was obtained after contact for 3 hours for the three scenarios. In conclusion, the synthesized LALF protein was stable and functional in the range between 4˚C and 37˚C, where the bead:protein contact did not show substantial differences on the protein uptake and denaturalization did not occur.

LALF-LPS Interaction isotherms. Influence of temperature and bead: protein ratio

In order to study the ability of the functionalized beads to capture LPS, a solution of lipopolysaccharides of 1 mg/mL was prepared, and as previously performed with the solid-liquid contact, the influence of temperature on the LPS capture isotherms was studied.

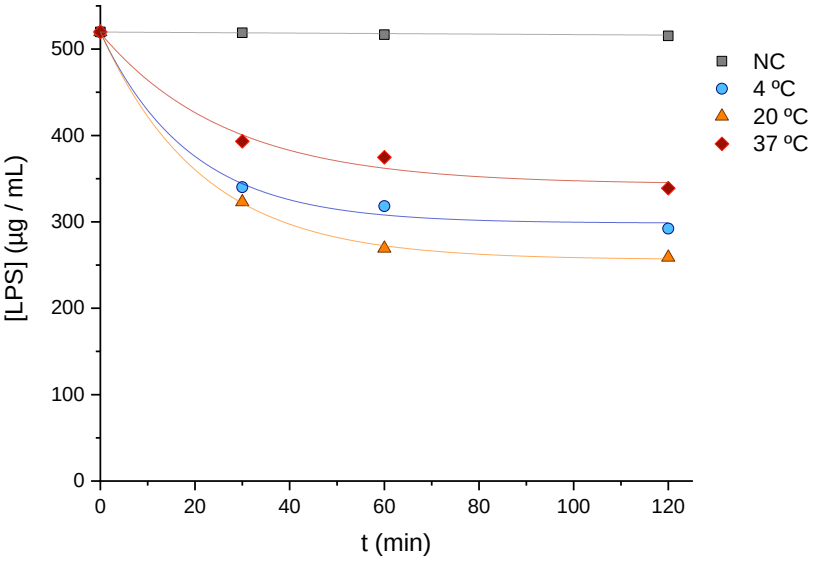

Figure 3.4. Influence of temperature on the LPS sequestration kinetics.

The contact between the functionalized beads and the LPS solution was carried out under three different temperatures: 4˚C, 20˚C and 37˚C. **Figure 3.4** shows the influence of temperature on the LPS sequestration at the explained temperatures as well as the behavior of the negative

control (no protein presence in the contact). Initially, 6.8 mg of protein were contacted to the beads and, as a result of contacting those beads to the 1 mg/mL LPS solution, the protein: LPS resultant ratio was 61. Although this ratio may seem to be too high, as a reference, LPS concentration in septic patients is around 300 pg/mL while the lipid binding protein (LBP) presence is 30 µg/mL [25], a significative ratio that is even higher than the tried for the first protein: LPS contact. LPS percentage removed at 4˚C was 43%, at 20˚C was 50.2% and at 37˚C it was 35%. Within these data the most favorable scenario for the LPS removal corresponded to 20˚C.

Protein:LPS optimum ratio

As the LPS captured in previous experiments was considered too low, and the protein concentration in a septic patient is 10000 times higher than that of LPS [25], the protein: LPS ratio (ϕ) was increased to promote LPS removals closer to 100% and was calculated with the expression below:

$$C_{LPS} \cdot V_{LPS} \cdot \phi = C_{Protein} \cdot V_{Protein}$$

where C_{LPS} corresponds to the LPS concentration (1 mg/mL for all the experiments) and the LPS volume (V_{LPS}) was set on 75 µL. Protein concentration ($C_{Protein}$) was already known from the binding stage and the functionalized beads were always resuspended in 75 µL.
Based on that, several runs were carried out at different protein: LPS ratio (ϕ and the measured supernatant concentrations are shown in the graph below (**Figure 3.5**). As the negative control did not change, it is assumable that the concentration of the supernatant decreased as LPS were trapped on the beads surface.

As expected, the LPS removal was significantly improved as ϕ factor increased as shown in **Figure 3.5 a**. In particular, 85% of LPS removal from the initial solution was reached when the protein:LPS ratio was 392, in

accordance to the 83.4% LPS removal using PMB cartridges (Toraymyxyn) and reported by Malard et al, 2018 [26]. The first sample measured for that ratio was taken at 5 minutes, when the equilibrium in the interaction between LALF and LPS had been already achieved, so that an in-depth study of the contact was conducted. In this case, the ϕ factor was slightly higher and, under those conditions, the system achieved 95% of LPS removal in less than 1-minute (**Figure 3.5 b**), pointing to an instantaneous binding between the bead-protein complex and LPS and achieving an acceptable percentage for LPS removal processes.

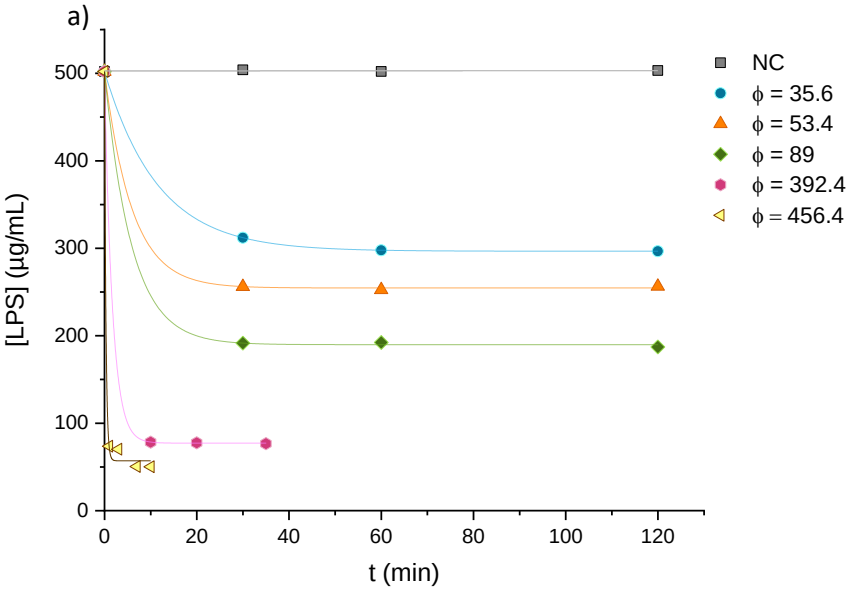

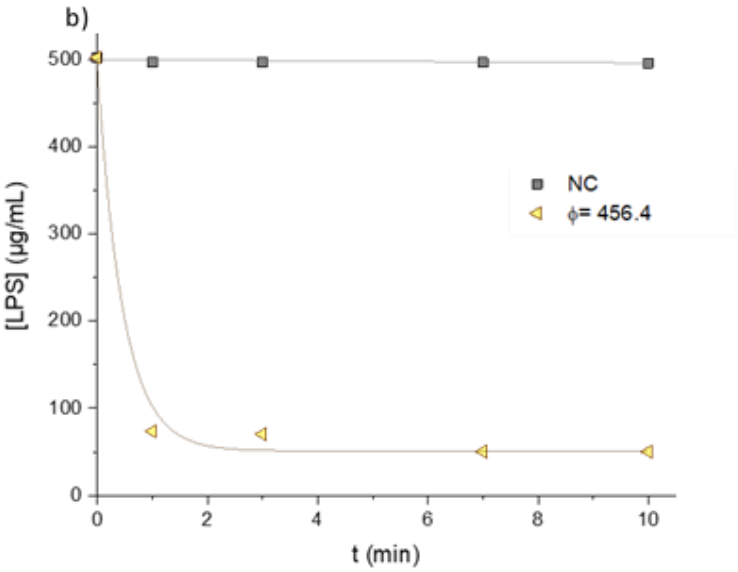

Figure 3.5. a) LPS concentration decrease in the supernatant at different protein-LPS ratios. b) LPS supernatant concentration change with time at ϕ factor of 456.4.

3.4.2. Apparent equilibrium constant

Previous adsorption measurements results were plotted in **Figure 3.6** where, based on the previously described constant expression, eq. (4) the resulting complex between the protein and LPS [P-LPS] divided by the free protein [P] and the free LPS present in the supernatant [LPS_{SN}] are represented. The obtained slope corresponds to the apparent equilibrium constant expression with a resulting value of 2.8 10^3 M^{-1}.

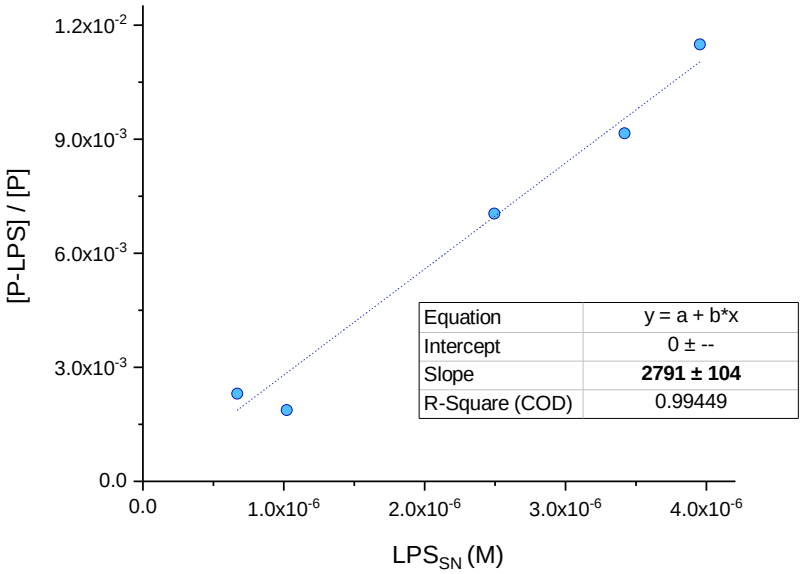

Figure 3.6.Adsorption isotherm for LPS-LALF protein interaction.

Association constant values reported for PMB (K_A= 2.1 10^6 M^{-1}) based on FRET-based experiments) or the biomolecules involved in the cascade mechanisms (LBP, sCD14) were higher than the value we have obtained in this work. This can be explained both by the determination method and also because of the characteristics of the synthesized LALF protein. While binding constants reported in the literature were obtained by immobilizing the protein on a chip surface and via binding analysis techniques, in this work an experimental procedure was carried out where the peptide was firstly immobilized on an agarose matrix through nickel coordination bonds and then contacted to LPS solution; furthermore, LPS capture was carried out at ambient conditions similar to those expected in extracorporeal treatment. Regarding the protein structure, although molecular tags can improve the solubility to target proteins, they can also generate steric hindrance [27] as our protein synthesis required an MBP tag to avoid formation of inclusion bodies and the 6x Histidines to covalently bond to the beads. These modifications

changed the molecular weight of our protein from 15 to 76 kDa so that this steric effect could prevent from better LPS removal. Despite that fact, protein: LPS ratios of 400 satisfactorily removed 95% of the initial LPS in the contacted solution and, considering the higher protein:LPS ratios in septic humans (10000) our approach is a good starting point for LPS cleansing systems.

In this regard, the aim here, is to advance on the state-of-the-art of the experimental evaluation of the LPS binding interaction through a methodological approach that combines protein and separation engineering. Thus, further work could consist of applying this advance to a continuous device to analyze the removal efficacy of the system as a potential alternative to the existing therapies that unfortunately, are not completely efficient as today one-third to one-half of all septic patients in-hospital die.

3.5. Conclusions

LPS toxicity has boosted the research on effective methods for its separation from biofluids where micro-magnetophoretic devices deserve special attention. In this process the first stage aims at LPS entrapment on functionalized MNPs followed by the removal of the loaded particles from the biofluid in a second stage. While the particles deflection in microdevices has been studied in detail with outstanding results, the LPS-MNPs complex formation requires LPS easy to obtain selective binding agents and a quantitative and systematic methodology to experimentally determine the binding kinetics is fundamental for the rigorous and correct design of removal devices. In this regard, previously synthesized LALF protein has shown binding capacity to agarose beads selected as particle model system. Initial experiments were carried out to select the variables that provided the best LPS separation performance, i.e., bead-protein and temperature of the protein supporting process. With a bead:protein ratio 2:1 the protein uptake on the beads surface reached 90% of the initial

concentration in 5 h and 94% in 22 h. The temperature in the range 4˚C to 37˚C did not exert influence on protein fixation.

Regarding the LPS sequestration stage, the experimental planning analyzed the influence of the temperature on LPS removal at 4, 20 and 37 ˚C reaching the highest value, ca. 50.2%, at 20 ˚C. To increase LPS removal, runs with variable protein: endotoxin ratio (ϕ), were carried out, observing that with a protein: endotoxin ratio (ϕ), around 95% of LPS removal from the initial solution was achieved in the first minute of contact. The obtained apparent association constant value was $2.8\ 10^{3}$ M^{-1}, determined through an experimental approach based on a cost-effective protein synthesis process contributing to the development of micro-magnetophoretic cleansing devices.

3.6. References

[1] C.J. Thomas, B.P. Gangadhar, N. Surolia, A. Surolia, Kinetics and mechanism of the recognition of endotoxin by polymyxin B, J. Am. Chem. Soc. 120 (1998) 12428–12434. https://doi.org/10.1021/ja981777j.

[2] C.J. Thomas, A. Surolia, Kinetics of the interaction of endotoxin with polymyxin B and its analogs: a surface plasmon resonance analysis, FEBS Lett. 445 (1999) 420–424. https://doi.org/10.1016/S0014-5793(99)00150-7

[3] P.S. Tobias, K. Soldau, J.A. Gegner, D. Mintz, R. Ulevitch, Lipopolysaccharide Binding Protein-mediated Complexation of lipopolysaccharide with soluble CD14, J. Biol. Chem. 270 (1995) 10482–10488. doi: 10.1074/jbc.270.18.10482.

[4] S. Viriyakosol, J.C. Mathison, P.S. Tobias, T.N. Kirkland, Structure-function analysis of CD14 as a soluble receptor for lipopolysaccharide, J. Biol. Chem. 275 (2000) 3144–3149. https://doi.org/10.1074/jbc.275.5.3144.

[5] C.J. Thomas, M. Kapoor, S. Sharma, H. Bausinger, U. Zyilan, D. Lipsker, D. Hanau, A. Surolia, Evidence of a trimolecular complex involving LPS, LPS binding protein and soluble CD14 as an effector of LPS response, FEBS Lett. 531 (2002) 184–188. https://doi.org/10.1016/S0014-5793(02)03499-3.

[6] H.J. Shin, H. Lee, J.D. Park, H.C. Hyun, H.O. Sohn, D.W. Lee, Y.S. Kim, Kinetics of binding of LPS to recombinant CD14, TLR4, and MD-2 proteins., Mol. Cells. 24 (2007) 119–24.

[7] S. Akashi, S. Saitoh, Y. Wakabayashi, T. Kikuchi, N. Takamura, Y. Nagai, Y. Kusumoto, K. Fukase, S. Kusumoto, Y. Adachi, A. Kosugi, K. Miyake, Lipopolysaccharide Interaction with Cell Surface Toll-like Receptor 4-MD-2: Higher affinity than that with MD2 or CD14, J. Exp. Med. 198 (2003) 1035–1042. https://doi.org/10.1084/jem.20031076.

[8] S. Viriyakosol, P.S. Tobias, L. Kitchens, T.N. Kirkland, R.L. Kitchens, MD-2 Binds to Bacterial Lipopolysaccharide *, 276 (2001) 38044–

38051. https://doi.org/10.1074/jbc.M105228200.

[9] A.D. Romaschin, C. V. Obiezu-Forster, H. Shoji, D.J. Klein, Novel Insights into the Direct Removal of Endotoxin by Polymyxin B Hemoperfusion, Blood Purif. 44 (2017) 193–197. https://doi.org/10.1159/000475982.

[10] K. Teramoto, Y. Nakamoto, T. Kunitomo, H. Shoji, T. Tani, K. Hanazawa, M. Kodama, Removal of endotoxin in blood by polymyxin B immobilized polystyrene-derivative fiber, Ther. Apher. 6 (2002) 103–108. https://doi.org/10.1046/j.1526-0968.2002.00411.x.

[11] T. Shimizu, T. Miyake, M. Tani, History and current status of polymyxin B-immobilized fiber column for treatment of severe sepsis and septic shock, Ann. Gastroenterol. Surg. 1 (2017) 105–113. https://doi.org/10.1002/ags3.12015.

[12] J. Gómez-Pastora, I. Karampelas, E. Bringas, E.P. Furlani, I. Ortiz, Computational Analysis of a Two-Phase Continuous-Flow Magnetophoretic Microsystem for Particle Separation from Biological Fluids, Comput. Aided Chem. Eng. 40 (2017) 1183–1188. https://doi.org/10.1016/B978-0-444-63965-3.50199-9.

[13] J. Gómez-Pastora, C. González-Fernández, E. Real, A. Iles, E. Bringas, E.P. Furlani, I. Ortiz, Computational modeling and fluorescence microscopy characterization of a two-phase magnetophoretic microsystem for continuous-flow blood detoxification, Lab Chip. 18 (2018) 1593–1606. https://doi.org/10.1039/c8lc00396c.

[14] J. Gómez-Pastora, I.H. Karampelas, X. Xue, E. Bringas, E.P. Furlani, I. Ortiz, Magnetic Bead Separation from Flowing Blood in a Two-Phase Continuous-Flow Magnetophoretic Microdevice: Theoretical Analysis through Computational Fluid Dynamics Simulation, J. Phys. Chem. C. 121 (2017) 7466–7477. https://doi.org/10.1021/acs.jpcc.6b12835.

[15] J. Gómez-Pastora, I.H. Karampelas, E. Bringas, E.P. Furlani, I. Ortiz, Numerical Analysis of Bead Magnetophoresis from Flowing Blood in a Continuous-Flow Microchannel: Implications to the Bead-Fluid

Interactions, Sci. Rep. 9 (2019) 1–13. https://doi.org/10.1038/s41598-019-43827-x.

[16] J. Gómez-Pastora, X. Xue, I.H. Karampelas, E. Bringas, E.P. Furlani, I. Ortiz, Analysis of separators for magnetic beads recovery: From large systems to multifunctional microdevices, Sep. Purif. Technol. 172 (2017) 16–31. https://doi.org/10.1016/j.seppur.2016.07.050.

[17] M. Berger, J. Castelino, R. Huang, M. Shah, R.H. Austin, Design of a microfabricated magnetic cell separator, Electrophoresis. 22 (2001) 3883–3892. https://doi.org/10.1002/1522-2683(200110)22:18<3883::AID-ELPS3883>3.0.CO;2-4.

[18] N. Pamme, A. Manz, On-chip free-flow magnetophoresis: Continuous flow separation of magnetic particles and agglomerates, Anal. Chem. 76 (2004) 7250–7256. https://doi.org/10.1021/ac049183o.

[19] N. Pamme, Magnetism and microfluidics, Lab Chip. 6 (2006) 24–38. https://doi.org/10.1039/b513005k.

[20] B.D. Plouffe, L.H. Lewis, S.K. Murthy, Erratum: “Computational design optimization for microfluidic magnetophoresis” [Biomicrofluidics 5, 013413 (2011)], Biomicrofluidics. 5 (2011) 2013–2015. https://doi.org/10.1063/1.3668225.

[21] I.S. Novikau, E.S. Minina, P.A. Sánchez, S.S. Kantorovich, Suspensions of magnetic nanogels at zero field: Equilibrium structural properties, ArXiv. (2019) 1–5. https://doi.org/10.1016/j.jmmm.2019.166152

[22] C. Biglione, J. Bergueiro, S. Wedepohl, B. Klemke, M.C. Strumia, M. Calderón, Revealing the NIR-triggered chemotherapy therapeutic window of magnetic and thermoresponsive nanogels, Nanoscale. 12 (2020) 21635–21646. https://doi.org/10.1039/d0nr02953j.

[23] J.C. Cuggino, E.R.O. Blanco, L.M. Gugliotta, C.I. Alvarez Igarzabal, M. Calderón, Crossing biological barriers with nanogels to improve drug delivery performance, J. Control. Release. 307 (2019) 221–246. https://doi.org/10.1016/j.jconrel.2019.06.005.

[24] K. S. Soni, S. S. Desale, T. K. Bronich, Nanogels: an overview of properties, biomedical applications and obstacles to clinical translation, Physiol. Behav. 176 (2016) 139–148. https://doi.org/10.1016/j.physbeh.2017.03.040.

[25] S.M. Opal, P.J. Scannon, J. Vincent, M. White, S.F. Carroll, J.E. Palardy, N.A. Parejo, J.P. Pribble, J.H. Lemke, Relationship between Plasma Levels of Lipopolysaccharide (LPS) and LPS-Binding Protein in Patients with Severe Sepsis and Septic Shock, J. Infect. Dis. 180 (1999) 1584–1589. https://doi.org/10.1086/315093.

[26] B. Malard, C. Lambert, J.A. Kellum, In vitro comparison of the adsorption of inflammatory mediators by blood purification devices, Intensive Care Med. Exp. 6 (2018). https://doi.org/10.1186/s40635-018-0177-2.

[27] W.S. Hlavacek, R.G. Posner, A.S. Perelson, Steric effects on multivalent ligand-receptor binding: Exclusion of ligand sites by bound cell surface receptors, Biophys. J. 76 (1999) 3031–3043. https://doi.org/10.1016/S0006-3495(99)77456-4.

4

Design of flow-through microdevices. Methodological guidelines

Abstract

This chapter aims to provide the methodological guidelines for the implementation of the capture stage of dissolved solutes using selective agents and operating in continuous microdevices setting the grounds for the capture of LPS from biological fluids using LALF functionalized nanoparticles. As a first approach, the microdevices design for reactive liquid phase separation is carried out employing aqueous solutions of Cr (VI) flowing through a Y-Y shaped microchannel in a homogeneous system where water is the receiving phase, and in a heterogeneous system where the solute moves to an organic receiving phase and is removed by facilitated transport mechanism. In the homogeneous system, mass transfer took place essentially by diffusion and both phases reached half of the initial solute inlet concentration whereas 85% chromium extraction was achieved by the addition of the selective extractant at a residence time of 5s. Model simulations with ANSYS FLUENT based on multiphasic Eulerian-Eulerian model have been assessed against a set of experimental runs fitting with an error less than 10%.

4.1. Introduction

The biofluid detoxification process proposed in this Thesis is based on two stages; the first one in which endotoxins are captured on the surface of functionalized particles and a second one in which the decorated-bead-LPS complex is removed from the target fluid.

After the synthesis of the LALF protein and determination of its activity in the capture of LPS, the next step consists of developing an application to carry out the continuous capture step aimed at fluid detoxification.

To this end, the advantages of microfluidics were addressed to propose the capture step as scaling down allows for handling smaller volume of fluids, which entails small quantities of reagents and samples, reducing waste products and hazardous substances and therefore, decreasing costs [1,2]. Besides, high surface-to-volume ratio enhances mass transfer and thermal dissipation, which makes liquid-liquid separation a suitable technique to be combined with microfluidic devices [3,4].

In this regard, and as depicted in **Figure 4.1**, the basic process would be comprised of a step where an endotoxin solution flows in parallel to a receptor phase that contains the functionalized beads, allowing the LPS binding on the particles surface as a function of the residence time and the operating temperature.

Although the objective to be achieved in the capture stage is well defined, the novelty of this approach requires of three essential steps: i) the design of microdevices for reactive L-L separation, ii) the design of microdevices for reactive L-S separation and finally, iii) its application to LPS capture.

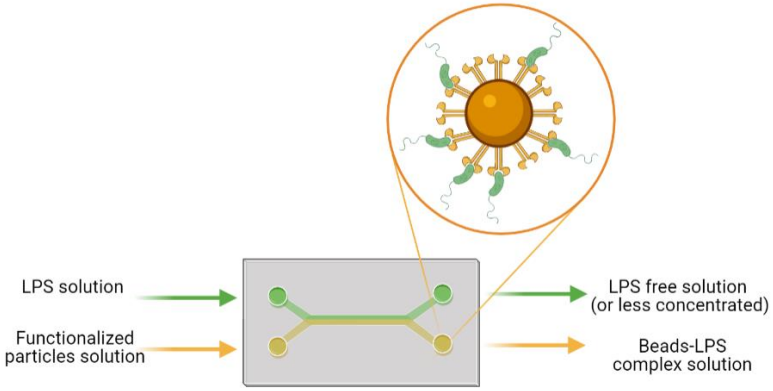

Figure 4.1. Functionalized beads-LPS capture stage illustration.

This Thesis addresses the first point concerning the design of microdevices for L-L separations. For this purpose, a system with chemical similarity consisting of the reactive separation of anionic solutions by means of functionalized amino groups has been chosen due to its fast kinetics.

To approach the study, the references and applications of microfluidics have been taken into account, specifically those related to extraction systems. In fact, during the last few years, great expectations have been aroused about countless applications of micro-solvent extraction in diverse fields that range from food safety control in applications such as extraction and pre-concentration of pesticides from juice samples [5] to forensics, detecting different antidepressant compounds in human urine and plasma samples [6].

Besides, as many materials employed in microfluidics as PDMS or SU-8 report biocompatibility [7], there are several studies focused on the development of microfluidic analytical techniques of biological substrates, isolation of leukocyte and erythrocyte cells from blood cells [8], detection of cocaine and its derivatives in hair samples [9] or even tumor progression tracking [10].

The crux of solvent extraction (SX) techniques often lies in molecular diffusion. Since down scaling predominantly implies laminar flow (Re< 1) with no turbulences and a streamlined flow, net transport of molecules occurs due to their random motion (McNaught and Wilkinson 1997). Based on this principle, several studies regarding the separation of solutes have been applied in two differentiated systems: homogenous, where two aqueous phases are contacted, and solute transport occurs by simple diffusion, and heterogeneous systems, where an aqueous phase is brought into contact with an organic receptor phase and the separation is carried out by facilitated transport.

Regarding homogeneous systems, since the pioneering work of Brody and Yager [13] reporting the diffusive transport of carboxifluorescein in an aqueous phase, different authors have contributed with interesting studies on molecular diffusion combining experimental runs and computational techniques as recently reported by Gómez-Pastora et al. [14] who studied the solute mass transport performance in Y-Y shaped microchannels as function of flow patterns and mass transport kinetics.

Moreover, microfluidic techniques have been also applied to protein extraction in aqueous two-phase systems, Novak et al. [15]. In this context, mathematical models to characterize microchannels mixing and flow quality and models aimed to determine the necessary operation conditions to verify laminar flow and predicting diffusivity and concentration profiles of the solute have been already reported [16–19]. Different solutes such as glucose, benzoic acid, sucrose and glycine among others were contacted with water and the experimental results were satisfactorily validated with the predicted ones. Afterwards, Ciceri and co-workers [20] focused on the diffusion of Co (II) from an aqueous feed solution to an aqueous buffer and validated the experimental diffusion study with model simulated results based on the previous work of McCulloch et al. [21] who, using “Instaspec” III software, developed an analytical solution starting from Fick`s second diffusion law in order to predict the target specie concentration in the receptor phase.

Concerning heterogeneous systems, Sato et al. [22] firstly experimentally demonstrated the molecular transport of Ni (II) into a chloroform reservoir and Bowden et al. [23] reported the rapid hydrocarbon extraction to an hexane phase. In addition, different reports [12,20] developed a treatment to control the degree of hydrophilicity /hydrophobicity of the microdevices walls. They further reviewed stabilizing methods of stratified micro flows and studied the molecular diffusion to describe the solute transfer across the water/oil interface. Recently, experimental micro extraction has been applied by Kolar et al. [24] to validate the viability of rare earth elements extraction into Cyannex® 572.

Furthermore, experimental work coupled with computational techniques has been reported as in the work of Kuban et al. [25] to determine the influence of physical parameters such as interfacial area, density, viscosity and flow velocity on the performance of micro-solvent extraction processes. Despite most solvent extraction processes are developed and simulated in 2 layer microdevices, Surmeian et al. [26] and Tetala et al. [25] carried out the simultaneous forward and backward extraction steps in a water/oil/water system. While Surmeian et al. assured the stability between the 3 phases and achieved a rapid transport of methyl red into cyclohexane, Tetala et al. studied the extraction effectiveness of alkaloids from plants extracts. Phase stabilization in a 2 phase system was also reported by Žnidaršič-Plazl and Plazl. [29] who estimated the diffusion coefficients by correlations and mathematically described a non-linear equation system where the esterification of isoamyl acetate took place at the interface between n-hexane and an aqueous phase.

Moreover, Mason et al. [30] focused on heterogeneous transport and developed a simplified model under steady state conditions; they assumed a stable interface and estimated the mass transfer coefficients by four different approaches to determine the best correlation to describe the solute transfer to a receptor phase. This analysis gave rise to a subsequent work carried out by Ciceri et al. [31] to determine the extraction kinetics of Co (II) into DEHPA. A numerical model was

constructed and solved using CFD techniques assuming a flat interface between the fluids in contact as well as a streamline flow along the device. In addition, a no-slip velocity condition was considered as boundary condition on the walls of the micro device and a pressure driven gradient set the flow rate of each phase.

On the basis of previous studies, this work pursues the advance on micro-extractors design solving the coupling between fluid dynamics and mass transfer kinetics and allowing the interface tracking along the complete geometry of the microdevice as an initial step in the methodological development for the implementation of the LPS capture stage in microdevices.

The analysis has been developed for the transport of hexavalent chromium as target solute from an aqueous phase flowing through a Y-Y shaped microchannel and considering two different scenarios: i) a homogeneous system, where the solute is separated by simple diffusion across two aqueous phases and, ii) a heterogeneous system where facilitated transport promoted the solute transport across the aqueous-organic interface.

ANSYS FLUENT software was used to develop a flexible model that solves under dynamic conditions both Navier-Stokes and species balance equations; the model also implements the surface tension between the liquid phases that had been experimentally determined, and the fluid-wall interaction through the measurement of the contact angle.

The main objective of the study was to address the hydrodynamics and flow patterns, analyzing the conditions that ensure the co-flow of the fluids in contact, guaranteeing a stable interface without mixing of the fluids. Besides, as a key variable in the design of microdevices, the influence of the residence time of the target solute diffusion along the device for the homogeneous system was also tackled. Likewise, the effect of the addition of the selective extractant to the process was also studied in terms of chromium removal performance as function of the residence time. Furthermore, a set of experimental runs was carried out for the two

cases of study and the results fitted satisfactorily to simulated data using CFD modelling together with physical-chemical parameters already reported [32].

Consequently, the rigorous and flexible model developed here constitutes a useful tool for the design of micro-separators and is applicable to the subsequent study of reactive L-S separation prior to its application in the LPS capture stage.

4.2. Materials

4.2.1. Chemical reagents

$KCrO_4$ (99%, Panreac Quimica S.A.) was used to prepare the feed solution and Shellsol D-70® (Kremer) and Alamine 336® (BASF) were employed for the organic phase of the heterogeneous system. Hydrochloric acid (37%, Panreac) was also added to the initial solution to adjust the pH. Furthermore, in order to verify the interface stabilization of the homogeneous system, sodium fluorescein, $C_20H_{10}Na_2O_5$, (Scharlau) was employed as fluorescent tracer to better visualize the aqueous phases in contact. All aqueous solutions were prepared with milli-Q water.

4.2.2. Y-Y microfluidic device

A Y-Y shaped microdevice made of SU8 (MICRUX Technologies S.L.) as substrate was used to perform the experimental procedure. The contact zone after the Y-inlet was 2 mm long, 300 µm wide and 300 µm deep and the angle between both inlets was 60˚ (same angle as between the outlet branches) as shown in **Figure 4.2**. The cross-sectional shape was rectangular and the interfacial area between phases was approximately 0.6 mm^2.

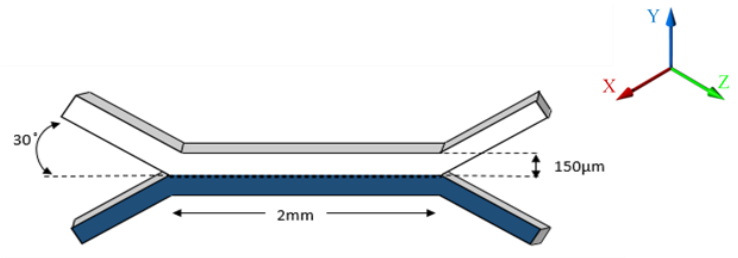

Figure 4.2. Micro-device geometry and dimensions.

4.3. Experimental procedure

The micro device was placed in a polymethyl methacrylate (PMMA) holder (16 x 8.5 mm) with a magnetic closure and interchangeable inlets and outlets connections of ¼" UNF (MicruX Technologies). At the same time, two 50 mL stainless steel syringes (Harvard Apparatus) were loaded with their respective solutions, placed in two infusion pumps (KD Scientific Legato series 200) and connected to the micro device inlets through Tygon ® tubes of 0.8 mm of internal diameter (Saint-Gobain). For each scenario, the fluid phases were brought in contact along the microdevice and for both cases of study, fluids co-flow and the interface track were controlled on a stereo microscope (Nikon SMZ18) equipped with a green fluorescence filter (light wavelengths of around 550 nm) and a Jenoptik ProgRes C5 camera. Images were taken using the ProgRes® CapturePro software (CapturePro V2.10.0.0).

Samples were collected in Eppendorf tubes (1 mL) and the chromium concentration of the aqueous phases was measured by atomic absorption spectroscopy (Perkin Elmer 3110). Absorption standards were prepared with a chromium standard solution of 1000 mg/L (PanReac). Experiments were executed in triplicate to verify their reproducibility. A schematic diagram of the experimental set-up is shown in **Figure 4.3**.

Firstly, the interface stability was experimentally verified. For the homogeneous case, as both fluids in contact were aqueous solutions, sodium fluorescein was employed as colouring agent to distinguish the two phases. For the heterogeneous system that involved the contact between an aqueous feed and an organic receptor, the colorant was not needed.

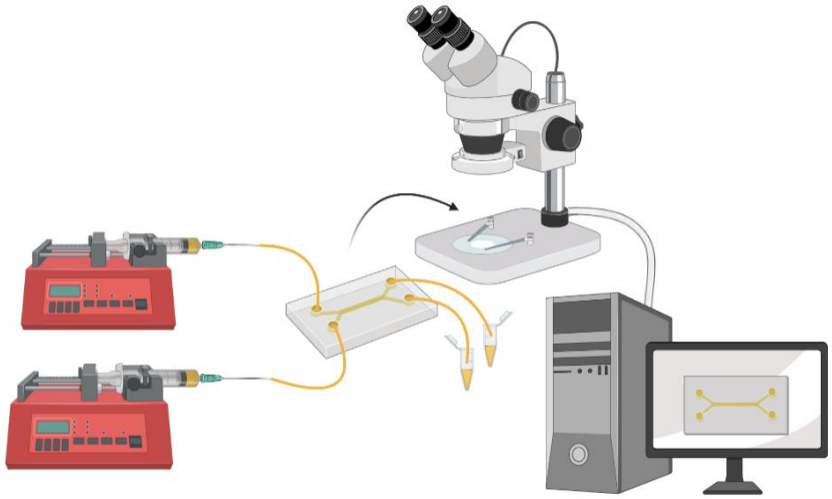

Figure 4.3. Experimental set-up diagram.

For both scenarios, an aqueous solution of hexavalent chromium of 20 mgL^{-1} as feed phase was used. Diffusive mass transport of the metal (homogeneous system) was determined by contacting the feed phase with water as receptor phase. Due to the symmetric geometry and similar properties of the phases in contact, with a viscosity (μ_{aq}) of 0.001 kg $m^{-1}s^{-1}$, the same flow rate values (0.6 μLs^{-1} – 0.01 μLs^{-1}) along the microchannel were applied for both streams. Furthermore, in the facilitated transport experiments, the aqueous chromium-based stream was contacted with an organic solution composed of Shellsol D-70® as solvent and Alamine 336® (10% wt.) as selective extractant. The pH of the initial solution was adjusted to 1.5 with hydrochloric acid to protonate the amino functional groups present in the extractant agent. As fluids in contact for this scenario had different rheological properties (viscosity values of μ_{aq}

=0.001 $kgm^{-1}s^{-1}$, μ_{org} = 0.0009 $kgm^{-1}s^{-1}$), different throughputs were applied in order to control the pressure drop along the microchannels (9.5 µL/s – 0.003 µL/s). The residence time for both scenarios ranged from 0.01s to 10s and the experimental operating conditions for homogeneous and heterogeneous experiments are detailed in **Table 4.1**.

Table 4.1.Experimental flow- rates and residence time for both systems.

Homogeneous system			**Heterogeneous system**		
F_{feed} (µL/s)	$F_{receptor}$ (µL/s)	τ (s)	F_{feed} (µL/s)	$F_{receptor}$ (µL/s)	τ (s)
0.6	0.6	0.15	9.526	4.763	0.006
0.105	0.105	0.573	0.263	0.132	0.228
0.051	0.051	1.168	0.103	0.052	0.581
0.025	0.025	2.353	0.012	0.006	4.81
0.015	0.015	4	0.006	0.003	9.58
0.01	0.01	5.968			
0.009	0.009	7			
0.006	0.006	9.285			

4.4. Theoretical background

ANSYS FLUENT R17.0 was employed to simulate both the simple diffusion and the facilitated transport cases. The model was based on the Eulerian finite volume algorithm combined with Volume of Fluid (VOF) parameters, which allow defining the position of the interface as a result of the calculation of each phase volume fraction.

The model is governed by mass and momentum equations (1-3). Eq. 1 is the general expression of the mass conservation equation applicable for both incompressible fluids, expressed as:

$$\frac{\partial \rho}{\partial t} + \nabla(\rho\vec{v}) = 0 \quad (1)$$

where ρ is the density and $\vec{v}$ the velocity vector.

The VOF method solves a set of momentum equations in an inertial system (non-accelerating) throughout the computational domain, which depends on the volume fraction of all the phases through the density and viscosity [33]. The volume fraction of each fluid along the micro device can be calculated from:

$$\frac{\partial}{\partial t}(\rho\vec{v}) + \nabla \cdot (\rho\vec{v}\,\vec{v}) = -\nabla p + \nabla \cdot (\bar{\tau}) \quad (2)$$

$$\bar{\tau} = \mu\left[\left(\nabla\vec{v} + \nabla\vec{v}^{T}\right) - \frac{2}{3}\nabla\vec{v}I\right] \quad (3)$$

where p is the static pressure and ($\bar{\tau}$) is the stress tensor given by Eq. 3, which includes the molecular viscosity (μ), the unit tensor "I" and the effect of volume dilatation.

Due to the spatial distribution of the concentration values that change along the microchannel length, ANSYS FLUENT implements the Fick´s Law to model mass diffusion rate as:

$$\vec{J_i} = -\rho\mathcal{D}_{i,m}\nabla Y_i - D_{T,i}\frac{\nabla T}{T} \quad (4)$$

In Eq. 4, $\vec{J_i}$ represents the diffusive flux of the specie "i" and Y_i is the predicted local mass fraction of each specie, $D_{T,i}$ is the thermal (Soret) diffusion coefficient and $\mathcal{D}_{im}$ denotes the chromium diffusion coefficient. Due to the isothermal regime of our system, the energy contribution of the system was neglected.

A conservation expression is also included to model the transport of different chemical species describing the convection, diffusion and chemical reaction phenomena previously reported by Bringas et al. [34], as follows:

$$\frac{\partial(\alpha_q \rho_q Y_q^i)}{\partial t} + \nabla(\alpha_q \rho_q \vec{V}_q\, Y_q^i) = -\nabla(\alpha_q \vec{J}_q^i) + \alpha_q R_q^i \quad (5)$$

Eq. (5) describes the variation of local mass fraction (α_q) with time of the specie "i" in the feed phase (q), "$\vec{V_q}$" is the velocity of the feed phase and " R^i_q " is the net rate of production of homogeneous species "i" through chemical reaction in phase q.

In order to simulate the single chromium diffusion, Equations (1-5) were solved including the diffusion coefficient for chromate in the aqueous phase with a value of 1.76 10^{-9} m^2/s. For this simple diffusion scenario, the second term on the right-hand side of Eq. 5 was neglected; thus, the change in chromium concentration along the channel length was due to the diffusive flux $\vec{J_i}$. Facilitated transport was modelled in this work by the addition of chemical reactions, R^i_q as presented in Eq. 5. In this case, the diffusion coefficient for the organometallic complex in the organic phase takes the value of 7.39 10^{-11} m^2/s. At the interface, the target specie reacts with the selective extractant agent ($\overline{R_3NH}$) as detailed in Eqs. (6-8):

$$HCrO_4^- \overset{k_1}{\Leftrightarrow} Cr_2O_7^{2-} + H_2O \quad (6)$$

$$\overline{R_3N} + 2H^+ + HCrO_4^- \overset{K_2}{\Leftrightarrow} \overline{(R_3NH)\,HCrO_4} \quad (7)$$

$$\overline{2R_3N} + 2H^+ + Cr_2O_7^{2-} \overset{K_3}{\Leftrightarrow} \overline{(R_3NH)_2\,CrO_7} \quad (8)$$

Chemical reaction takes place instantaneously at the interface so that, this phenomenon was included in the model by a molar concentration equilibrium ratio K>>10^3 [35] as reported in Eq. (9):

$$Y^i_{q,e} = K_{q^i p^j}\, Y^i_{p,e} \quad (9)$$

In addition, the surface tension between the aqueous and organic phase was included by the expression proposed by Brackbill et al. [36] as follows:

$$p_2 - p_1 = \sigma\left(\frac{1}{R_1} - \frac{1}{R_2}\right) \quad (10)$$

where p_1 and p_2 denote the pressure of both fluids, R_1 and R_2 is the surface curvature measured by two radii in orthogonal directions. Surface tension coefficient (σ) was experimentally determined in a Krüss K11 tensiometer using the method of the Wilhelmy plate with an estimated uncertainty of ca. 0.3 mNm^{-1} and its value is 3.55 mNm^{-1}. This is a key feature of this work since it was not assumed a flat interface nor a fully developed profile for the entire pass length so that, the surface tension value between the fluids in contact was experimentally measured and implemented in the model. **In Table 4.2**, the values of all the parameters included in our simulations are presented.

Table 4.2. Values of parameters employed in our computational model.

Parameter (T=20˚C)	**Feed phase**	**Receptor phase**	
		Homogeneous system	**Heterogeneous system**
Density (kg/m^3)	998.2	998.2	789
Viscosity (cP)	10^{-3}	10^{-3}	$9\ 10^{-4}$
Diffusion coefficient (m^2/s)	$1.76\ 10^{-9}$	$1.76\ 10^{-9}$	$7.39\ 10^{-11}$
Partition Coefficient	-	1	$>10^3$
Interfacial tension (mN/m)	-	-	3.55

4.5. Results

4.5.1. Interface stabilization

The fluid co-flow for the simple diffusion case is presented in **Figure 4.4**. This figure gathers the volume fraction of each phase along the micro device: the feed phase flows through the upper part of the channel represented in blue and the receptor phase is coloured in red in the lower part of the device. This chart is referred to the receptor phase volume fraction, the blue colour of the upper microchannel denotes the absence of the receptor phase in the feed one verifying that each fluid flows through each branch without mixing. In this case, the co-flow results in a clear and straight interface when both fluids are introduced into the domain at the same velocity value. This is due to the similar fluid properties of both phases, which ensures the same pressure drop along the channel length and thus, the separation of the phases at the channel outlets.

For the facilitated transport model, simulations run under the assumption of a non-stable interface between the phases in contact so that the interfacial tension value was implemented to avoid bulges along the pass length. To assess the accuracy of this assumption, simulated results with and without the interfacial tension were obtained to analyse its influence and to assure a flat interface along the micro device under the different studied conditions. The results are presented in **Figures 4.4 b)** and **c)**. For both figures, the applied velocities at the micro-channel inlets were different for each stream in order to facilitate phase separation at the Y outlet. This is due to the different properties reported by the feed and receptor phase, as previously observed by other authors Gómez-Pastora et al. [14] and Ciceri et al. [20]. **Figure 4.4 b)**, which corresponds to a simulation that does not include the interfacial tension coefficient, shows a dented interface between the feed and the organic phase where fluids come together at the initial part of the device. On the contrary, the stabilization of the interface was confirmed thanks to the implementation

of the interfacial tension value combined with the VOF method. Fluids flowed in the downstream x-direction and the interface was balanced in the centreline of the micro device as depicted in **Figure 4.4 c)**.

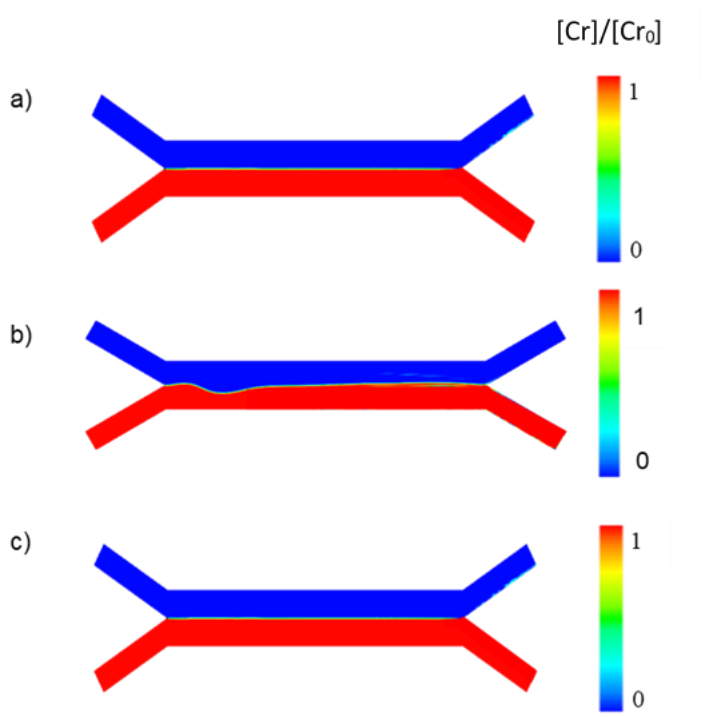

Figure 4.4.a) Simple diffusion simulation. b) Co-flow and interface simulation without implementing the interfacial tension value between the fluid phases of the heterogeneous system. c) Heterogeneous system interface verification showing a straight interface after including the interfacial tension model.

As a fully developed profile along the micro device was not assumed, simulations provided velocity vectors of the phases through the pass length as well as fluids distribution at the micro device to prove this assumption. As depicted in **Figure 4.5**, for both the homogeneous (**Figure 4.5 a**) and the heterogeneous (**Figure 4.5 b**) systems, it is appreciable a turbulent flow when the fluids converge and split up, coinciding at the inlet and outlet of the micro device where fluids collide with each other.

Despite this fact, both phases rapidly reach the laminar flow along the x-direction of the microchip achieving the maximum velocity at the inlet of the branches and at the centreline and the minimum at the micro device walls.

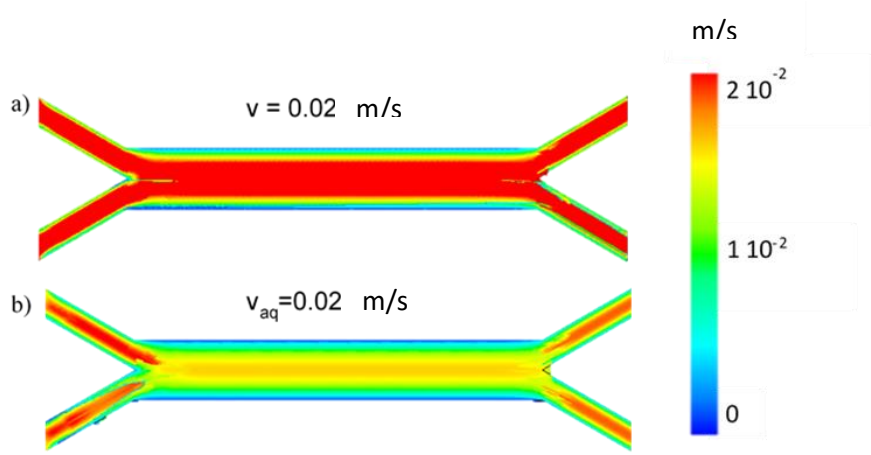

Figure 4.5. Velocity profiles of a) homogeneous system and b) heterogeneous system.

Once simulations run satisfactorily, it was also necessary to experimentally verify the interface stabilization. For the homogeneous case, as fluids in contact were both aqueous phases, one of the phases was dyed with sodium fluorescein Therefore, due to the symmetric geometry and similar properties of the feed and receptor phases, the applied velocities along the microchannel were the same for both fluids as presented in **Figure 4.4**. On the other hand, as the heterogeneous system involved an aqueous feed contacted with an organic receptor, the applied velocities were different for each stream along the device as previously reported by Ciceri et al. [37]. As depicted in **Figure 4.6** the fluid phases flow in parallel along the device separated by a stable interface at the microchannel centreline in good agreement with the simulated pathways presented in **Figure 4.4**.

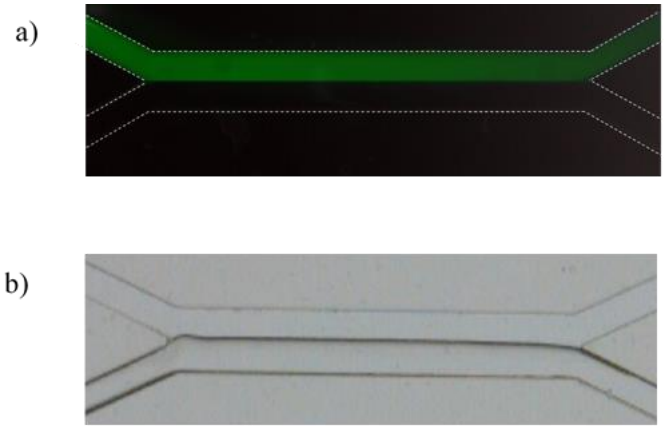

Figure 4.6. Experimental interface verification. a) Homogeneous system; b) Heterogeneous system.

4.5.2. Single-solute removal by diffusion

After studying the system hydrodynamics and the flow patterns, in this subsection the removal of chromium by simple diffusion in the homogeneous system is analysed. In this case, the removal of this component from the feed phase was studied as a function of the residence time of the feed phase in the microchannel. The results are presented in **Figure 4.7**, where it can be seen that both simulated and experimental results show a dependence of chromium migration from the feed to the receptor phase as function of the residence time. As previously studied by Bruss [38] it was observed that the lower the flow rate, the higher the chromium concentration in the receptor phase as detailed in **Figure 4.7**. Increasing the residence time benefits the separation as chromium diffuses along the device from the donor phase to the receptor phase. At larger residence times, the receptor phase is much more enriched in chromium that at shorter residence times where the metal is mainly present in the feed solution because the insufficient time for diffusion. Moreover, the process is controlled by the mass transfer kinetics, which means that the chromium outlet concentration of the feed phase is half of the initial inlet concentration.

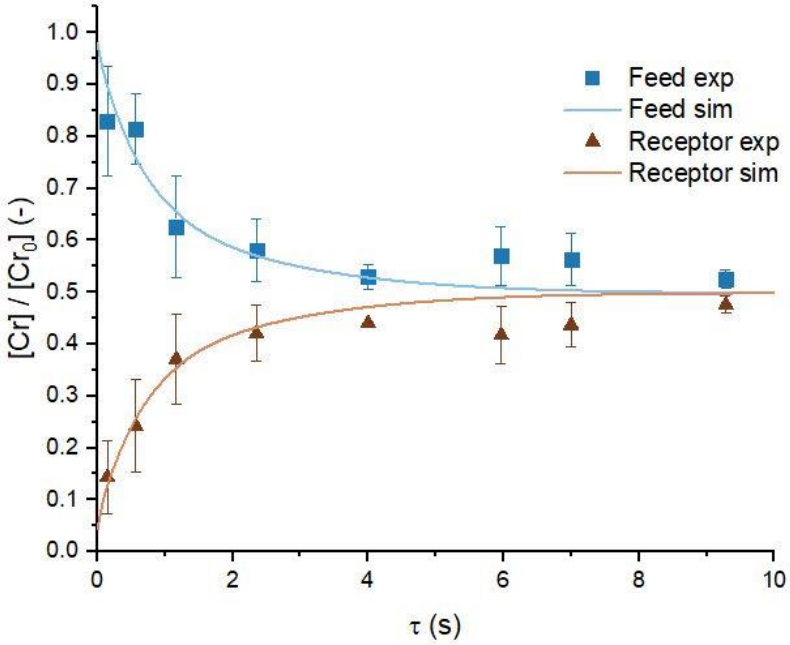

Figure 4.7. Homogeneous simulated and experimental results comparison for the chromium removal by simple diffusion. Squares correspond to feed phase (aqueous chromium solution) and triangles to the receptor phase (water), whereas solid lines correspond to the simulated results.

The system reaches the equilibrium after approximately 4 s. According to Bruus and Gomez-Pastora et al. [39], diffusion dominates convection when the diffusion time is larger than the residence time. Diffusion time is proportional to the square of the channel width and inversely proportional to the diffusivity of the target compound. Diffusion along the "x" and "z" axis was negligible and it was only taken into account in the direction perpendicular to the interface. For our case of study, the required time for the solute to diffuse from the wall to the interface is around 3.7 s, which is in good agreement with the experimental observations. Moreover, computational simulations verified this diffusion time as it can be appreciated in **Figure 4.8** where the green colour indicates that chromium concentration in both phases is equalised as the system reaches the equilibrium.

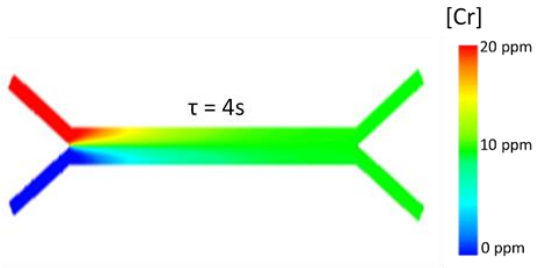

Figure 4.8.Chromium concentration profile of the homogeneous system at τ=4s.

In **Figure 4.9,** chromium concentration profiles of the feed and receptor phases along the microdevice for this system are provided at representative residence times of 0.1 and 10 seconds. As presented in **Figure 4.9 a**, for low residence times, where $t_{diffusion} >> t_{residence}$, chromium molecules do not reach the interface and go out with the feed water stream; therefore, the system is unable to reach equilibrium and as consequence, the feed solution concentration is substantially higher than the receptor phase concentration. However, increasing the residence time for situations where $t_{residence} >> t_{diffusion}$ implies that chromium concentration in the receptor phase is much higher and the outlet concentration of both phases in contact is balanced at 10 ppm (**Figure 4.9 b**).

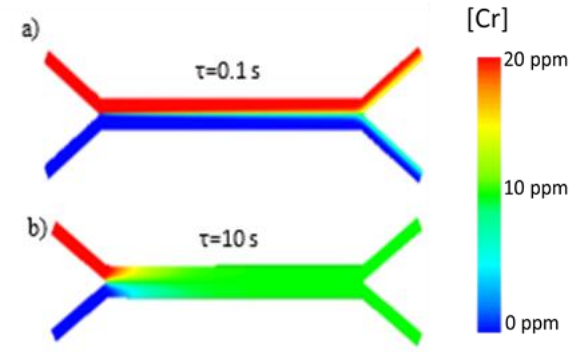

Figure 4.9. Chromium concentration profiles for the homogeneous system for different feed residence times. a) 0.1 s; b) 10 s.

4.5.3. Solute removal by facilitated transport

In this subsection, we examine the chromium extraction by facilitated transport, for which a chemical reaction at the interface between the immiscible fluid phases was implemented [35,40]. Thus, facilitated transport was carried out by contacting the chromium-based feed phase with an organic solution containing a selective carrier (Alamine 336) to enhance the extraction of the target compound. The micro device aqueous outlet concentration of chromium was measured and compared to simulated results. **Figure 4.10** reports a comparison between simulated and experimental results where it can be noticed the effect of the addition of the selective extractant to the process. Thus, the chromium outlet concentration of the receptor phase is much higher than the values reached in the homogeneous case presented in **Figure 4.7**, achieving extraction percentages between 85% and 97% for a residence time ranging from 5 to 10 seconds.

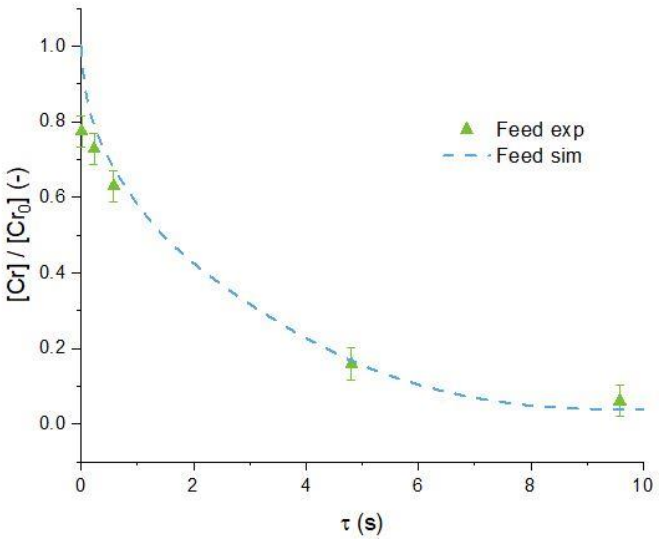

Figure 4.10. Chromium extraction by facilitated transport as a function of the feed phase residence time in the heterogeneous system. Dashed lines correspond to simulated results whereas triangles represent experimental chromium concentration variation in the feed phase.

Furthermore, the benefits of the facilitated transport are provided by examining the chromium concentration profiles along the microdevice. **Figure 4.11** represents the chromium contours of feed and receptor phase for the heterogeneous system at residence times of 0.1 (**Figure 4.11 a**) and 10 (**Figure 4.11 b**) seconds. For this case, chromium concentration in both phases is different at the outlets of the microdevice contrary to what is observed in the homogeneous system and consequently, the higher the residence time, the higher chromium extraction percentage obtained: the feed outlet chromium concentration at 0.1s of residence time is around 17 mg/L (**Figure 11 a)** while at 10 s, the concentration decreases to less than 1 mg/L as presented in **Figure 4.11 b)**. Moreover, extraction percentages range from 20% to 96% within the residence time varying between 0.01s and 10s, whereas for the homogeneous system the maximum removal percentage was 50%, after the chromium concentration was equal in both phases.

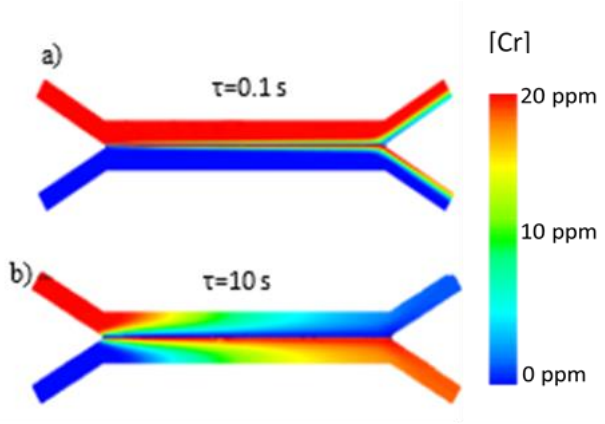

Figure 4.11.Chromium concentration profiles for the facilitated transport analysis at a) 0.1 s and b) 10 s.

By comparing both scenarios, it is noticed that mass transport of chromium from the feed to the receptor phase is improved in the heterogeneous system with regard to the homogenous system. However, at low residence times there is a small difference in the behaviour of the chromium concentration present in the feed of both scenarios, as shown in **Figures 7 and 10**. These results from the fact that both systems are

limited by diffusion phenomena, especially when the contact time is short (approximately less than 2 seconds). On the contrary, increasing the residence times avoids limitations of diffusion through the aqueous feed phase and enhances the chromium facilitated transport thanks to the chemical reaction equilibrium with the selective extractant. Consequently, higher extraction ratios are achieved and the chromium concentration of the feed phase decreases by 90% for residence times higher than 5 s.

4.5.4. CFD theoretical analysis and experimental validation

Although we presented the theoretical predictions along with experimental measured data in the previous subsection, we also calculated the standard deviation on the results for validating our computational model. We calculated the error between experimental and model predicted data with the following equation:

$$E\ (\%)=\frac{\sum_{i=1}^{n}\left|\left(\frac{[Cr]_{Sim}-[Cr]_{exp}}{[Cr]_{sim}}\right)\right|}{n}\times 100 \qquad (11)$$

where $[Cr]_{Sim}$ represents simulated chromium concentration, $[Cr]_{exp}$ represents the chromium concentration experimentally measured for the same conditions and n is the number of the experiments performed.

Based on the previous equation, our model predictions fit with experimental results with an average error less than 10% for both scenarios, i.e., simple diffusion and facilitated transport. Furthermore, in **Figure 4.12** we present a graphical comparison between the experimental and simulated results for the homogeneous and heterogeneous system. It could be seen that the simulated results satisfactorily predict the system performance within a 10% deviation.

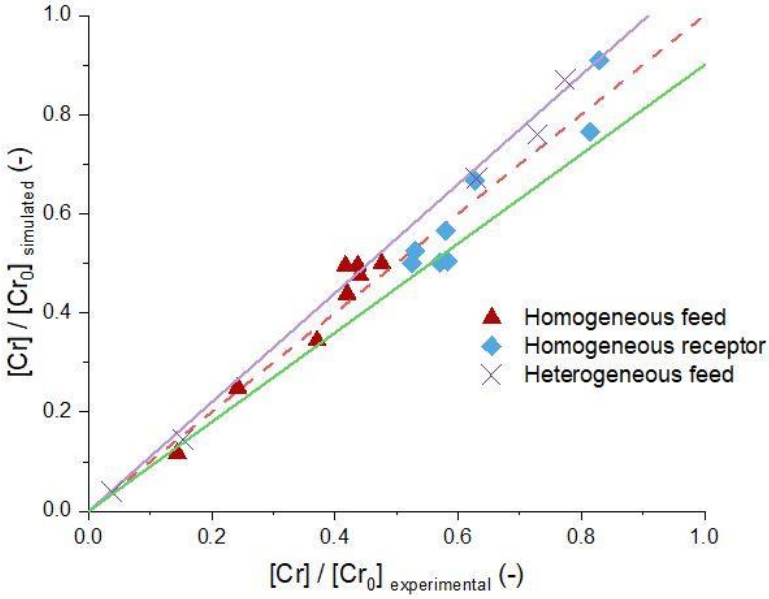

Figure 4.12.Simulated and experimental results comparison. Triangles represent homogenous feed phase and diamonds correspond to homogeneous receptor phase while crosses denote the heterogeneous feed phase.

4.6. Conclusions

Previous studies and applications on solvent extraction at the micro-scale have motivated the work of this chapter whose main objective is to contribute to the design of microdevices to be applied at continuous LPS capture process.

Therefore, a L-L reactive system using hexavalent chromium as a methodological example in a Y-Y shaped microchannel has been conducted as initial approach. Thus, a deep analysis of the fluid dynamics and mass transport phenomena involved in homogeneous and heterogeneous micro-separation systems has been carried out.

Firstly, a mathematical model solved using ANSYS FLUENT R17.0 was developed not restricted to previously adopted assumptions of flat interface and fully developed profile for the entire pass length, in order to analyze the fluids behavior and interface stabilization along the device. The fluid dynamic study disclosed that, for the homogeneous system, the applied velocities for both phases should be equal. However, phases in contact for the heterogeneous system were different due to the distinct rheological properties of each phase so that, the applied velocities were different for the feed and the receptor phase. Moreover, while fluids flowed under laminar conditions along the x-axis, it is appreciated turbulent regime where fluids meet and separate from each other. It means that, when fluids come into contact and when they branch into their respective channel, they experience a slight mixing. The interface stability was simulated as well as experimentally assessed for both cases of study and it was proven that, for the heterogeneous system, in order to avoid crumpling effects at the interface, it was necessary to implement the interfacial tension coefficient between the aqueous and the organic phase which was previously determined and whose value was 3.55 mNm^{-1}.

Regarding the mass transport analysis, in the homogeneous system mass transfer took place essentially by diffusion and both phases reached the same solute concentration when the values of diffusion time and residence time matched each other, which occurred at 3.7 s in the experimental system of this work. Nonetheless, the addition of Alamine 336 as selective carrier for chromium (VI) enhanced the mass transfer rate and displaced equilibration of chromium concentration between both phases, minimizing its limitation and thereby the transport to the receptor phase was increased; it was achieved an extraction percentage of 84.75% at a residence time of 5 seconds in the experimental system.

The model was validated through a set of experimental runs, fitting to the experimental data with an error less than 10%. Thus, this modelling effort constitutes a comprehensive tool for the design of microdevices as it points out the key variables that determine the separation performance.

The achievement of the model represents the attainment of the first objective of the capture stage in the path towards the design of biofluids cleaning systems in which, the subsequent step would be its implementation in a reactive S-L system and finally, its application to continuous LPS sequestration.

4.7. References

[1] P.T. Anastas, J.C. Warner, Green Chemistry: Theory and Practice, Oxford Uni, Oxford, 2000.

[2] R. Van Dam, Solvent-resistant elastomeric microfluidic devices and applications, California Institute of Technology, 2006. http://resolver.caltech.edu/CaltechETD:etd-12052005-234258.

[3] J.G. Kralj, H.R. Sahoo, K.F. Jensen, Integrated continuous microfluidic liquid–liquid extraction, Lab Chip. 7 (2007) 256–263. https://doi.org/10.1039/B610888A.

[4] G.M. Whitesides, The origins and the future of microfluidics., Nature. 442 (2006) 368–73. https://doi.org/10.1038/nature05058.

[5] D. Moreno-González, L. Gámiz-Gracia, A.M. García-Campaña, J.M. Bosque-Sendra, Use of dispersive liquid-liquid microextraction for the determination of carbamates in juice samples by sweeping-micellar electrokinetic chromatography, Anal. Bioanal. Chem. 400 (2011) 1329–1338. https://doi.org/10.1007/s00216-011-4682-3.

[6] M.A. Farajzadeh, P. Khorram, H. Ghorbanpour, Simultaneous derivatization and solid-based disperser liquid-liquid microextraction for extraction and preconcentration of some antidepressants and an antiarrhythmic agent in urine and plasma samples followed by GC-FID, J. Chromatogr. B Anal. Technol. Biomed. Life Sci. 983–984 (2015) 55–61. https://doi.org/10.1016/j.jchromb.2015.01.004.

[7] P.N. Nge, C.I. Rogers, A.T. Woolley, Advances in Micro fl uidic Materials , Functions , Integration , and Applications, Chem. Rev. 113 (2013) 2550–2583. https://doi.org/10.1021/cr300337x.

[8] M. Tsukamoto, S. Taira, S. Yamamura, Y. Morita, N. Nagatani, Y. Takamura, E. Tamiya, Cell separation by an aqueous two-phase system in a microfluidic device, Analyst. 134 (2009) 1994–1998. https://doi.org/10.1039/b909597g.

[9] A.M.F. Pego, F.L. Roveri, R.Y. Kuninari, V. Leyton, I.D. Miziara, M. Yonamine, Determination of cocaine and its derivatives in hair

samples by liquid phase microextraction (LPME) and gas chromatography–mass spectrometry (GC–MS), Forensic Sci. Int. 274 (2017) 83–90. https://doi.org/10.1016/j.forsciint.2016.12.024.

[10] V. Kiseliovas, M. Milosevic, M. Kojic, L. Mazutis, M. Kai, Y.T. Liu, K. Yokoi, M. Ferrari, A. Ziemys, Tumor progression effects on drug vector access to tumor-associated capillary bed, J. Control. Release. 261 (2017) 216–222. https://doi.org/10.1016/j.jconrel.2017.05.031.

[11] A. McNaught, A. Wilkinson, Compendium of Chemical Terminology, 2nd ed., Oxford, 1997. https://doi.org/10.1351/goldbook.I03352.

[12] A. Aota, K. Mawatari, T. Kitamori, Parallel multiphase microflows: fundamental physics, stabilization methods and applications., Lab Chip. 9 (2009) 2470–2476. https://doi.org/10.1039/b904430m.

[13] J.P. Brody, P. Yager, Diffusion-based extraction in a microfabricated device, Sensors Actuators A Phys. 58 (1997) 13–18. https://doi.org/10.1016/S0924-4247(97)80219-1.

[14] J. Gómez-Pastora, C. González-Fernández, M. Fallanza, E. Bringas, I. Ortiz, Flow patterns and mass transfer performance of miscible liquid-liquid flows in various microchannels: Numerical and experimental studies, Chem. Eng. J. 344 (2018) 487–497. https://doi.org/10.1016/j.cej.2018.03.110.

[15] U. Novak, A. Pohar, I. Plazl, P. Žnidaršič-Plazl, Ionic liquid-based aqueous two-phase extraction within a microchannel system, Sep. Purif. Technol. 97 (2012) 172–178. https://doi.org/10.1016/j.seppur.2012.01.033.

[16] A.E. Kamholz, B.H. Weigl, B.A. Finlayson, P. Yager, Quantitative analysis of molecular interaction in a microfluidic channel: The T-sensor, Anal. Chem. 71 (1999) 5340–5347. https://doi.org/10.1021/ac990504j.

[17] T. Hotta, S. Nii, T. Yajima, F. Kawaizumi, Mass transfer characteristics of a microchannel device of split-flow type, Chem. Eng. Technol. 30 (2007) 208–213.

https://doi.org/10.1002/ceat.200600285.

[18] J.T. Adeosun, A. Lawal, Numerical and experimental studies of mixing characteristics in a T-junction microchannel using residence-time distribution, Chem. Eng. Sci. 64 (2009) 2422–2432. https://doi.org/10.1016/j.ces.2009.02.013.

[19] M. van Leeuwen, X. Li, E.E. Krommenhoek, H. Gardeniers, M. Ottens, L.A.M. van der Wielen, J.J. Heijnen, W.M. van Gulik, Quantitative determination of glucose transfer between cocurrent laminar water streams in a H-shaped microchannel, Biotechnol. Prog. 25 (2009) 1826–1832. https://doi.org/10.1002/btpr.271.

[20] D. Ciceri, J.M. Perera, G.W. Stevens, A study of molecular diffusion across a water/oil interface in a Y-Y shaped microfluidic device, Microfluid. Nanofluidics. 11 (2011) 593–600. https://doi.org/10.1007/s10404-011-0824-3.

[21] A. Mineral, Direct Spectroscopic Measurement and Theoretical Modeling of the Diffusion of a Single Species in a Two-Phase Unstirred System, 405 (1996) 399–405. https://doi.org/10.1006/jcis.1996.0634..

[22] K. Sato, M. Tokeshi, T. Sawada, T. Kitamori, Molecular Transport between Two Phases in a Microchannel., Anal. Sci. 16 (2000) 455–456. https://doi.org/10.2116/analsci.16.455.

[23] S.A. Bowden, P.B. Monaghan, R. Wilson, J. Parnell, J.M. Cooper, The liquid–liquid diffusive extraction of hydrocarbons from a North Sea oil using a microfluidic format, Lab Chip. 6 (2006) 740–743. https://doi.org/10.1039/B518162C.

[24] E. Kolar, R.P.R. Catthoor, F.H. Kriel, R. Sedev, S. Middlemas, E. Klier, G. Hatch, C. Priest, Microfluidic solvent extraction of rare earth elements from a mixed oxide concentrate leach solution using Cyanex?? 572, Chem. Eng. Sci. 148 (2016) 212–218. https://doi.org/10.1016/j.ces.2016.04.009.

[25] P. Kuban, J. Berg, P.K. Dasgupta, Vertically stratified flows in microchannels. Computational simulations and applications to solvent extraction and ion exchange, Anal. Chem. 75 (2003) 3549–3556. https://doi.org/10.1021/ac0340713.

[26] M. Surmeian, M.N. Slyadnev, H. Hisamoto, A. Hibara, K. Uchiyama, T. Kitamori, Three-layer flow membrane system on a microchip for investigation of molecular transport, Anal. Chem. 74 (2002) 2014–2020. https://doi.org/10.1021/ac0112317.

[27] M. Surmeian, M.N. Slyadnev, H. Hisamoto, A. Hibara, K. Uchiyama, T. Kitamori, Three-layer flow membrane system on a microchip for investigation of molecular transport, Anal. Chem. 74 (2002). https://doi.org/10.1021/ac0112317.

[28] K.K.R. Tetala, J.W. Swarts, B. Chen, A.E.M. Janssen, T. a. van Beek, A three-phase microfluidic chip for rapid sample clean-up of alkaloids from plant extracts., Lab Chip. 9 (2009) 2085–92. https://doi.org/10.1039/b822106e.

[29] P. Žnidaršič-Plazl, I. Plazl, Modelling and experimental studies on lipase-catalyzed isoamyl acetate synthesis in a microreactor, Process Biochem. 44 (2009) 1115–1121. https://doi.org/10.1016/j.procbio.2009.06.003.

[30] L.R. Mason, D. Ciceri, D.J.E. Harvie, J.M. Perera, G.W. Stevens, Modelling of interfacial mass transfer in microfluidic solvent extraction: Part I. Heterogenous transport, Microfluid. Nanofluidics. 14 (2013) 197–212. https://doi.org/10.1007/s10404-012-1038-z.

[31] D. Ciceri, L.R. Mason, D.J.E. Harvie, J.M. Perera, G.W. Stevens, Modelling of interfacial mass transfer in microfluidic solvent extraction: Part II. Heterogeneous transport with chemical reaction, Microfluid. Nanofluidics. 14 (2013) 213–224. https://doi.org/10.1007/s10404-012-1039-y.

[32] H. Redl, S. Bahrami, G. Schlag, D.L. Traber, Clinical detection of LPS and animal models of endotoxemia, Immunobiology. 187 (1993) 330–345. https://doi.org/10.1016/S0171-2985(11)80348-7.

[33] J.M. Fernández Oro, Técnicas numéricas en ingeniería de fluidos: introducción a la dinámica de fluidos computacional (CFD) por el método de volúmenes finitos., Reverte, Barcelona, 2012.

[34] E. Bringas, M.F. San Román, J.A. Irabien, I. Ortiz, An overview of the mathematical modelling of liquid membrane separation

processes in hollow fibre contactors, J. Chem. Technol. Biotechnol. 84 (2009) 1583–1614. https://doi.org/10.1002/jctb.2231.

[35] E. Bringas, M.F. San Román, I. Ortiz, Removal of anionic pollutions from groundwaters using Alamine 336: Chemical equilibrium modelling, J. Chem. Technol. Biotechnol. 81 (2006). https://doi.org/10.1002/jctb.1610.

[36] J.U. Brackbill, D.B. Kothe, C. Zemach, A continuum method for modeling surface tension, J. Comput. Phys. 100 (1992) 335–354. https://doi.org/10.1016/0021-9991(92)90240-Y.

[37] D. Ciceri, L.R. Mason, D.J.E. Harvie, J.M. Perera, G.W. Stevens, Extraction kinetics of Fe(III) by di-(2-ethylhexyl) phosphoric acid using a Y-Y shaped microfluidic device, Chem. Eng. Res. Des. 92 (2014) 571–580. https://doi.org/10.1016/j.cherd.2013.08.033.

[38] K. Nishi, J.M. Perera, R. Misumi, M. Kaminoyama, G.W. Stevens, Study of diffusion of Co(II) and Co(II)-DEHPA complex in a microfluidic device, J. Chem. Eng. Japan. 43 (2010). https://doi.org/10.1252/jcej.09we175.

[39] J. Gómez-Pastora, X. Xue, I.H. Karampelas, E. Bringas, E.P. Furlani, I. Ortiz, Analysis of separators for magnetic beads recovery: From large systems to multifunctional microdevices, Sep. Purif. Technol. 172 (2017) 16–31. https://doi.org/10.1016/j.seppur.2016.07.050.

[40] A.I. Alonso, B. Galan, A. Irabien, I. Ortiz, Separation of Cr (VI) with Aliquat 336: Chemical Equilibrium Modeling, Sep. Sci. Technol. 32 (1997) 1543–1555. https://doi.org/10.1080/01496399708004065.

5

Conclusions and challenges for future research

Abstract

The main objective of this thesis is the development of a new process for the capture of endotoxins present in biofluids by combining the capture of LPS in specifically designed biomolecules by genetic engineering with continuous separation in microfluidic devices. After having described in detail the main aspects of this work, this chapter summarizes the main results obtained, highlights the conclusions derived from its analysis and exposes the challenges and perspectives for future research in the design of efficient systems for LPS capture and separation from biological fluids.

5.1. Conclusions

This thesis focuses on the development of a new process for the detoxification of biological fluids contaminated with endotoxins in which genetic engineering is integrated with microfluidic technology.

In this process, two main steps are distinguished; i) the capture of LPS on the surface of previously functionalized particles, and ii) the separation of the endotoxins, present in the target fluid using micro separators.

The work focuses on the first stage corresponding to endotoxins capture. Initially, a literature review was carried out to identify the molecules with greater activity against LPS and it was decided to synthesize, by means of genetic engineering techniques, the LALF protein (anti-lipopolysaccharide protein from the *Limulus Polyphemus* species).

The successful synthesis of LALF occurred when the genetic sequence was designed with a stability tail (Maltose Binding Protein) and subsequently expressed in the Artic Express strain, at 18˚C.

Once the protein was obtained, its kinetic activity was studied. For this purpose, the surface of agarose particles was functionalized with the previously synthesized LALF protein. Subsequently, the functionalized particles were contacted to fluorescent LPS solution, which made it possible to quantify the adsorption of endotoxins by the difference between the initial and final fluorescence signal.

At the same time, the variables that provided the highest performance in the separation of LPS were studied experimentally. In relation to the particle:protein contact, the optimal volume ratio was established at 2:1, achieving a retention of 90% of the initially contacted protein after 5 hours. In addition, temperature in the range of 4˚C to 37 ˚C did not exert influence on LALF binding.

Regarding LPS sequestration, the influence of the same temperature range was analyzed, reaching a maximum value of 50.2% capture at 20˚C. To increase endotoxin removal, tests were performed with a variable

protein: endotoxin ratio (ϕ), achieving about 95% removal of LPS from the initial solution in the first minute of contact for a ratio of 456.4. The results obtained in the adsorption measurements determined an apparent association constant value of 2.8 10^3 M^{-1} at a temperature of 20˚C.

Once the protein:LPS equilibrium was studied and in view of its application, the realization of the capture stage requires continuous operation. For this and, considering the advantages of microfluidics and the background of the research group, the use of micro devices has been proposed in which the fluid containing the LPS is contacted with another phase carrying the solid with LALF attached, determining the degree of capture as a function of residence time and temperature.

Considering the novelty and difficulty of the system under study, the design of the micro-fluidic capture has been structured in 3 stages, i) design of micro devices for L-L reactive separation, ii) design of micro devices for L-S reactive separation and finally, iii) application to the capture of LPS.

Specifically, this thesis hosts the study of the first stage of L-L reaction in which a system that maintains the fluid-dynamic analogy and of which the behavior of both the kinetics and the equilibrium of the chemical reaction is known has been subject to study. For this purpose, it has been worked with an initial aqueous solution composed of Cr (VI) flowing through a Y-Y microchannel in i) a homogeneous system in which the receiving phase is another aqueous phase and ii) a heterogeneous system in which facilitated transport promotes solute transport across an aqueous-organic interface.

As for the mass transport analysis, in the homogeneous system the mass transfer took place essentially by diffusion and both phases reached the same concentration at the exit of the microdevice corresponding to 50% of the initial concentration. However, the addition of Alamine 336 as a selective carrier for chromium (VI) improved the rate of mass transport and shifted the chromium concentration distribution between the two

phases, reaching an extraction percentage of 84.75% at a residence time of 5 s.

In addition, a mathematical model has been developed using ANSYS FLUENT R17.0 with a Eulerian approximation for multiphase systems. This model solves under dynamic conditions, both ta set of momentum equations as well as conservation equations. In addition, it implements the experimentally determined surface tension between the liquid phases, and the fluid-wall interaction. The experimentally obtained results were compared with the simulated ones with a 90% agreement.

Overall, the work reported in this thesis lays the foundations for the separation of endotoxins in fluids whose potential application represents an alternative to conventional endotoxin capture treatments and contributes to the development of new detoxification processes.

5.2. Challenges for future research

This thesis aims to open new ways for the microfluidic separation of endotoxins contained in biological fluids applicable, for example, to the treatment of patients with sepsis. Despite the achievements described in this thesis, there are still improvements to be implemented to accomplish the desired system that lie in i) the improvement of the activity of the LALF protein, determinant in the efficiency (kinetics and equilibrium) of endotoxin capture ii) the functionalization of a magnetic substrate and iii) the application of the mathematical model for L-S systems.

The activity of the protein could be improved by switching the synthesis and expression from bacteria to insect cells. This process requires the construction of recombinant baculovirus that serves as a vector to transfect the insect cells responsible for producing the LALF protein. Using this new expression system would allow the purification of an *E. coli*-free protein since the initial culture would not contain Gram-negative bacteria. Although the cost of working with insects is higher in both

material and equipment than working with *E.coli*, the activity of the protein of interest can be significantly improved.

On the other hand, the synthesis and characterization of magnetic nanogels carried out in this work represents a first step towards the implantation of a magnetic substrate in the micro-magnetophoretic system. Its functionalization with the protein, as well as the study of the variables involved in its adsorption on its surface, could be approached analogously as described in this work with agarose particles.

Finally, a robust mathematical model has been developed with ANSYS FLUENT to describe L-L reaction systems as a first approach for the improvement of the LPS capture step. To properly define the overall process, the model should be extended to the study of L-S reactive systems and once defined, it could be implemented in the endotoxin capture system.

5

Conclusiones y retos para investigaciones futuras

Abstract

El objetivo del trabajo descrito en esta tesis es el desarrollo de un nuevo proceso de separación de endotoxinas (LPS) presentes en biofluidos conjugando la captura en biomoléculas con diseño específico mediante ingeniería genética con la separación en continuo en dispositivos microfluídicos. Después de haber descrito en detalle los principales aspectos de este trabajo, este capítulo resume los principales resultados obtenidos, destaca las conclusiones que se derivan del análisis de los resultados y expone los retos y perspectivas para futuras investigaciones en el diseño de sistemas eficaces para la captura de LPS y su separación de fluidos biológicos.

5.1. Conclusiones

Esta tesis se centra en el desarrollo de un nuevo proceso de detoxificación de fluidos biológicos contaminados con endotoxinas en el que se integra la ingeniería genética con la tecnología microfluídica.

En este proceso se distinguen dos etapas principales; i) la captura de LPS en la superficie de una partícula previamente funcionalizada, y ii) la separación de las endotoxinas presentes en el fluido objetivo utilizando micro separadores.

El trabajo se centra en la primera etapa correspondiente a la captura de endotoxinas. Inicialmente, se realizó una revisión bibliográfica para identificar las moléculas con mayor actividad contra el LPS y de decidió sintetizar, mediante técnicas de ingeniería genética, la proteína LALF (proteína anti lipopolisacáridos procedente de la especie *Limulus Polyphemus*).

La síntesis de LALF resultó exitosa al diseñar la secuencia genética con una cola de estabilidad (proteína de unión a maltosa) y posteriormente expresarse en la cepa Artic Express, a 18˚C.

Una vez obtenida la proteína, se abordó el estudio de su actividad. Para ello, se funcionalizó la superficie de partículas de agarosa con la proteína LALF previamente sintetizada. Posteriormente, se llevó a cabo el contacto entre las partículas funcionalizadas y una disolución de LPS fluorescente, lo que permitió cuantificar la adsorción de las endotoxinas por diferencia entre la señal inicial y final de fluorescencia de la fase líquida.

A su vez, se estudiaron experimentalmente las variables que proporcionaron el mayor rendimiento en la separación de LPS. En relación al contacto partícula:proteína, la relación óptima se estableció en 2:1, consiguiéndose una retención del 90% de la proteína inicialmente contactada tras 5 horas. Además, la temperatura en el rango de 4˚C a 37˚C no ejerció influencia en la fijación de LALF.

Al respecto del secuestro de LPS, se analizó la influencia del mismo rango de temperatura, alcanzándose un valor máximo del 50.2% de captura a 20˚C. Para aumentar la eliminación de endotoxinas se realizaron ensayos con una relación variable de proteína: endotoxina (ϕ), lográndose alrededor del 95% de eliminación del LPS de la disolución inicial en el primer minuto de contacto para una relación de 456.4. Los resultados obtenidos en las medidas de adsorción determinaron un valor de la constante de asociación aparente de 2.8 10^3 M^{-1} a una temperatura de 20˚C.

Una vez estudiado el equilibrio de captación de LPS en la proteína sintetizada y de cara a su aplicación, la siguiente etapa comenzó el estudio de la separación en continuo. Para ello y considerando las ventajas de la microfluídica y los antecedentes del grupo de investigación, se ha propuesto el uso de micro dispositivos en los que, el fluido conteniendo el LPS se contacta con otra fase que porta el sólido con LALF adherido, determinando el grado de captura en función el tiempo de residencia y la temperatura.

Considerando la novedad y dificultad que entraña el sistema objeto de estudio, el diseño de la captación microfluídica se ha estructurado en 3 etapas, i) diseño de micro dispositivos para separación reactiva L-L, ii) diseño de micro-dispositivos para separación reactiva L-S y finalmente, iii) aplicación a la captura de LPS.

En concreto, esta tesis alberga el estudio de la primera etapa de reacción L-L en la que un sistema que mantiene la analogía fluidodinámica y del que se conoce el comportamiento tanto de la cinética como del equilibrio de la reacción química se ha sometido a estudio. Con este objetivo se ha trabajado con una disolución acuosa inicial compuesta de Cr (VI) que fluye a través de un micro canal en forma de Y-Y en i) un sistema homogéneo en el que la fase receptora es otra fase acuosa e ii) un sistema heterogéneo en el que el transporte facilitado promueve el transporte del soluto a través de una interfase acuosa-orgánica.

En cuanto al análisis de transporte de materia, en el sistema homogéneo la transferencia de materia tuvo lugar esencialmente por difusión y ambas fases alcanzaron la misma concentración a la salida del micro-dispositivo correspondiente al 50% de la concentración inicial. No obstante, la adición de la Alamine 336 como portador selectivo del cromo (VI) mejoró la velocidad de transporte de materia y desplazó el reparto de la concentración de cromo entre ambas fases, alcanzando un porcentaje de extracción del 84,75% a un tiempo de residencia de 5 segundos.

Además, se ha desarrollado un modelo matemático realizado con ANSYS FLUENT R17.0 con una aproximación euleriana para sistemas multifásicos. Este modelo resuelve en condiciones dinámicas, tanto las ecuaciones de Navier-Stokes como las de equilibrio de especies. Además, implementa la tensión superficial entre las fases líquidas determinada experimentalmente, y la interacción fluido-pared mediante la medición del ángulo de contacto. Los resultados conseguidos experimentalmente fueron comparados con los simulados con una concordancia del 90%.

En conjunto, el trabajo recogido en esta tesis sienta las bases de la separación de endotoxinas en fluidos cuya potencial aplicación supone una alternativa a los tratamientos convencionales de captura de endotoxinas y contribuye al desarrollo de nuevos procesos de detoxificación.

5.2. Retos para investigaciones futuras

Esta tesis pretende abrir nuevas vías para la separación microfluídica de endotoxinas contenidas en fluidos biológicos aplicable por ejemplo al tratamiento extracorpóreo de pacientes con sepsis. A pesar de los logros descritos en esta tesis, todavía existen mejoras a implementar para conseguir el sistema deseado que radican en i) la mejora de la actividad de la proteína LALF, determinante en la eficacia (cinética y equilibrio) de la captura de la endotoxina ii) la funcionalización de un sustrato magnético y iii) la aplicación del modelo matemático para sistemas L-S.

La actividad de la proteína podría ser mejorada al pasar de obtenerse en bacterias y expresarse en células de insecto. Este proceso requiere la construcción de un baculovirus recombinante que sirve como vector para transfectar las células de insectos encargadas de fabricar la proteína LALF. El hecho de utilizar este nuevo sistema de expresión permitiría purificar una proteína libre de *E.coli* ya que en el cultivo inicial no habría presencia de bacterias Gram negativas. Aunque el coste de trabajar con insectos es mayor tanto en material como en equipamiento del que supone trabajar con *E.coli*, la actividad de la proteína de interés puede verse significativamente mejorada.

Por otro lado, la síntesis y caracterización de nanogeles magnéticos llevada a cabo en este trabajo supone un primer paso hacia la implantación de un sustrato magnético en el sistema micromagnetoforético. Su funcionalización con la proteína, así como el estudio de las variables que intervienen en la adsorción de la misma en su superficie, podrían ser abordados de manera análoga a la descrita en este trabajo con las partículas de agarosa.

Por último, se ha desarrollado un modelo robusto con ANSYS FLUENT para describir sistemas de reacción L-L como primera aproximación para la mejora de la etapa de captura de LPS. Para definir correctamente el proceso global, el modelo debería extenderse al estudio de sistemas reactivos L-S y una vez definido, se podría implementar en el sistema de captura de endotoxinas.

APPENDIX

APPENDIX A: Lipid binding molecules

Table A.1. Classification of LPS binding molecules.

Type of molecule	Example	Source / localization		Reference
Organic solvent	Triton X-114	(-)	Synthetic molecules	[1]
	Tetra(ethyleneoxide) decyl ether			[2]
	Butanol			[2]
	Octanol			[3]
Polymer	Polysulfone	(-)		[4]
	Polyamide			[5]
	Polyetherimide			[6]
Antibiotic	Polymyxin B	Gram (+) bacteria	Proteins extracted from other living organisms	[7,8]
Protein	FhuA	E.Coli membrane		[9–11]
	OmpT			
	MsbA			
	Attacin	Insect (Silk moth)		[12]
	Sarcotoxin IA	Insect (Fresh fly)		[13]
	Melittin	Insect (Honey bee)		[14]
	Papiliocin	Insect (Swallowtail butterfly)		[15]
	Magainin 2	Amphibians (African clawed frog)		[16]
	Limulus factor C	Horseshoe crab (Limulus Polyphemus)		[17]
	LALF			[18,19]
	TALF	Horseshoe crab (Tachypleus tridentatus)		[20]

Continuation of Table A.1. Classification of LPS binding molecules.

Type of molecule	Example	Source / localization		Reference
Protein	Surfactant proteins	Lungs	Human proteins with potential LPS binding capacity	[21,22]
	SLPI	Human mucosa		[23–25]
	Hystatins	Saliva		[26,27]
	Factor XII	Human plasma		[28]
	Tissue factor			[29]
	PLTP			[30,31]
	CETP			[32]
	Complement components			[33,34]
	HDL			[35–37]
	Hemoglobin			[38–40]
	BPI	Human leukocytes		[41–43]
	Lactoferrin			[44,45]
	Heparin-binding protein			[46,47]
	Cathelicidins			[48]
	Lysozyme			[44,49]
	α-defensins	Cells of the human immune system		[48,50]
	Growth differentiation factor 5 (GDF5)	Membranes of human cells		[51]

Continuation of Table A.1. Classification of LPS binding molecules.

Type of molecule	Example	Source / localization		Reference
Protein	sCD14	Human plasma	Human proteins involved in the immune response	[52,53]
	LBP			[54–56]
	CD14	Human cells		[57–59]
	NKL	Porcine cells and human plasma		[60]
	TLR2, TLR4	Membranes of human cells		[61–63]
	Heat shock proteins (HSP70, HSP90)			[64]
	Chemokine receptor 4 (CXCR4)			[65]
	MD-2			[66,67]
	P2X7	Cytosol of human cells		[68]
	Histones			[51]
	Moesin	Cytoskeleton of human cells		[69]
	Tubulin			[4,70]

Synthetic molecules

The removal of LPS from LPS-biomolecules complexes by solvent extraction has been studied mainly for analytical purposes. These methods involve the contact of Triton X-114 or tetra(ethyleneoxide) decyl ether with the sample under controlled conditions in order to maintain phase immiscibility [1,2]. Due to their inherent hydrophobic character, endotoxins partition favorably into the organic phase, while the desired molecules remain in the aqueous phase. A serious drawback of these methods is that the detergent has to be removed prior to reliable endotoxin determination since even at low concentrations, it interferes with endotoxin determination by the LAL test [19]. In order to overcome these limitations, Szermer-Olearnik and Boratyńskil reported that the

endotoxin can be effectively removed from a bacteriophage lysate by extraction with water immiscible solvents such as butanol or octanol [2,3].

Additionally, LPS unspecific adsorption on dialysis membranes has been observed, especially on polysulfone or polyamide materials (due to hydrophobic interactions and the large relative surface of the membrane compared to LPS concentration) [4]. This suggests that hydrophobic polymeric materials can be effectively used for the removal of endotoxins from biological fluids. Mitzner et al. evaluated the performance of an extracorporeal endotoxin removal system by immobilized polyethylenimine (PEI) [71]. The results obtained indicate that PEI, is an effective endotoxin-binding substance with good selectivity and biocompatibility performances. However, as the LPS-PEI interaction is an unspecific hydrophobic interaction, the binding selectivity towards LPS can be compromised in complex matrixes.

Human proteins

Proteins involved in the human immune system response

Human LPS-binding proteins are involved in the recognition of LPS to signal the presence of potentially harmful bacteria and activate the immune system response. Among them, MD-2, a small secreted protein associated with TLR4, is largely responsible for the direct binding of LPS, an event that results in TLR4 homodimerization and proinflammatory gene expression [72]. LBP, a plasma protein which is mainly produced by hepatocytes and is by far the most extensively studied soluble protein with LPS-binding capacity [54,55]. LBP and CD14 are two proteins whose coordinate actions result in the disaggregation and delivery of LPS monomers to the TLR4·MD-2 complex.

Recently, heat shock proteins 70 and 90 (HSP70 and HSP90) [64], chemokine receptor 4 (CXCR4) [65] and growth differentiation factor 5 (GDF-5) [51] have been identified as cell surface proteins that bind LPS and are involved in LPS-induced signaling. After binding to the cell

surface, LPS is internalized in the cytoplasm of macrophages [73]. Once there, it can also interact with other intracellular LPS binding molecules. Such molecules can belong to the cytoplasmic domain or may form part of the membrane proteins. This is the case of P2X7, a nucleotide receptor which potentiates the LPS-induced activation of macrophages [68]. Moesin, a cytoskeletal linker actin-binding protein [69] that interacts with tubulin [4,70], an heterodimer of the structural subunit of microtubules, can also bind LPS as well. Additionally, Chaby et al. recently found that histones (H1, H2A, H2B, H3 and H4) can all bind LPS [51,74] .

Other human proteins with potential LPS binding capacity

In addition to lipid transport proteins, a wide variety of circulating proteins with LPS-binding capacity exists in human plasma like heparin, lipoproteins and hemoglobin [75]. Such is the case of polycationic molecules like heparin which interacts with a highly cationic region of LPS-binding site [34,76–79]. Moreover, LPS also binds all major plasma lipoproteins: HDLs, low-density lipoproteins (LDLs), very low density lipoproteins (VLDLs) and chylomicrons [80,81]. Besides, hemoglobin is an oxygen-carrying globular protein located in erythrocytes with proven LPS binding capacity. In this case the binding does not involve ionic interactions with lipid A, but rather hydrophobic and/or hydrogen interactions, with the lipid A acyl chains [38–40,82].

In some parts of the human body specially exposed to pathogens, such as epithelial tissues and mucosa, specific antimicrobial molecules are produced providing protection against infectious surfactant proteins, hystatins and secretory protease inhibitor (SLPI). The respiratory system is continuously exposed to LPS due to the inhalation of airborne particles. Lungs are provided with a protective layer composed by surfactant proteins; some proteins (SP-A and SP-D) are hydrophilic, whereas others (SP-C) are hydrophobic. It has been established that hydrophilic surfactant proteins bind phospholipids and LPS. However, there are some specificities: SP-D, binds to the core carbohydrates of LPS, whereas SP-A reacts with the lipid A region [23,25]. It has been reported that SP-C

interacts with the lipid A region showing an effective LPS-binding capacity as well [24,25]. Other antimicrobial type of molecule is the secretory leukocyte protease inhibitor (SLPI), which was found to interact directly with different sulphated polysaccharides and with LPS [21,22]. Moreover, histatins are small histidine-rich peptides (HRPs), secreted by salivary glands that can bind LPS and neutralize its effects as they also repair oral tissues and defend against different microbes [26,27].

Although neutrophils and epithelial cells are the main producers of soluble LPS-binding proteins, other cell types can also do the same. This is the case of natural killer (NK) cells, which produce a cationic polypeptide, NK-lysin (NKL); they were initially isolated from porcine cells, but it has been also reported that human lymphocytes produce a counterpart that also exhibits LPS-binding and neutralizing activity [60].

The last important group of antimicrobial proteins is produced in the surface of the cells, especially in those responsible for executing the immune response, playing an essential role in the defense of the organism against estrange substances or infectious agents. This is the case of the bactericidal permeability-increasing protein (BPI), a cationic antimicrobial protein that is present principally in leukocytes and on the surface of human mucosal epithelia. BPI is toxic only towards Gram-negative bacteria [41–43] and has both heparin and LPS-binding capacity [42,43]. Other protein with multi-specific character is Lactoferrin that can be found at mucosal surfaces and in biological fluids and has the capability of binding iron, heparin, proteoglycan, DNA, oligodeoxynucleotides and LPS [44,45]. Heparin-binding protein (HBP) is a cationic antimicrobial protein produced by human neutrophils. This multifunctional protein has an ionic and hydrophilic pocket with strong affinity for binding the phosphate groups of lipid A and a hydrophobic pocket suitable for binding the fatty acid chains of lipid A [46,47]. Lysozyme, a major cationic protein present in leukocytes, did also bind LPS. Like polymyxin B, lysozyme binds to the phosphate groups of lipid A first electrostatically followed by a hydrophobic interaction [44,49]. Human neutrophils contain two structurally distinct types of antimicrobial peptides, defensins and

cathelicidins. Human α-defensins (HNP-1 to HNP-4) interact with LPS, although less efficiently than BPI [48]. Cathelicidins SMAP-29, rCAP18 and hCAP18 are antimicrobial peptides found in sheep, rabbit and human leukocytes, that show antimicrobial and LPS-binding activity [83].

Proteins extracted from other living organisms

Bacteria

Bacterial proteins inserted in the outer membrane such as FhuA or OmpT interact with the lipid A region of LPS. FhuA is found on the surface of *Escherichia coli* and mediates the active transport of siderophores, small, high-affinity iron-chelating compounds (such as iron ions). OmpT is an outer-membrane protease found on the surface of *E. coli*. It contains an LPS-binding site that is strictly required for proper activity [10,11]. MsbA, located in the inner membrane, is a 'lipid flippase', involved in lipid A and glycerophospholipid export and therefore in the biogenesis of the outer membrane [9].

Similarly, other microorganisms, mainly Gram-positive bacteria, produce antibiotic-type structures with LPS recognition and binding capacity. An example is polymyxin B (PMB), which are cyclic lipopeptide antibiotics comprised of hydrophobic and hydrophilic domains that are critical for their antibacterial activity and bind to phospholipids present in the anionic outer cellular membrane of the LPS of G(-) bacteria increasing membrane permeability, which triggers apoptosis that sometimes is related to nephrotoxic effects as reviewed elsewhere [8,84–87].

Invertebrates

Antimicrobial peptides are naturally produced by different organisms such as insects, amphibians or crustaceans and have shown significant capacity to control and neutralize bacteria. Along their evolution, insects improved their resistance to bacterial infections by producing molecules able to interact with LPS. Among these antimicrobial cationic peptides,

cecropins, constitute a main component of the innate immune system of insects. Cecropins are small proteins (31 - 37 amino acids) that electrostatically interact with the negatively charged phospholipid membrane surface causing leaky membranes in both Gram-positive and Gram-negative bacteria [88,89]. They were firstly isolated from the hemolymph of the silk moth as attacin, and similar antibacterial peptides such as sarcotoxin IA was found in the hemolymph of the fresh fly while melittin is a major component of the honey bee venom and Papiliocin was recently isolated from the swallowtail butterfly [12–15]. These antimicrobial insect peptides consist of two synthetic α-helical peptides that selectively bind LPS with an affinity equivalent to that of polymyxin B. Similar molecules have also been found in amphibians. It is the case, for example, of magainin 2, isolated from the skin of the African clawed frog [16].

Invertebrates developed an innate immune system that recognizes minute amounts of surface components of potential pathogens. The horseshoe crab (Limulus Polyphemus) produces in its hemocytes a factor called Limulus factor C, a component of the serine protease cascade, able to interact with minute amounts of LPS leading to coagulation of the horseshoe crab hemolymph. This factor is used in the quantitative detection of LPS either by gelation or colorimetric assays [17]. Other proteins of this type are TALF [20], a similar anti-LPs factor produced by a Japanese variety of horseshoe crab or the Limulus anti-LPS factor (LALF), a small basic protein that inhibits the LPS-mediated coagulation cascade [18,19].

References

[1] Y. Aida, M.J. Pabst, Removal of endotoxin from protein solutions by phase separation using Triton X-114, 132 (1990) 191–195.

[2] B. Szermer-Olearnik, J. Boratyński, Removal of endotoxins from bacteriophage preparations by extraction with organic solvents, PLoS One. 10 (2015) 1–10. https://doi.org/10.1371/journal.pone.0122672.

[3] J.D. Van Belleghem, M. Merabishvili, B. Vergauwen, R. Lavigne, M. Vaneechoutte, A comparative study of different strategies for removal of endotoxins from bacteriophage preparations, J. Microbiol. Methods. 132 (2017) 153–159. https://doi.org/10.1016/j.mimet.2016.11.020.

[4] U.B. Bommer J , Becker KP , Urbaschek R , Ritz E, No evidence for endotoxin transfer across high flux polysulfone membranes, Clin. Nephrol. 27 (1987) 278–282. https://doi.org/10.1111/lam.12667.

[5] G. Lonnemann, T.C. Behme, B. Lenzner, J. Floege, M. Schulze, C.K. Colton, K.M. Koch, S. Shaldon, Permeability of dialyzer membranes to TNFα-inducing substances derived from water bacteria, Kidney Int. 42 (1992) 61–68. https://doi.org/10.1038/ki.1992.261.

[6] D. Petsch, F.B. Anspach, Endotoxin removal from protein solutions, J. Biotechnol. 76 (2000) 97–119. https://doi.org/10.1016/S0168-1656(99)00185-6.

[7] P.J. Koch, J. Frank, J. Schüler, C. Kahle, H. Bradaczek, Thermodynamics and structural studies of the interaction of polymyxin B with deep rough mutant lipopolysaccharides, J. Colloid Interface Sci. 213 (1999) 557–564. https://doi.org/10.1006/jcis.1999.6137.

[8] P. Pristovšek, J. Kidrič, Solution structure of polymyxins B and E and effect of binding to lipopolysaccharide: An NMR and molecular modeling study, J. Med. Chem. 42 (1999) 4604–4613. https://doi.org/10.1021/jm991031b.

[9] Z. Zhou, K.A. White, A. Polissi, C. Georgopoulos, C.R.H. Raetz,

Function of Escherichia coli MsbA, an essential ABC family transporter, in lipid A and phospholipid biosynthesis, J. Biol. Chem. 273 (1998) 12466–12475. https://doi.org/10.1074/jbc.273.20.12466.

[10] S. Stumpe, R. Schmid, D.L. Stephens, G. Georgiou, E.P. Bakker, Identification of OmpT as the Protease That Hydrolyzes the\rAntimicrobial Peptide Protamine before It Enters, J. Bacteriol. 180 (1998) 4002–4006. https://doi.org/10.1007/s00520-014-2245-9.

[11] L. Vandeputte-Rutten, R.A. Kramer, J. Kroon, N. Dekker, M.R. Egmond, P. Gros, Crystal structure of the outer membrane protease Ompt from Escherichia coli suggests a novel catalytic site, EMBO J. 20 (2001) 5033–5039. https://doi.org/10.1093/emboj/20.18.5033.

[12] A. Carlsson, T. Nystrom, H. De Cock, H. Bennichl, Attacin - an insect immune protein- binds to LPS and triggers the specific inhibition of bacterial oyter-membrane protein sysnthesis, Microbiol. (1998) 2179–2188.

[13] K. Okemoto, Y. Nakajima, T. Fujioka, S. Natori, Participation of two N-terminal residues in LPS-neutralizing activity of sarcotoxin IA, J. Biochem. 131 (2002) 277–281. https://doi.org/10.1093/oxfordjournals.jbchem.a003099.

[14] S.A. David, V.I. Mathan, P. Balaram, Interaction of melittin with endotoxic lipid A, Biochim. Biophys. Acta (BBA)/Lipids Lipid Metab. 1123 (1992) 269–274. https://doi.org/10.1016/0005-2760(92)90006-H.

[15] J.K. Kim, E. Lee, S. Shin, K.W. Jeong, J.Y. Lee, S.Y. Bae, S.H. Kim, J. Lee, S.R. Kim, D.G. Lee, J.S. Hwang, Y. Kim, Structure and function of papiliocin with antimicrobial and anti-inflammatory activities isolated from the swallowtail butterfly, Papilio xuthus, J. Biol. Chem. 286 (2011) 41296–41311. https://doi.org/10.1074/jbc.M111.269225.

[16] K. Matsuzaki, K. Sugishita, K. Miyajima, Interactions of an antimicrobial peptide, magainin 2, with outer and inner

membranes of Gram-negative bacteria, Biochim. Biophys. Acta - Biomembr. 1327 (2002) 119–130. https://doi.org/10.1016/s0005-2736(97)00051-5.

[17] N.S. Tan, M. Lon, P. Ng, Y.I.N.H.O.E. Yau, P. Kat, W. Chong, B.O.W. Ho, J.L. Ding, Definition of endotoxin binding sites in horseshoe crab Factor C recombinant sushi proteins and neutralization of endotoxin by sushi peptides, FASEB J. (2000) 1801–1813.

[18] J. Aketagawa, T. Miyata, S. Ohtsubo, T. Nakamura, T. Morita, H. Hayashida, T. Miyata, S. Iwanaga, T. Takao, Y. Shimonishi, Primary structure of limulus anticoagulant anti-lipopolysaccharide factor, J. Biol. Chem. 261 (1986) 7357–7365.

[19] A. Hoess, S. Watson1, G.R. Siber2, R. Liddington4, E. Schulz, Crystal structure of an endotoxin-neutralizing protein fromothe horseshoe crab, Limulus anti-LPS factor, at 1.5 A resolution Munchen, Germany 4Corresponding author Communicated by G, EMBO J. 12 (1993) 3351–3356. https://www.ncbi.nlm.nih.gov/pmc/articles/PMC413608/pdf/emboj00081-0013.pdf.

[20] M. Kloczewiak, K.M. Black, P. Loiselle, J. Cavaillon, H.S. Warren, N. Wainwright, Synthetic Peptides that Mimic the Binding Site of Horseshoe Crab Factor Antilipopolysaccharide, Culture. 170 (2010) 1490–1497.

[21] M.A. Fath, X. Wu, R.E. Hileman, R.J. Linhardt, M.A. Kashem, R.M. Nelson, C.D. Wright, W.M. Abraham, Interaction of secretory leukocyte protease inhibitor with heparin inhibits proteases involved in asthma, J. Biol. Chem. 273 (1998) 13563–13569. https://doi.org/10.1074/jbc.273.22.13563.

[22] A. Ding, N. Thieblemont, J. Zhu, F. Jin, J. Zhang, S. Wright, Secretory leukocyte protease inhibitor interferes with uptake of lipopolysaccharide by macrophages, Infect. Immun. 67 (1999) 4485–4489.

[23] J.F. Van Iwaarden, J.C. Pikaar, J. Storm, E. Brouwer, J. Verhoef, R.S. Oosting, L.M.G. van Golde, J.A.G. van Strijp, Binding of surfactant protein A to the lipid A moiety of bacterial lipopolysaccharides,

Biochem. J. 303 (2015) 407–411. https://doi.org/10.1042/bj3030407.

[24] L.A. Augusto, J. Li, M. Synguelakis, J. Johansson, R. Chaby, Structural basis for interactions between lung surfactant protein C and bacterial lipopolysaccharide, J. Biol. Chem. 277 (2002) 23484–23492. https://doi.org/10.1074/jbc.M111925200.

[25] M. Andersson, T. Curstedt, H. Jörnvall, J. Johansson, An amphipathic helical motif common to tumourolytic polypeptide NK-lysin and pulmonary surfactant polypeptide SP-B, FEBS Lett. 362 (1995) 328–332. https://doi.org/10.1016/0014-5793(95)00268-E.

[26] Y. Muramaki, S. Shizukuishi, A. Tsunemitsu, K. Nakashima, Y. Kato, Aim, Binding of a histidine-rich peptide to Porphyromonas gingivalis, Virulence. 5 (2014) 463–464. https://doi.org/10.4161/viru.28930.

[27] G. Belibasakis, T. Thurnheer, N. Bostanci, Porphyromonas gingivalis, Virulence. 5 (2014) 463–464. https://doi.org/10.4161/viru.28930.

[28] D. C Morrison, C. G Cochrane, Dircet evidence for Hageman factor (Factor XII) activation by baterial lipopolysaccharides (endotoxins), 134 (1971) 986–1004.

[29] C.T. Park, A.A. Creasey, S.D. Wright, Tissue factor pathway inhibitor blocks cellular effects of endotoxin by binding to endotoxin and interfering with transfer to CD14, Blood. 89 (1997) 4268–4274. http://ovidsp.ovid.com/ovidweb.cgi?T=JS&PAGE=reference&D=emed4&NEWS=N&AN=1997184961.

[30] E. Hailman, J.J. Albers, G. Wolfbauer, A.Y. Tu, S.D. Wright, Neutralization and transfer of lipopolysaccharide by phospholipid transfer protein, J. Biol. Chem. 271 (1996) 12172–12178. https://doi.org/10.1074/jbc.271.21.12172.

[31] C.J. Vesy, R.L. Kitchens, G. Wolfbauer, J.J. Albers, R.S. Munford, Lipopolysaccharide-binding protein and phospholipid transfer protein release lipopolysaccharides from gram-negative bacterial

membranes, Infect. Immun. 68 (2000) 2410–2417. https://doi.org/10.1128/IAI.68.5.2410-2417.2000.

[32] R.R. Schumann, S.R. Leong, G.W. Flaggs, P.W. Gray, D. Samuel, J.C. Mathison, P.S. Tobias, R.J. Ulevitch, R.R. Schumann, S.R. Leong, G.W. Flaggs, P.W. Gray, S.D. Wright, J.C. Mathison, P.S. Tobias, R.J. Ulevitcht, Structure and Function of Lipopolysaccharide Binding Protein Published by : American Association for the Advancement of Science Stable URL : http://www.jstor.org/stable/2878192 Structure and Function of Lipopolysaccharide Binding Protein, 249 (2017) 1429–1431.

[33] C. Tetta, R. Bellomo, P. Inguaggiato, M. Lou Wratten, C. Ronco, Endotoxin and cytokine removal in sepsis, Ther. Apher. 6 (2002) 109–115. https://doi.org/10.1046/j.1526-0968.2002.00413.x.

[34] A. Zohair, S. Chesne, R.H. Wade, M.G. Colomb, Interaction between complement subcomponent C1q and bacterial lipopolysaccharides, Biochem. J. 257 (2015) 865–873. https://doi.org/10.1042/bj2570865.

[35] K. Brandenburg, G. Jürgens, J. Andrä, B. Lindner, M.H.J. Koch, A. Blume, P. Garidel, Biophysical characterization of the interaction of high-density lipoprotein (HDL) with endotoxins, Eur. J. Biochem. 269 (2002) 5972–5981. https://doi.org/10.1046/j.1432-1033.2002.03333.x.

[36] B. Yu, S.D. Wright, Catalytic Properties of Lipopolysaccharide (LPS) Binding Protein, J. Biol. Chem. 271 (2002) 4100–4105. https://doi.org/10.1074/jbc.271.8.4100.

[37] S. Tanaka, D. Diallo, S. Delbosc, C. Genève, N. Zappella, J. Yong-Sang, J. Patche, A. Harrois, S. Hamada, E. Denamur, P. Montravers, J. Duranteau, O. Meilhac, High-density lipoprotein (HDL) particle size and concentration changes in septic shock patients, Ann. Intensive Care. 9 (2019) 1–9. https://doi.org/10.1186/s13613-019-0541-8.

[38] W. Kaca, R.I. Roth, J. Levin, Hemoglobin, a newly recognized lipopolysaccharide (LPS)-binding protein that enhances LPS biological activity, J. Biol. Chem. 269 (1994) 25078–25084.

[39] G. Jürgens, M. Müller, M.H.J. Koch, K. Brandenburg, Interaction of hemoglobin with enterobacterial lipopolysaccharide and lipid A, Eur. J. Biochem. 268 (2003) 4233–4242. https://doi.org/10.1046/j.1432-1327.2001.02338.x.

[40] C. Liepke, S. Baxmann, C. Heine, N. Breithaupt, L. Ständker, W.G. Forssmann, Human hemoglobin-derived peptides exhibit antimicrobial activity: A class of host defense peptides, J. Chromatogr. B Anal. Technol. Biomed. Life Sci. 791 (2003) 345–356. https://doi.org/10.1016/S1570-0232(03)00245-9.

[41] M. Gough, R.E.W. Hancock, N.M. Kelly, Antiendotoxin activity of cationic peptide antimicrobial agents, Infect. Immun. 64 (1996) 4922–4927.

[42] O. Levy, G. Canny, C.N. Serhan, S.P. Colgan, Expression of BPI (bactericidal/permeability-increasing protein) in human mucosal epithelia., Biochem. Soc. Trans. 31 (2003) 795–800. https://doi.org/10.1042/.

[43] R.G. Little, D.N. Kelner, E. Lim, D.J. Burke, P.J. Conlon, Functional domains of recombinant bactericidal/permeability increasing protein (rBPI 23), J. Biol. Chem. 269 (1994) 1865–1872.

[44] P. Berkel, M. Geerts, H. Veen, M. Mericskay, H. Boer, J. Nuijens, N-terminal stretch Arg 2 , Arg 3 , Arg 4 and Arg 5 of human lactoferrin is essential for binding to heparin, bacterial lipopolysaccharide, human lysozyme and DNA, Biochem. J. 328 (1997) 145–151.

[45] B.E. Britigan, T.S. Lewis, M. Waldschmidt, M.L. McCormick, A.M. Krieg, Lactoferrin Binds CpG-Containing Oligonucleotides and Inhibits Their Immunostimulatory Effects on Human B Cells, J. Immunol. 167 (2014) 2921–2928. https://doi.org/10.4049/jimmunol.167.5.2921.

[46] R. B, F. Christoph, K. I, Structure of HBP, a multifunctional protein with a serine proteinase fold, 4 (1996) 265–268.

[47] D.J. Brackett, M.R. Lerner, M.A. Lacquement, R. He, H.A. Pereira, A synthetic lipopolysaccharide-binding peptide based on the neutrophil- derived protein CAP37 prevents endotoxin-induced responses in conscious rats, Infect. Immun. 65 (1997) 2803–2811.

[48] A.J. Waring, J. Turner, Y. Cho, N.-N. Dinh, R.I. Lehrer, Activities of LL-37, a Cathelin-Associated Antimicrobial Peptide of Human Neutrophils, Antimicrob. Agents Chemother. 42 (2018) 2206–2214. https://doi.org/10.1128/aac.42.9.2206.

[49] K. Brandenburg, M.H.J. Koch, U. Shydel, Biophysical characterisation of lysozyme binding to LPS Re and lipid A, Eur. J. Biochem. 258 (1998) 686–695. https://doi.org/10.1046/j.1432-1327.1998.2580686.x.

[50] O. Levy, C.E. Ooi, P. Elsbach, M.E. Doerfler, R.I. Lehrer, J. Weiss, Antibacterial proteins of granulocytes differ in interaction with endotoxin. Comparison of bactericidal/permeability-increasing protein, p15s, and defensins, J. Immunol. 154 (1995) 5403–5410.

[51] R. Chaby, Lipopolysaccharide-binding molecules: Transporters, blockers and sensors, Cell. Mol. Life Sci. 61 (2004) 1697–1713. https://doi.org/10.1007/s00018-004-4020-4.

[52] M.O. Labeta, J. -J Durieux, N. Fernandez, R. Herrmann, P. Ferrara, Release from a human monocyte-like cell line of two different soluble forms of the lipopolysaccharide receptor, CD14, Eur. J. Immunol. 23 (1993) 2144–2151. https://doi.org/10.1002/eji.1830230915.

[53] R.I. Tapping, P.S. Tobias, Cellular binding of soluble CD14 requires lipopolysaccharide (LPS) and LPS-binding protein, J. Biol. Chem. 272 (1997) 23157–23164. https://doi.org/10.1074/jbc.272.37.23157.

[54] G. Ramadori, K.-H.M. zum Buschenfelde, T. P.S, M. J.C, U. R.J, Biosynthesis of Lipopolysaccharide-Binding protein in rabbit hepatocytes, Pathobiology. 58 (1990) 89–94.

[55] M. Müller, O. Scheel, B. Lindner, T. Gutsmann, U. Seydel, The role of membrane-bound LBP, endotoxin aggregates, and the MaxiK channel in LPS-induced cell activation, J. Endotoxin Res. 9 (2003) 181–186. https://doi.org/10.1179/096805103125001595.

[56] J.K. Eckert, Y.J. Kim, J.I. Kim, K. Gürtler, D.Y. Oh, S. Sur, L. Lundvall, L. Hamann, A. vanderPloeg, P. Pickkers, E. Giamarellos-Bourboulis, A. V. Kubarenko, A.N. Weber, M. Kabesch, O. Kumpf, H.J. An, J.O.

Lee, R.R. Schumann, The crystal structure of lipopolysaccharide binding protein reveals the location of a frequent mutation that impairs innate immunity, Immunity. 39 (2013) 647–660. https://doi.org/10.1016/j.immuni.2013.09.005.

[57] E. Hailman, H. Lichenstein, M. Wurfel, D. Miller, D. Johnson, M. Kelley, L. Busse, M. Zukowski, S. Wright, Lipopolysaccharide (LPS)-binding protein accelerates the binding of LPS to CD14., J. Exp. Med. 179 (1994) 269–77. http://www.pubmedcentral.nih.gov/articlerender.fcgi?artid=2191344&tool=pmcentrez&rendertype=abstract%5Cnhttp://jem.rupress.org/content/179/1/269.abstract.

[58] T.N. Kirkland, F. Finley, D. Leturcq, A. Moriarty, J.D. Lee, R.J. Ulevitch, P.S. Tobias, Analysis of lipopolysaccharide binding by CD14, J. Biol. Chem. 268 (1993) 24818–24823.

[59] D. Heumann, R. Lauener, B. Ryffel, The dual role of LBP and CD14 in response to Gram-negative bacteria or Gram-negative compounds, J. Endotoxin Res. 9 (2003) 381–384. https://doi.org/10.1179/096805103225003312.

[60] M. Andersson, R. Girard, P.A. Cazenave, Interaction of NK lysin, a peptide produced by cytolytic lymphocytes, with endotoxin, Infect. Immun. 67 (1999) 201–205.

[61] D. Artner, A. Oblak, S. Ittig, J.A. Garate, S. Horvat, C. Arrieumerlou, A. Hofinger, C. Oostenbrink, R. Jerala, P. Kosma, A. Zamyatina, Conformationally constrained lipid a mimetics for exploration of structural basis of TLR4/MD-2 activation by lipopolysaccharide, ACS Chem. Biol. 8 (2013) 2423–2432. https://doi.org/10.1021/cb4003199.

[62] J.A. Garate, J. Stöckl, M. Del Carmen Fernández-Alonso, D. Artner, M. Haegman, C. Oostenbrink, J. Jiménez-Barbero, R. Beyaert, H. Heine, P. Kosma, A. Zamyatina, Anti-endotoxic activity and structural basis for human MD-2·TLR4 antagonism of tetraacylated lipid A mimetics based on ßGlcN(1-1)αGlcN scaffold, Innate Immun. 21 (2015) 490–503. https://doi.org/10.1177/1753425914550426.

[63] N. Inohara, G. Nuez, ML - A conserved domain involved in innate immunity and lipid metabolism, Trends Biochem. Sci. 27 (2002) 219–221. https://doi.org/10.1016/S0968-0004(02)02084-4.

[64] J. Shiu, A.A. Gaspari, Toll-like receptors, Clin. Basic Immunodermatology Second Ed. (2017) 11–34. https://doi.org/10.1007/978-3-319-29785-9_2.

[65] A.M. Wengner, S.C. Pitchford, R.C. Furze, S.M. Rankin, W. Dc, The coordinated action of G-CSF and ELR + CXC chemokines in neutrophil mobilization during acute inflammation The coordinated action of G-CSF and ELR ƨ CXC chemokines in neutrophil mobilization during acute inflammation, Blood. 111 (2016) 42–49. https://doi.org/10.1182/blood-2007-07-099648.

[66] F. Cochet, F.A. Facchini, L. Zaffaroni, J.M. Billod, H. Coelho, A. Holgado, H. Braun, R. Beyaert, R. Jerala, J. Jimenez-Barbero, S. Martin-Santamaria, F. Peri, Novel carboxylate-based glycolipids: TLR4 antagonism, MD-2 binding and self-assembly properties, Sci. Rep. 9 (2019) 1–13. https://doi.org/10.1038/s41598-018-37421-w.

[67] J. Gao, J.-X. Wang, X.-W. Wang, MD-2 Homologue Recognizes the White Spot Syndrome Virus Lipid Component and Induces Antiviral Molecule Expression in Shrimp, J. Immunol. 203 (2019) 1131–1141. https://doi.org/10.4049/jimmunol.1900268.

[68] L.C. Denlinger, P.L. Fisette, J.A. Sommer, J.J. Watters, U. Prabhu, G.R. Dubyak, R.A. Proctor, P.J. Bertics, Cutting Edge: The Nucleotide Receptor P2X7 Contains Multiple Protein- and Lipid-Interaction Motifs Including a Potential Binding Site for Bacterial Lipopolysaccharide, J. Immunol. 167 (2014) 1871–1876. https://doi.org/10.4049/jimmunol.167.4.1871.

[69] S. Amar, K. Oyaisu, L. Li, T. van Dyke, Moesin: a potential LPS receptor on human monocytes, J. Endotoxin Res. 7 (2004) 281–286. https://doi.org/10.1179/096805101101532855.

[70] M. Torres, A. Casadevall, The immunoglobulin constant region contributes to affinity and specificity, Trends Immunol. 29 (2008) 91–97. https://doi.org/10.1016/j.it.2007.11.004.

[71] S. Mitzner, J. Schneidewind, D. Falkenhagen, F. Loth, H. Klinkmann, Extracorporeal Endotoxin Removal by Immobilized Polyethylenimine, Artif. Organs. 17 (1993) 775–781. https://doi.org/10.1111/j.1525-1594.1993.tb00630.x.

[72] Y. Nagai, S. Akashi, M. Nagafuku, M. Ogata, Y. Iwakura, S. Akira, T. Kitamura, A. Kosugi, M. Kimoto, K. Miyake, Essential role of MD-2 in LPS responsiveness and TLR4 distribution, Nat. Immunol. 3 (2002) 667–672. https://doi.org/10.1038/ni809.

[73] G.D. Kutuzova, R.M. Albrecht, C.M. Erickson, N. Qureshi, Diphosphoryl Lipid A from Rhodobacter sphaeroides Blocks the Binding and Internalization of Lipopolysaccharide in RAW 264.7 Cells, J. Immunol. 167 (2014) 482–489. https://doi.org/10.4049/jimmunol.167.1.482.

[74] L. Augusto, K. Le Blay, G. Auger, D. Blanot, R. Chaby, Interaction of bacterial lipopolysaccharide with mouse surfactant protein C inserted into lipid vesicles, Am. J. Physiol. Cell. Mol. Physiol. 281 (2017) L776–L785. https://doi.org/10.1152/ajplung.2001.281.4.l776.

[75] I.D. Kuntz, E.C. Meng, B.K. Shoichet, Structure-Based Molecular Design, Acc. Chem. Res. 27 (1994) 117–123. https://doi.org/10.1021/ar00041a001.

[76] S.W. Vukajlovich, Antibody-independent activation of the classical pathway of human serum complement by lipid A is restricted to re-chemotype lipopolysaccharide and purified lipid A, Infect. Immun. 53 (1986) 480–485.

[77] V. Brade, G. Kreuzpaintner, Interaction of Lipopolysaccharides and of Lipid A from Yersinia Enterocolitica with Purified Guinea Pig C3, Immunobiology. 156 (1980) 441–453. https://doi.org/10.1016/S0171-2985(80)80077-5.

[78] D. Liu, S. Cai, X. Gu, J. Scafidi, X. Wu, A.E. Davis, C1 Inhibitor Prevents Endotoxin Shock Via a Direct Interaction with Lipopolysaccharide, J. Immunol. 171 (2014) 2594–2601. https://doi.org/10.4049/jimmunol.171.5.2594.

[79] J.L. Edwards, M.A. Apicella, The role of lipooligosaccharide in

Neisseria gonorrhoeae pathogenesis of cervical epithelia: Lipid A serves as a C3 receptor molecule, Cell. Microbiol. 4 (2002) 585–598. https://doi.org/10.1046/j.1462-5822.2002.00212.x.

[80] T.S. Parker, D.M. Levine, J.C.C. Chang, J. Laxer, C.C. Coffin, A.L. Rubin, Reconstituted high-density lipoprotein neutralizes gram-negative bacterial lipopolysaccharides in human whole blood, Infect. Immun. 63 (1995) 253–258.

[81] J. Zweigner, H.J. Gramm, O.C. Singer, K. Wegscheider, R.R. Schumann, High concentrations of lipopolysaccharide-binding protein in serum of patients with severe sepsis or septic shock inhibit the lipopolysaccharide response in human monocytes, Blood. 98 (2001) 3800–3808. https://doi.org/10.1182/blood.V98.13.3800.

[82] A.M. Kleinfeld, J. Storch, Transfer of Long-Chain Fluorescent Fatty Acids between Small and Large Unilamellar Vesicles, Biochemistry. 32 (1993) 2053–2061. https://doi.org/10.1021/bi00059a024.

[83] B.F. Tack, M. V. Sawai, W.R. Kearney, A.D. Robertson, M.A. Sherman, W. Wang, T. Hong, L.M. Boo, H. Wu, A.J. Waring, R.I. Lehrer, SMAP-29 has two LPS-binding sites and a central hinge, Eur. J. Biochem. 269 (2002) 1181–1189. https://doi.org/10.1046/j.0014-2956.2002.02751.x.

[84] L. Poirel, J. Aurélie, P. Nordmann, Polymyxins: Antibacterial Activity, Susceptibility Testing, and Resistance Mechanisms Encoded by Plasmids or Chromosomes Laurent Poirela,b,c, Aurélie Jayola,b,c and Patrice Nordmann, Clin. Microbiol. Rev. 30 (2017) 557–596. https://doi.org/10.1128/CMR.00064-16.

[85] I.M. Helander, I. Kilpeläinen, M. Vaara, Increased substitution of phosphate groups in lipopolysaccharides and lipid A of the polymyxin-resistant pmrA mutants of Salmonella typhimurium: a 31P-NMR study, Mol. Microbiol. 11 (1994) 481–487. https://doi.org/10.1111/j.1365-2958.1994.tb00329.x.

[86] A.P. Zavascki, R.L. Nation, Nephrotoxicity of polymyxins: Is there any difference between colistimethate and polymyxin B?, Antimicrob. Agents Chemother. 61 (2017).

https://doi.org/10.1128/AAC.02319-16.

[87] R. Aggarwal, A. Dewan, Comparison of nephrotoxicity of Colistin with Polymyxin B administered in currently recommended doses: A prospective study, Ann. Clin. Microbiol. Antimicrob. 17 (2018) 4–11. https://doi.org/10.1186/s12941-018-0262-0.

[88] A.J. De Lucca, T.J. Jacks, K.A. Brogden, Binding between lipopolysaccharide and cecropin A, Mol. Cell. Biochem. 151 (1995) 141–148. https://doi.org/10.1007/BF01322336.

[89] J.M. Bland, A.J. De Lucca, T.J. Jacks, C.B. Vigo, All-D-cecropin B : Synthesis , conformation , lipopolysaccharide binding , and antibacterial activity, Mol. Cell. Biochem. 218 (2001) 105–111.

APPENDIX B: Strains and oligosaccharides employed in this thesis

Table B.1. Different strains used in this thesis.

Name	Genotype	Description	Ref
DH5α	F-, endA1, glnV44, thi-1, recA1, relA1, gyrA96, deoR, nupG, ϕ80dlacZΔM15, Δ(lacZYA-argF) U169, hsdR17 (rK-mK+, λ-[Nx^R]	Maximize transformation efficiency.	[1]
BL21 (DE3)	F^-, ompT, gal, dcm,lon, hsdSB(r_B^- m_B^-),λ(DE3[lacI lacUV5-T7p07 ind1 sam7 nim5]), [$malB^+$]$_{K-12}$(λ^S)	Reduce the degradation of heterologous proteins. (Lack of OmpT and Ion proteases)	[2]
Rosetta	F^-, ompT hsdSB (r_B^- m_B) gal dcm (DE3)	Enhance eukaryotic proteins expression that contain codons rarely used in *E.coli*	[3]
Origami	F^- *ompT hsd*SB(r_B^- m_B^-) *gal dcm lacY1 ahpC* (DE3) *gor522*:: Tn*10 trxB* (Kan^R, Tet^R)	Facilitate proper disulfide bond formation	[4]
Artic Express	F^- ompT hsdS(r_B^- m_B^-) dcm^+ Tet^r gal endA Hte [cpn10 cpn60 $Gent^R$]	Increase the yield of soluble protein produced in *E. coli*	[5]
P. Pastoris SMD1168H	Mut^Shis4$^-$	Avoid protein degradation	[6]

Table B.2. Primers employed for *E.coli* plasmids construction.

Name	Sequence (5´> 3´)
pET_gen_F	TAGAAATAATTTTGTTTAACTTTAAGAAGG
pET_gen_R	TAGCAGCCGGATCTCAGTG
pET_vector_F	ATGTATATCTCCTTCTTAAAGTTAAAC
pET_vector_R	GAGCACCACCACCACCA
pET29c_LALF_TAGsinsert_R	TGTTATCCGCTCACAATTCCCCTA
pET29c_LALF_TAGsinsert_F	ATGGATGGTATTTGGACACAGTTAATTTTCACC
TAGsmplpET_prom	CGATCCCGCGAAATTAATACGACTCAC
LALF+ SenP2	TGACCAGGGTGAAAATTAACTGTGTCCAAATACCATCCATTCCACCGGTCTGCTGCTGGA
LALF + TEV	TGACCAGGGTGAAAATTAACTGTGTCCAAATACCATCCATGCCCTGGAAGTAAAGGTTTTCGGTC
MBP_seq	CGATGAAGCCCTGAAAGACGCGCAGAC
GALF_pET29c_F	AATAATTTTGTTTAACTTTAAGAAGGAGATATACATATGCGTGTATCCGTGCTTGTATCTCTAG
GALF_pET29c_R	CTTTGTTAGCAGCCGGATCTCAGTGGTGGTGGTGGTGGTGCTCGAGGGAACTCAACCATTGATT
TRXout_TEVin	TACCATCCATGCCCTGGAAGTAAAGGTTTTCGGTCGTTGGGATATCGGCCAGGTTAGCGTCGAGGA
TEV_F	GATATCCCAACGACCGAAAACCT
TRX_pET3a_NdeI	AAAAA<u>CATATG</u>GGTACCAGCGATAAAATTATTCACC

Continuation of Table B.2. Primers employed for *E.coli* plasmids construction.

TRX_pET3a_BamHI	AAAAAGGATCCGCCCTGGAAGTAAAGGTTTTCG
pET_iso_F	CACCACCACCACCACCACTGAGATCCGGCTGCTAAC
pDBHISGST_iso_R	CGATATCCCAACGACCGAAAACCTTTACTTCCAGGGC
Pgst_iso_F	CGAATCTAGAGCCTGCAGTCTCGAGCGGC
pGST_iso_R	CGATACGACCGAAAACCTGTATTTTCAGGGCGCC
pET_iso_F	CACCACCACCACCACCACTGAGATCCGGCTGCTAAC
pHisMBP_iso_R	GGATATCCCAACGACCGAAAACCTGTATTTTCAGGGCGCC
pETSumo3_iso_R	CGAGGACACCATCGACGTGTTCCAGCAGCAGACCGGTGGA
Pet_iso_F	CACCACCACCACCACCACTGAGATCCGGCTGCTAAC
pHis_iso_R	CGATATCCCAACGACCGAAAACCTGTATTTTCAGGGC

Underlined nucleotides indicate the restriction target for cloning through enzyme restriction.

Table B.3. Primers utilized for *Pichia Pastoris* plasmids construction.

Name	Sequence (5´>3´)
LBP_pPIC gen F	TTGATTTTAACGACTTTTAAC
LBP_pPIC gen R	CAACTTGAACTGAGGAACAG
LBP_pPIC_vector_F	GTT TGT AGC CTT AGA CAT GAC
LBP_pPIC_vector_R	TTGATCTTCTCAAGTTGTCG
LALF_pPIC	AGAAGAAGGGGTATCTCTCGAGAAAAGAGAGGCTGAAGCT ATG GATGGTATTTGGACCCAACTG

pPICZ_vector	AGCTTCAGCCTCTCTTTTC
LBP_pPICZ	AGAAGAAGGGGTATCTCTCGAGAAAAGAGAGGCTGAAGCT**ATG GGCGCACTAGCTCG**

Bold nucleotides indicate the homology domains needed for cloning through isothermal assembly.

Table B.4. Oligonucleotides employed for PCR and Sanger sequencing.

Primer	Sequence (5´>3´)	Description
T7	TAA TAC GAC TCA CTA TAG GGG	Universal promotor T7
pT7	GCT AGT TAT TGC TCA GCG G	Universal terminator T7
NdeI	CAT ATG CAT CAC CAC CAC C	Restriction enzyme
XhoI	CTC GAG AGG CGG ATG ATC	Restriction enzyme
BanHI	AAAAAGGATCCGCCCTGGAAGTAAAGG	Restriction enzyme
Seq_pET_T7	CGATCCCGCGAAATTAATACGACTCACTATAGGG	Sequencing primer
Seq_GST_F	GTATATAGCATGGCCTTTGCAGGGCTGGC	Sequencing primer
Seq_pET_R	CCACCGCTGAGCAATAACTAGCATAACCCC	Sequencing primer
Seq_Pgex_f	GCGCCGACATCATAACGGTTCTGGC	Sequencing primer

References

[1] S.G.N. Grant, J. Jessee, F.R. Bloom, D. Hanahan, Differential plasmid rescue from transgenic mouse DNAs into Escherichia coli methylation-restriction mutants, Proc. Natl. Acad. Sci. U. S. A. 87 (1990) 4645–4649. https://doi.org/10.1073/pnas.87.12.4645.

[2] F. William Studier, A.H. Rosenberg, J.J. Dunn, J.W. Dubendorff, Use of Bacteriophage T7 RNA polymerase to direct expression of cloned genes, Methods Enzymol. 185 (1990) 60–89. https://doi.org/10.1016/0076-6879(90)85008-C.

[3] R. Novy, D. Drott, K. Yaeger, R. Mierendorf, Overcoming the codon bais of E. coli for enhanced protein expression, Innovations. (2001) 4–6. https://doi.org/https://doi.org/10.1021/acssynbio.8b00332.

[4] P.W.K. Rothemund, Folding DNA to create nanoscale shapes and patterns (Supplementary Notes), Nature. (2006) 1–82. https://doi.org/Folding DNA to create nanoscale shapes and patterns.

[5] M. Ferrer, T. N. Cherikova, M. M. Yakimov, P. N. Golyshin, K. N. Timmis, Chaperonins govern growth of Escherichia coli at low temperatures, Nat. Biotechnol. 21 (2003) 1266–1267.

[6] J.M. Cregg, K.J. Barringer, A.Y. Hessler, K.R. Madden, Pichia pastoris as a host system for transformations., Mol. Cell. Biol. 5 (1985) 3376–3385. https://doi.org/10.1128/mcb.5.12.3376.

APPENDIX C: Polymerase Chain Reaction (PCR)

The principles behind every PCR independently of the DNA sample are the same. It is required a DNA template to be copied that contains the target sequence. Primers are short pieces of single-strained DNA previously designed and complementary to the target sequence which initiate the reaction. Besides, nucleotides (dNTPs or deoxynucleotide triphosphates) are also necessary to construct the new strand of DNA. Finally, a DNA polymerase enzyme with high fidelity is required as it synthesizes the new strands of DNA complementary to the target sequence. The first and most common used is TaqDNA (used in this work) as it can generate the new strand together with the DNA template and primers as well as it is heat resistant.

PCR process involves three main stages depicted in **Figure C.1**: 1) denaturing where stranded DNA is heated to separate it into single news, 2) annealing, when the temperature is lowered to enable the DNA primers to attach to the template DNA and 3) extension, when temperature is raised and the new strand of DNA is made by the Taq polymerase enzyme.

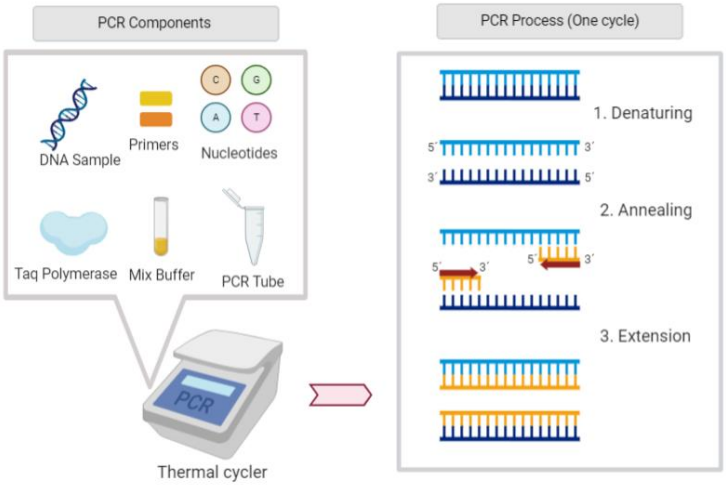

Figure C.1. Polymerase Chain Reaction (PCR) required components and process stage

APPENDIX D: Protein synthesis results

As a sample of the multiple expression attempts, **Figure D.1** shows the absence of protein bands from different overexpressions of pET29c_LALF and pET29c_LBP both in BL21 and Origami strains at different temperatures (37˚C, 25˚C, 20˚C, 18˚C). Protein production was induced with 1 mM IPTG when the OD_{600} was around 0.5-0.7.

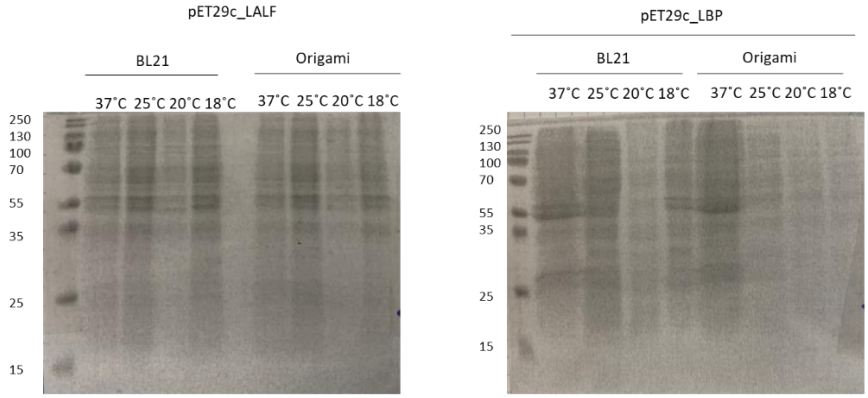

Figure D.1. pET29c_LALF overexpression test in BL21 and Origami at different temperature conditions.

Besides, **Figure D.2** depicts the unsatisfactory expression of pPICZ_LALF expressed in *P. pastoris* using two different mediums, BMGY and BMMY. Similar results were obtained when pPICZ_LBP was overexpressed in yeast cells.

After introducing fusion vectors, the TRX_LALF construction seemed a suitable alternative for protein obtention. Since previous expressions indicated better performance at 18˚C, in this case, temperature was set and the influence of both BL21 and Origami *E.coli*-derived strains was analyzed. As depicted in **Figure D.3**, TRX_LALF protein was successfully expressed in BL21 but not in Origami.

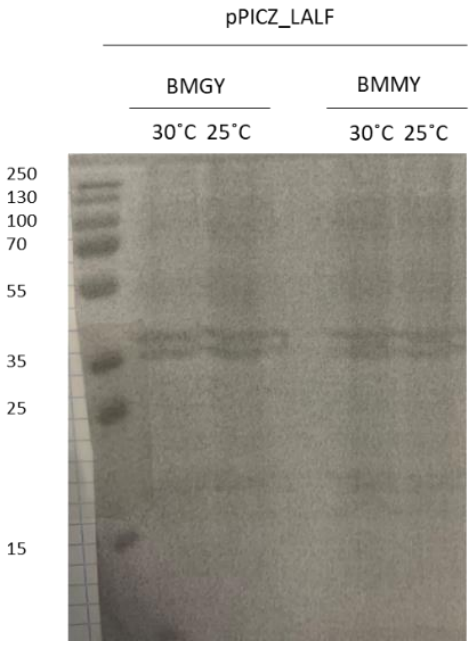

Figure D.2. pPICZ_LALF protein expression in *P.pastoris* using different mediums at different temperatures.

Unfortunately, TRX_LALF protein was found in the insoluble fraction. This means that its conformation was not correct and therefore, it was non active as it tends to aggregate with each other and form the so-called "inclusion bodies". As an example, samples of TRX-LALF in BL21 (expressed at 18˚C) electrophoresis gel results are shown in **Figure D.4**.

The culture was resuspended in lysis buffer and sonicated before separating the soluble (SN) and insoluble (P) fraction through ultracentrifugation. It can be observed a wider band corresponding to the insoluble fraction (P), that contains 90% of the protein, while the SN protein band was almost unappreciable, indicating the absence of soluble protein.

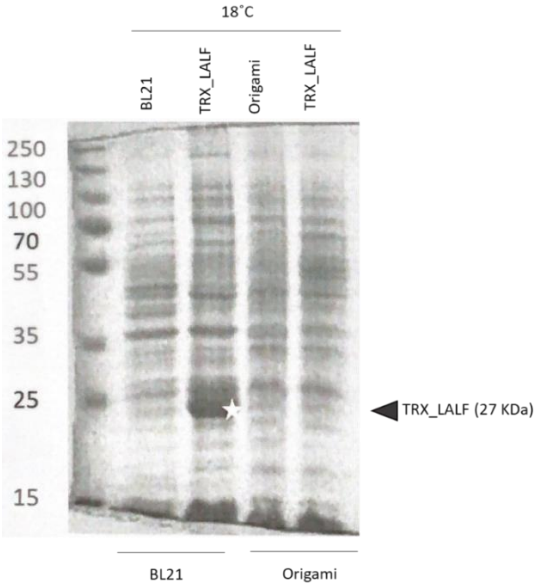

Figure D.3. Protein analysis through SDS-PAGE of BL21 and Origami *E.col*i strains of TRX_LALF fusion protein at 18˚C.

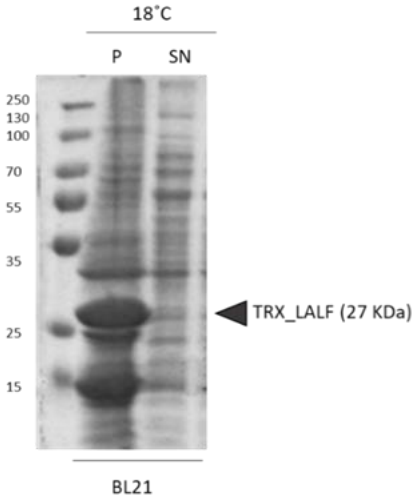

Figure D.4. Insoluble TRX_LALF protein visualized in the pellet (P) fraction after the expression at 18˚C in BL21.

In an attempt to partially solubilize the aggregates, a detergent was added to the lysis buffer to decrease the interaction between the proteins. Attending to the work of Sun et al. 2014 **[1]**, between 1% and 5% Triton X-100 was added to the lysis buffer but, in combination with the sonication, undesired bubbles generation occurred and consequently, the lysis method was insufficient. Accordingly, enzymatic lysis was introduced to assure the complete cells rupture by adding 100 µg/mL lysozyme to the buffer.

Solubility test were carried out and SN and P samples previously treated with different concentrations of Triton X-100 and enzymatically lysed were visualized in an SDS-PAGE gel. Results are depicted in **Figure D.5** where it can be observed that the addition of 1% Triton X-100 improved protein solubility whereas the higher concentrations did not show any improvement. However, despite 1% Triton X-100 sample implied the better results, most of the protein still remained in the insoluble fraction.

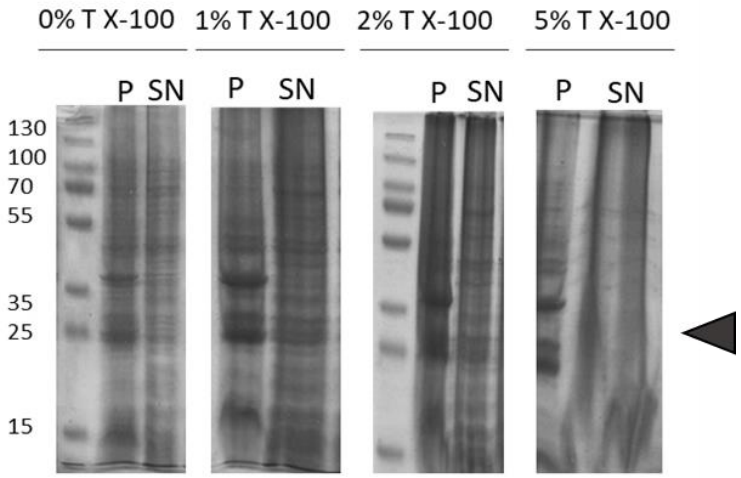

Figure D.5. Influence of Triton X-100 on protein solubilization.

Another addressed strategy was to synthesize the binding domain of the LBP, also known as LBD, both BL21 and Origami and Artic express to compare their yields as illustrated in **Figure D.6**. Induction was carried out with 1 mM IPTG and overexpression took place at 18˚C. As appreciable,

protein expression in Origami did not succeed whereas BL21 and Artic Express production showed protein but in the insoluble fraction.

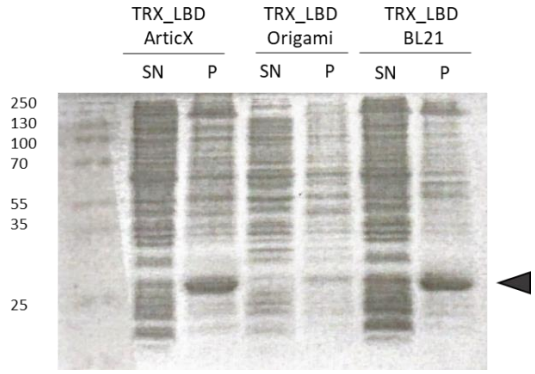

Figure D.6. TRX_LBD expression in Artic express, origami and BL21 where protein production in BL21 and Artic express was found in the insoluble fraction.

APPENDIX E: Kinetic parameters determination techniques

Kinetic studies, whose main objective is the determination of the equilibrium constant from the kinetic parameters of the direct and reverse binding reactions, employ either surface plasmon resonance (SPR), micro calorimetry (ITC), or fluorescence resonance energy transfer (FRET).

Surface Plasmon resonance (SPR)

Surface Plasmon Resonance is a mass-sensitive transductor procedure that monitors in real-time the association and dissociation events between a binding molecule immobilized on a surface and a partner injected on the surface. The sensor surface is composed of a thin gold film on a transparent material illuminated by a polarized light as depicted in **Figure E.1**. Once the wavelength, angle and refractive indices are adjusted, a resonance takes place between the light and the free electrons clouds (plasmon wave). Binding and dissociation between the immobilized compound and its partner change the refractive index and allows the real-time tracking of the resonance conditions [1,2].

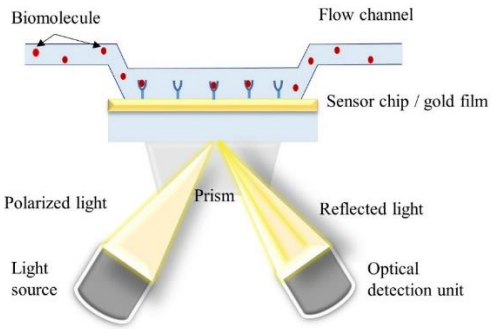

Figure E.1. Surface Plasmon Resonance detection system.

SPR screening offers detailed binding characteristics such as kinetic measurements, thermodynamic parameters and binding stoichiometry [3]. The kinetics measurement procedure implies the injection of different samples of analyte with already known concentrations on a surface with low ligand level in order to favor kinetic conditions. The main instrument of SPR is the Biacore^{TM} biosensor, where k_1 (M^{-1} s^{-1}) is the rate of analyte-surface binding and the K_{-1} (s^{-1}) is the analyte removed from the surface. As result, it is generated a primary sensogram that allows calculating interaction parameters like association (K_A) or dissociation (K_D) constants as well as the maximal binding capacity of the surface (R_{max}) [4,5].

Isothermal titration calorimetry (ITC).

Isothermal titration calorimetry (ITC) is playing a key role in the exhaustive study of protein-ligand interactions. Measuring protocol involves two different cells: a cell with around 1 mL of the reactant and a second cell for temperature reference. A syringe that also serves as stirrer injects the ligand to the sample cell. Initially, both cells are equilibrated at the desired temperature but, when the experiment is started, a constant power is supplied to the reference cell and a compensating one is also supplied to the other cell in order to equilibrate temperatures. Based on pre-set intervals, the ligand is added and the associated absorbed or released heat is compensated thanks to the power supplied to the initial cell as depicted in **Figure E.2**. The feedback-supplied power is directly proportional to the heat-flow (dQ/dt) [6,7] . As a result of this procedure, different panels show relevant information about the interaction as the association constant (K_A), the enthalpy change (AH) and the stoichiometry (n) for the reaction.

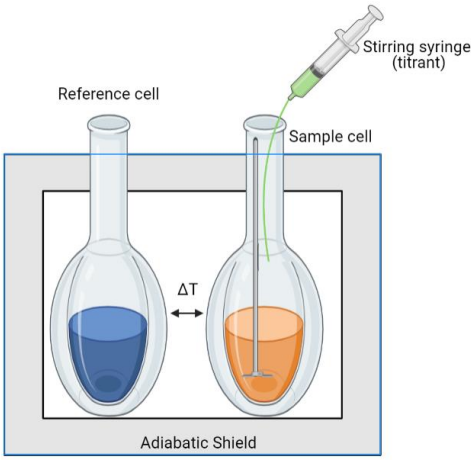

Figure E.2. Isothermal Titration Calorimetry measurement system.

Fluorescence resonance energy transfer

Fluorescence resonance energy transfer (FRET) is a useful technique based on the distance dependent transfer of energy between a donor fluorophore (D) and an acceptor fluorophore (A) whose absorption spectrum must overlap partially with the emission spectrum of D [8,9]. When both fluorophores are approached, the donor excited-stage energy is transferred through a dipole-dipole coupling. As a result of FRET, the fluorescence of the donor decreases and the fluorescence of A increases by means of the rate of energy transfer, K_T, from D to A,

Fluorescence techniques allow determining kinetic rate constants under stopped-flow techniques of fast reactions. Stopped flow is a type of flow injection analysis where reactants are rapidly driven from syringes into a high efficiency mixer as shown in **Figure E.3**. To perform a run, two syringes are filled with the reagent, the content is expelled into the flow circuit, and a small volume of each reagent is displaced through the mixer observation cell. When the flow is stopped, the reaction initiated by mixing proceeds in the observation cell and the change in absorbance is monitored by the spectrophotometer following the absorbance change in

the millisecond time range. The flow is stopped with the reactant stream in the flow cell photometric detector that usually is fluorescence detector as it is more sensitive. The sensitivity of the fluorescence detection is very useful to limit the amount of the material needed by the technique. Kinetic determination is obtained by monitoring the concentration of the reactants over time using absorption or fluorescence spectroscopy [10,11].

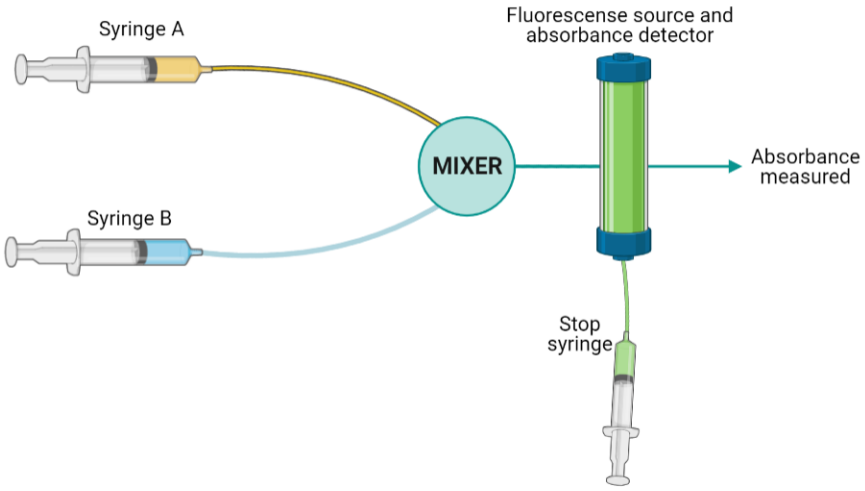

Figure E.3. Stopped flow injection analysis system.

References

[1] E. Hutter, J.H. Fendler, Exploitation of localized surface plasmon resonance, Adv. Mater. 16 (2004) 1685–1706. https://doi.org/10.1002/adma.200400271.

[2] L.J. Sherry, R. Jin, C.A. Mirkin, G.C. Schatz, R.P. Van Duyne, Localized surface plasmon resonance spectroscopy of single silver triangular nanoprisms, Nano Lett. 6 (2006) 2060–2065. https://doi.org/10.1021/nl061286u.

[3] J. Homola, S.S. Yee, G. Gauglitz, Surface plasmon resonance sensors:review, 54 (1999) 3–15. https://doi.org/10.1016/S0925-4005(98)00321-9.

[4] L. Bo, N. Claes, L. Ingemar, Surface plasmon resonance for gas detection and biosensing, Sensors and Actuators. 4 (1983) 299–304. https://doi.org/10.1016/0250-6874(83)85036-7.

[5] R.H. Ritchie, E.T. Arakawa, J.J. Cowan, R.N. Hamm, Surface-plasmon resonance effect in grating diffraction, Phys. Rev. Lett. 21 (1968) 1530–1533. https://doi.org/10.1103/PhysRevLett.21.1530.

[6] M.R. Duff, Jr., J. Grubbs, E.E. Howell, Isothermal Titration Calorimetry for Measuring Macromolecule-Ligand Affinity, J. Vis. Exp. (2011) 2–5. https://doi.org/10.3791/2796.

[7] D. Amit K, J. Rösgen, K. Rajarathnam, Using isothermal titration calorimetry to determine thermodynamic parameters of protein-Glycosaminoglycans interactions, Handb. Glycomics. (2010) 59–80. https://doi.org/10.1016/B978-0-12-373600-0.00003-2.

[8] E. Ploetz, E. Lerner, F. Husada, M. Roelfs, S. Chung, J. Hohlbein, S. Weiss, T. Cordes, Förster resonance energy transfer and protein-induced fluorescence enhancement as synergetic multi-scale molecular rulers, Sci. Rep. 6 (2016) 1–18. https://doi.org/10.1038/srep33257.

[9] S.. Hussain, An Introduction to Fluorescence Resonance Energy Transfer (FRET), (2009) 1–4. https://doi.org/10.7237/sjp/268.

[10] E. Lerner, T. Orevi, E. Ben Ishay, D. Amir, E. Haas, Kinetics of fast

changing intramolecular distance distributions obtained by combined analysis of FRET efficiency kinetics and time-resolved FRET equilibrium measurements, Biophys. J. 106 (2014) 667–676. https://doi.org/10.1016/j.bpj.2013.11.4500.

[11] J. Xing, J.J. Jayasundar, Y. Ouyang, W.J. Dong, Förster resonance energy transfer structural kinetic studies of cardiac thin filament deactivation, J. Biol. Chem. 284 (2009) 16432–16441. https://doi.org/10.1074/jbc.M808075200.

APPENDIX F: Affinity and kinetics of lipid- ligand interactions

As lipid A, one of the most potent stimulators of the innate system, induces a wide spectrum of biological effects, which may be harmful for the host, theoretical, experimental and combined studies have been developed to analyze the interaction between the lipid A and different binding molecules. These approaches contribute to clarify the binding mechanism and make progress on advanced therapies for sepsis control. In this context, some authors focused their investigation on the kinetics and reaction mechanisms as they play an important role in the design and optimization of the analytical or treatment devices. Kinetic studies have been carried out by surface plasmon resonance (SPR), isothermal titration calorimetry (ITC), or fluorescence resonance energy transfer (FRET).

Table F.1 collects the information on the kinetics and affinity constants of the reaction between Lipid A and different receptor molecules specifying the technique that has been used in the reported studies; moreover, in order to facilitate the comparison of the data provided in the literature, **Table F.1** gives the association constant of the interactions calculated as the reverse of the dissociation constants ($K_A=1/K_D$) given by the authors. Along the text, the values of the original reported constants are provided.

Table F.1. Kinetic constants of the interaction between lipid A and different receptor molecules.

Lipid A-Receptor molecule	k_1 x 10^{-4} (M^{-1} s^{-1})	k_{-1} (s^{-1})	K_A x 10^{-6} (M^{-1})	Technique	Ref
FITC-LPS-LBP			286	FRET	[1]
FITC-LPS-sCD14			34.5		
LPS-dansylPMB	10.3 - 55	0.336	0.3-1.63	Stopped flow	[2]
			2.3	FRET	
LPS-PMB	9.3 - 11	0.07	1.33 - 1.58	SPR	[3]
LPS-PMBN	2.8 - 3.2	0.08	0.34 – 0.39	SPR	
			0.21	ITC	
LPS-cyclic decapeptide	4.8 - 5.2	0.09	0.51 - 0.58	SPR	
			0.35	ITC	
LPS-cyclic heptapeptide	0.2	1	0.002	SPR	
			0.002	ITC	
FITC LPS- CD14 wild type			13.5	FRET	[4]
FITC LPS- CD14 DDED delection			58.8		
FITC LPS- CD14 PQPD delection			58.8		
FITC LPS- CD14 DDED/PQPD delection			500		
FITC LPS- CD14 AVEVE delection			30.3		

FITC LPS- CD14 DPRQY delection			< 1		
FITC LPS- MD-2			15.4	FRET	[5]
LPS- Dansyl-magainins analogs	2-89	0.078-0.7	0.002-1.14	SPR	[6]
	2-83	0.071-0.73	0.002-1.18	Stopped flow	
			0.21-1.2	ITC	
LPS-rLBP	123	0.004	288	SPR	[7]
			140	Scatchard plot	
LPS-rsCD14	2.9	0.07	0.42	SPR	
			0.98	Scatchard plot	
LPS-rLBP-rsCD14	1300	0.06	216	SPR	
			100	Scatchard plot	
LPS-TLR4-MD-2			333	FRET	[8]
LPS-TLR4	0.323	0.045	0.07		
LPS-CD14	0.286	0.025	0.115	SPR	[9]
LPS-MD-2	0.561	0.013	0.429		

In this context, Tobias et al. reported the characterization of LPS-LBP and LPS-CD14 complexes using sucrose density gradients and fluorescent assays [1]. Rabbit LBP was isolated from rabbit serum, human recombinant soluble sCD14 was obtained by immunoaffinity chromatography and lipopolysaccharides were fluorescinated with fluorescein isothiocyanate (FITC-LPS). Equilibria and kinetic experiments were carried out by tracking the fluorescence signal for FITC-LPS-LBP and FITC-LPS-sCD14 complexes. For the first complex study, 4.2 10^{-9} M of FITC-

LPS was reacted with 4.2 10^{-8} M of LBP achieving a dissociation constant value (K_D) of 3.5 10^{-9} M. On the other hand, 10 ng/mL sCD14 were contacted with 10 µg/mL sCD14 but no color-changes were appreciated until addition of 0.04 µg/mL LBP as catalyst of the FITC-LPS-sCD14 complex formation who's averaged K_D was 2.9 10^{-8} M.

Afterwards, in 1998 and for the first time, Thomas et al. [2] reported the elementary steps involved in the recognition of lipopolysaccharides by polymyxin B (PMB). The amphiphilic nature of PMB is supposed to be a key factor in the specific interaction with LPS as its binding affinity was studied by displacements of fluorescence techniques. In order to elucidate the kinetics and mechanisms involved in the complex formation, Thomas et al. studied the LPS-PMB reaction attempting to contribute to the design of more potent LPS neutralizing agents through stopped flow analyses using N-dimethylaminonaphthalene-5-sulfonyl-PMB (dansyl-PMB) as common indicator. Therefore, by means of FRET-based experiments, the association constant yielded a value of 2.1 10^6 M^{-1} while, by stopped flow techniques, LPS (1 µM) was contacted to different concentrations of dansyl-PMB (10-75 µM) yielding a k_1 range of 1.03 10^5-5.5 10^5 $M^{-1}s^{-1}$ while k_{-1} remained invariant in 0.336s^{-1}; these kinetic constants provide values for the association constant in the range of 3.06 10^5 to 1.63 10^6 M^{-1}.

Staying on this subject, Thomas and Surolia investigated the interaction between LPS (from Escherichia Coli, 055:B5) and PMB, Polymyxin B nonapeptide (PMBN), and a cyclic hepta and decapeptide on-purpose synthetized using a solid phase peptide synthesizer (NovaSyn) [3]. Binding kinetics were analyzed by SPR using a BIAcore 2000 biosensor system. The association rates of the interaction of LPS to the peptides except the cyclic heptapeptide, ranged from 2.8 10^4 $M^{-1}s^{-1}$ to 11 10^4 $M^{-1}s^{-1}$, whereas dissociation rates were 0.07 - 0.09 s^{-1}, **Table F.1**. Moreover, ITC measures performed as described by Srimal et al. [10] provided binding affinities using an OMEGA high sensitivity microcalorimeter and the obtained binding constants (K_A) for each peptide complex were in good agreement with the ones obtained by SPR [3].

In 2000, Viriyakosol and coworkers based on their studies, constructed different CD14 mutants making 4-5 amino delections [11]. They analyzed the activity of those mutants and CD14 wild type by means of fluorescent assays of FITC- LPS binding after contact of 7 different concentrations of each ligand with 10ng/mL LPS. The apparent dissociation constant value (K_D) ranged from 7.4 10^{-8} M^{-1} to $< 10^{-6}$ M^{-1} [4]. Hence, in 2001, Viriyakosol et al. produced a recombinant human MD-2, which is a protein associated to toll-like receptor 4 (TLR-4), to study the viability of LPS binding in the absence of other associated binding proteins. Fluorescence assays gave an apparent dissociation constant value of K_D= 6.5 10^{-8} M [5].

As displayed in **Table F.1**, Thomas et al. [6] studied the interaction between LPS (E. Coli 55:B5, 111:B4) with synthesized magainins analogues with improved amphiphilicity. Isothermal Titration Calorimetry (ITC) provided a binding constant k_A ranging between 1.2 10^6 and 2.1 10^5 M^{-1}. Furthermore, fast reaction kinetic studies were performed by stopped-flow apparatus measuring the influence of the ionic strength on the kinetic parameters and suggesting the influence of ionic forces in the recognition of LPS by this kind of designed peptides. The association rate (k_1) values ranged from 0.2 10^3 $M^{-1}s^{-1}$ to 8.3 10^3 $M^{-1}s^{-1}$ and dissociation (k_{-1}) rates were between 0.071 s^{-1} and 0.730 s^{-1} resulting in association constant k_A (calculated as $k_A=k_1/k_{-1}$) ranging from 0.02 10^5 M^{-1} to 11.8 10^5 M^{-1}.

In addition, surface plasmon resonance SPR analysis with LPS concentration that varied from 25 nM -125 nM flowing at a rate of 5 µL/min. Association rate constants (k_1) values between 0.2 10^3 - 8.9 10^3 $M^{-1}s^{-1}$ and dissociation (k_{-1}) rates in the range of 0.078 and 0.7 s^{-1} resulted in affinity constant values in the range of 0.02 10^5 to 11.4 10^5 M^{-1}, standing in the same order of magnitude than the values previously measured with ITC and stopped flow techniques.

Besides kinetic studies on the formation of LPS complexes with antibiotics and different peptides, several studies have also been carried out to clarify the binding mechanisms between lipid A and LBP. Although the progress made on describing the interaction mechanisms of LPS-LBP is

significant, fundamental details of the LPS binding site of LPB are missing and the crystal structure of the LPS-LBP complex is still lacking. Focused on this specific interaction, Thomas et al. [7] analyzed the kinetics of interactions between LPS, LBP and recombinant soluble CD14 (rsCD14) based on the ability of LPS to interact with a variety of target cells. SPR assays at 25˚C with immobilized rLPB on a CM5 sensor chip at 40 µgm/L and LPS flowing over the surface of the chip at concentrations between 6 nM and 35 nM and a flow rate of 10 $\mu L min^{-1}$ were carried out. This interaction yielded k_1 and k_{-1} values of 1.23 10^6 $M^{-1}s^{-1}$ and 4.26 10^{-3} s^{-1} respectively, and K_A value of 2.88 10^8 M^{-1}, in good agreement with the association constant value obtained from the Scatchard plot (K_A= 1.4 10^8 M^{-1}).

Furthermore, these authors studied the LPS-rsCD14 binding. The same concentration of rsCD14 (40 µg/mL) was also covalently immobilized on a different sensor chip and LPS (200 nM) mixed with increasing concentrations of LBP (5, 10, 15, 80, 140 nM) was passed over the rsCD14 to study the interaction of the ternary complex. k_1 and k_{-1} values for the binding of LPS to immobilized rsCD14 were 2.9 10^4 $M^{-1}s^{-1}$ and 0.07 s^{-1}, yielding K_A of 4.2 10^5 M^{-1}; this constant had the same magnitude order as the K_A calculated from the Scatchard plot (9.8 10^5 M^{-1}).

Moreover, the interaction between LPS-rLBP and immobilized rsCD14 was studied in order to analyze the influence of LBP presence on the complex formation. After incubating a constant amount of LPS with LBP and once the complex was formed, it was passed over previously immobilized rsCD14. Data related to the binding LPS-LBP complex with CD14 displayed k_1 of 1.3 10^7 $M^{-1}s^{-1}$ whereas k_{-1} was 0.06 s^{-1}, obtaining an overall binding constant value of 2.16 10^8 M^{-1}. Subsequent data treatment by Scatchard analysis of the SPR data yielded K_A of 1 10^8 M^{-1} entailing a binding enhancement thanks to the LBP presence which, increased not only the association rate but also the association constant for the interaction between LPS and CD14 by three orders of magnitude.

References

[1] P.S. Tobias, K. Soldau, J.A. Gegner, D. Mintz, R. Ulevitch, Lipopolysaccharide Binding Protein-mediated Complexation of lipopolysaccharide with soluble CD14, J. Biol. Chem. 270 (1995) 10482–10488.

[2] C.J. Thomas, B.P. Gangadhar, N. Surolia, A. Surolia, Kinetics and mechanism of the recognition of endotoxin by polymyxin B, J. Am. Chem. Soc. 120 (1998) 12428–12434. https://doi.org/10.1021/ja981777j.

[3] C.J. Thomas, A. Surolia, Kinetics of the interaction of endotoxin with polymyxin B and its analogs: a surface plasmon resonance analysis, FEBS Lett. 445 (1999) 420–424.

[4] S. Viriyakosol, J.C. Mathison, P.S. Tobias, T.N. Kirkland, Structure-function analysis of CD14 as a soluble receptor for lipopolysaccharide, J. Biol. Chem. 275 (2000) 3144–3149. https://doi.org/10.1074/jbc.275.5.3144.

[5] S. Viriyakosol, P.S. Tobias, L. Kitchens, T.N. Kirkland, R.L. Kitchens, MD-2 Binds to Bacterial Lipopolysaccharide *, 276 (2001) 38044–38051. https://doi.org/10.1074/jbc.M105228200.

[6] C.J. Thomas, N. Surolia, A. Surolia, Kinetic and Thermodynamic Analysis of the Interactions of 23-Residue Peptides with Endotoxin, J. Biol. Chem. 276 (2001) 35701–35706. https://doi.org/10.1074/jbc.M011319200.

[7] C.J. Thomas, M. Kapoor, S. Sharma, H. Bausinger, U. Zyilan, D. Lipsker, D. Hanau, A. Surolia, Evidence of a trimolecular complex involving LPS, LPS binding protein and soluble CD14 as an effector of LPS response, FEBS Lett. 531 (2002) 184–188. https://doi.org/10.1016/S0014-5793(02)03499-3.

[8] S. Akashi, S. Saitoh, Y. Wakabayashi, T. Kikuchi, N. Takamura, Y. Nagai, Y. Kusumoto, K. Fukase, S. Kusumoto, Y. Adachi, A. Kosugi, K. Miyake, Lipopolysaccharide Interaction with Cell Surface Toll-like Receptor 4-MD-2: Higher affinity than that with MD2 or CD14, J. Exp. Med. 198 (2003) 1035–1042.

https://doi.org/10.1084/jem.20031076.

[9] H.J. Shin, H. Lee, J.D. Park, H.C. Hyun, H.O. Sohn, D.W. Lee, Y.S. Kim, Kinetics of binding of LPS to recombinant CD14, TLR4, and MD-2 proteins., Mol. Cells. 24 (2007) 119–24. http://www.ncbi.nlm.nih.gov/pubmed/17846506.

[10] S. Srimal, N. Surolia, S. Balasubramanian, A. Surolia, Titration calorimetric studies to elucidate the specificity of the interactions of polymyxin B with lipopoiysaccharides and lipid A, Biochem. J. 315 (1996) 679–686. https://doi.org/10.1042/bj3150679.

[11] S. Viriyakosol, T.N. Kirkland, A region of Human CD14 required for lipopolysaccharide binding, J. Biol. Chem. 270 (1995) 361–368.

APPENDIX G: Synthesis and characterization of magnetic nanogels (MNGs)

MNGs synthesis

MNGs synthesis comprises three main steps; i) magnetic particles fabrication followed by ii) MNGs synthesis and iii) MNGs surface decoration.

Synthesis of magnetic nanoparticles (MNPs)

The synthesis of iron oxide MNPs was carried out by coprecipitation of iron salts. Briefly, 16.14 g $FeCl_3.6H_2O$ and 5.56 g $FeCl_2.4H_2O$ were placed in a 250 mL round bottom flask together with 130 mL of MilliQ water. 70 mL of 3 M NH_4OH were added dropwise and left under magnetic stirring for 15 minutes. Then, the nanoparticles were magnetically separated, and the supernatant was discarded. MNPs were resuspended in 20 mL of 2M HNO_3 and stirred for 15 minutes more. To purify, several washes and magnetic separation were carried out using acetone and finally water.

Surface modification of MNPs with vinyl moieties (MNP@MEMO)

To perform the surface functionalization of the nanoparticles, 50 mg of MNPs were suspended in 26 mL of an EtOH: H_2O (1:1) mixture. Then, a silanizing gent (MEMO) was added to provide methacrylic groups on the particle surface. The influence of this agent was analyzed as depicted in **Table G.1**.

Different volumes of MEMO were added to the MNPs and the resulting dispersion was sonicated 5 times for 2 minutes (70% power). The reaction mixture was purified by magnetic separation and washed 3 times with acetone. Afterwards, MNP@MEMO were resuspended in MilliQ water.

Table G.1.Experimental design to study the influence of the MEMO silanizing agent on the MNPs size and polydispersity.

V_{MEMO} (mL)	MNPs (mg)	Objective
0.5	50	Study the silanizing agent effect on MNPs size and polydispersity
1	50	
1.5	50	
2	50	

Once the best silanizing condition was determined, and as MNP@MEMO were resuspended in water, samples were lyophilized to dry them and measure their spectra by FTIR.

Synthesis of magnetic nanogels (MNG)

When the silanization stage was satisfactorily completed, different monomers that give shape to the nanogel (DEGMA and OEGMA) and HEMA, which provides the OH groups to the surface, are added to the previously synthesized MNPs as shown in **Figure G.1**.

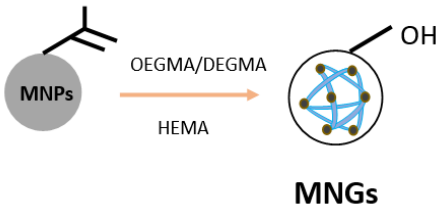

Figure G.1. MNGs formation from MPs@MEMO and DEGMA, OEGMA and HEMA monomers.

As an initial step, it was studied the optimum %HEMA that involved the desired shape of the MNGs as explained in **Table G.2**.

Table G.2. Experimental design to study the influence of % HEMA monomer on the MNGs size and polydispersity.

HEMA (%)	Objective
4	Study the influence of HEMA monomer on the MNGs shape and polydispersity
8	
15	
20	

To synthesize the MNGs, 0.8 mmol DEGMA, 0.2 mmol OEGMA, together with the optimal determined amount of HEMA, 1.8 mg of SDS and 1.6 mg of APS and MiliQ water to a total volume of 10 mL were added in a 20 mL flask. (It is advisable to prepare aqueous solutions of both SDS and APS and add 500 µL of each to the target solution due to the small amounts required for this step).

The monomer solution was stirred and homogenized for half an hour. Then, the mixture was heated up to 60˚C and once this temperature was reached, 0.3 mL of 0.25 M TEMED and 1.5 mg MNP@MEMO were added simultaneously. The reaction mixture was ultrasonicated discontinuously (6 times, 1 min) at 70% of power during 15 minutes. Finally, the nanogels were purified by magnetic separation and subsequent dialysis against water for 3 days at room temperature using a 50 kDa MWCO membrane (**Figure G.2**).

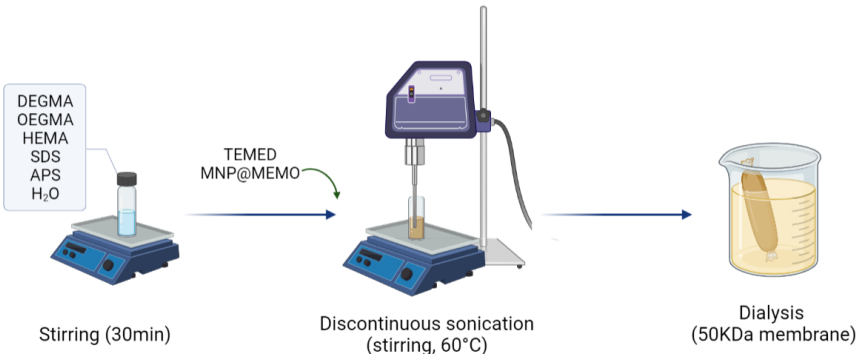

Figure G.2. Illustration of the overall process of MNGs synthesis.

MNGs surface functionalization

The aim of synthesizing MNGs was to anchor the LALF protein to its surface. For this to occur, it was necessary to functionalize the surface with nickel cations and thus, facilitate the nickel-protein coordination. This surface modification requires different steps.

Initially, succinic anhydride was used during the functionalization process to get an acid group on the surface of the MNGs and subsequently bind the linker. Since succinic anhydride has a cyclic structure, it was dissolved in DMF so that it opens up and can be anchored to the MNGs. In sequence, the nanogels had also to be dissolved in DMF so, after MNGs dialysis, the water was removed from the solution by magnetic separation and 50 mL of DMF were added and sonicated for 30 minutes in a bath with ice to avoid a temperature increase.

Once MNGs were dissolved in DMF, a previously prepared and stirred solution of succinic anhydride in DMF (0.2 g/mL, 10 mL) was added. This solution was then placed in contact with the nanogels in a round bottom flask under inert atmosphere (N_2) and stirred for 10 hours. After this time, the sample was centrifuged at 13,500 rpm for 25 minutes and the supernatant was discarded. To eliminate remains not anchored to the surface, 3 washes with methanol (30 minutes of resuspension by sonication, 30 minutes of centrifugation and supernatant removal) were carried out. Subsequently, this last rinsing process was performed twice with water and the nanogels were finally resuspended in 40 mL of deionized water.

In summary, what was achieved in terms of the nanogel´s surface was a linearization of the succinic anhydride getting an acid at the end of the chain to carry out the successive steps (**Figure G.3**).

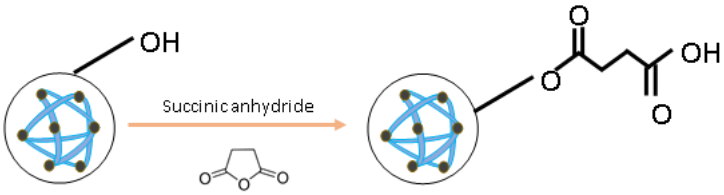

Figure G.3.MNGs surface decoration to obtain an acid at the end of the chain.

Before anchoring nickel particles to the MNGs surface, a prior step of linker (Nα,Nα-Bis(carboxymethyl)-L-lysine hydrate) addition was required. Since this compound has an amine group (**Figure G.4**) and the nanogels have an acid at their end, it was necessary an active ester to facilitate the binding between the two functional groups (**Figure G.5**).

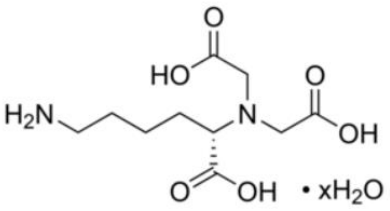

Figure G. 4. Linker chemical structure.

This process started with the resuspension of the MNGs to ensure good dispersion. Next, 100 mg EDC and 100 mg NHS were added and stirred for 30 minutes at room temperature. Then, 10 mg of the linker were added and allowed to react for 24 hours at room temperature. Subsequently, the sample was centrifuged for 30 minutes and the supernatant was removed. Lastly, it was resuspended in water and washed 3 times until final resuspension in 20 mL of deionized water.

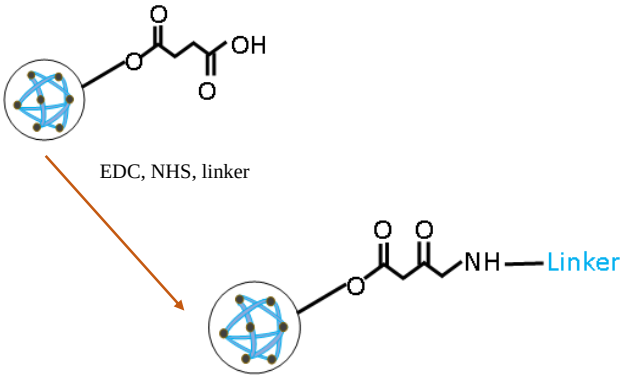

Figure G.5. MNGs surface structure after the linker addition.

Immobilizing Ni (II) Ions onto the Surface MNGs

The previously water resuspended MNGs were sonicated again to avoid aggregates. Then, they were vortex-mixed in aqueous nickel chloride solution (0.1 M, 200 µL) for 1 h. MNGs were separated from the solution under a magnetic field, and the MNGs-Ni(II) conjugates were three-times rinsed with deionized water (200 µL) and resuspended in 200 µL deionized water before use.

MNGs synthesis characterization

Initially, the influence of the silanizing agent (MEMO) was studied to determine the most suitable amount to ensure the desired particle size (around 200 nm) and polydispersity index (PDI) around 0.2, 0.3.

Attending to both size and PDI criteria (both measured through dynamic light scattering, DLS), and as shown in **Figure G.6**, the appropriate amount of MEMO to be added was determined to be 1 mL, since the previously mentioned requirement were accomplished. Higher values of MEMO implied ten times larger sizes and PDI three times greater than desired.

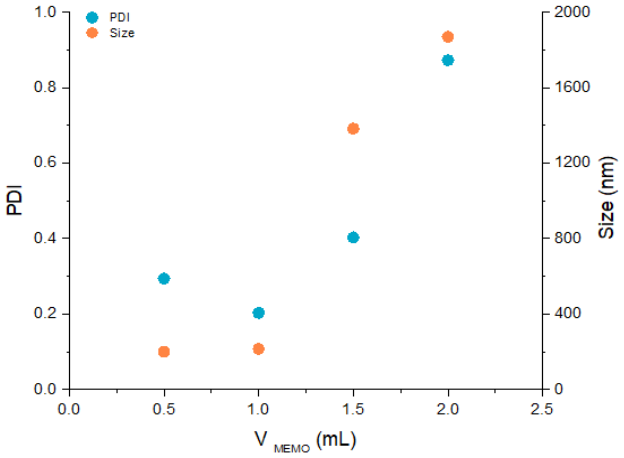

Figure G.6. MEMO influence on MNPs size and PDI.

Having determined the volume of MEMO, the silanization was corroborated by IR, and the peak corresponding to the Si-O-Si bond was observed in all the spectra measured as depicted in **Figure G.7**.

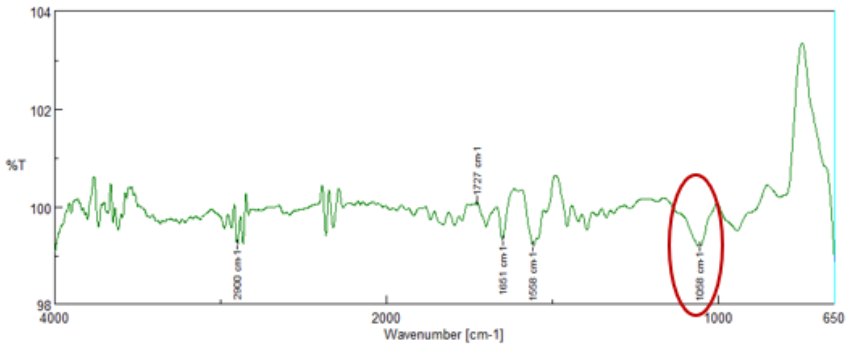

Figure G.7. MNP@MEMO spectrum obtained by IR where SI-O-Si desired bond is highlighted in red color.

When the synthesis of MNGs started, the influence of the HEMA monomer in the process was studied (4mol%, 8mol%, 15mol%) since it is the monomer in charge of providing the OH groups to the surface of the nanogel.

Particle size was measured by DLS for each percentage of HEMA and, as appreciable in **Figure G.8**, higher HEMA percentages entailed aggregates formation and very non-homogeneous and large nanogels. In conclusion, HEMA was decided to be added at 4 mol% since the obtained nanogels met size (200 nm) requirements.

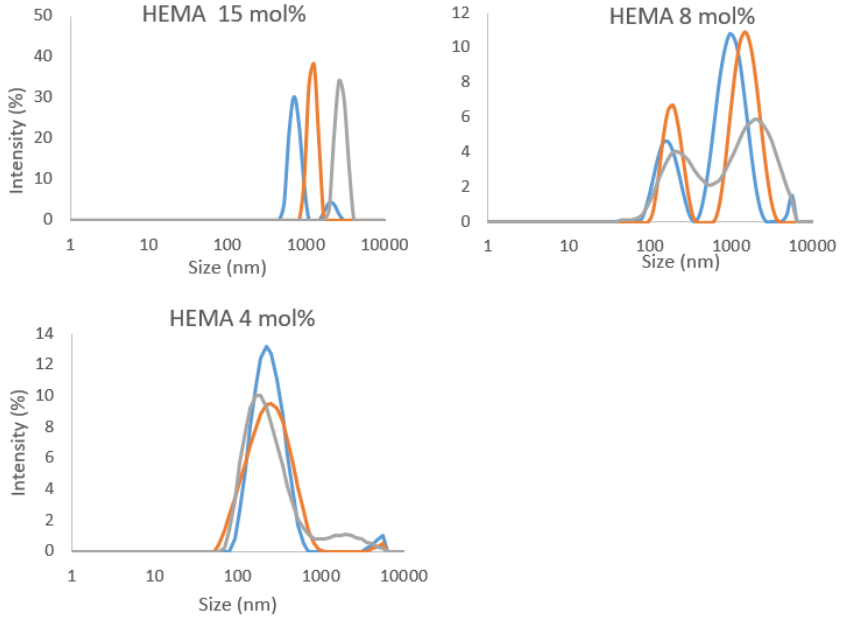

Figure G.8. HEMA percentage influence on MNGS size.

Plotting the percentage of HEMA as a function of nanogel size and PDI (**Figure G.9**), it is again observed that the appropriate amount of HEMA for optimal synthesis of MNGs is 4 mol%.

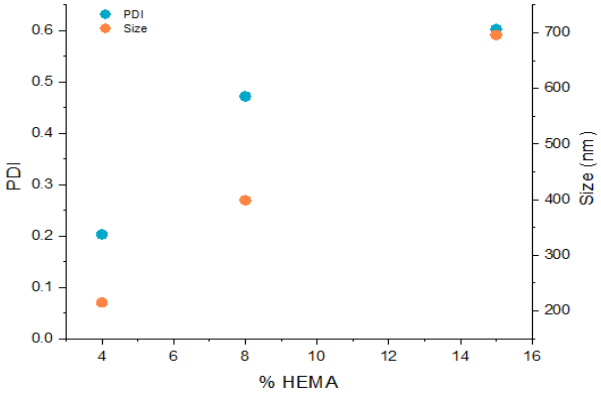

Figure G. 9.Influence of HEMA monomer on MMGs both size and PDI.

Afterwards, it was proceeded to the synthesis of MNGs by characterizing them using different techniques for which each sample was diluted and sonicated before performing the relevant measurements.

The morphology of the nanogels was studied by Transmission Electron Microscopy (TEM) and Atomic Force Microscopy (AFM). Due to the magnetic character of the nanogels, sometimes they stuck to the AFM tip and, consequently, obtaining images by this technique was harder. Even so, the structure of the nanogels can be appreciated and it was corroborated that they were dispersed and not aggregated in the sample (**Figure G.10)**.

At the same time, TEM was used to measure the size of the nanogels and compared to the data previously obtained by DLS, which were coincident (**Figure G.11**).

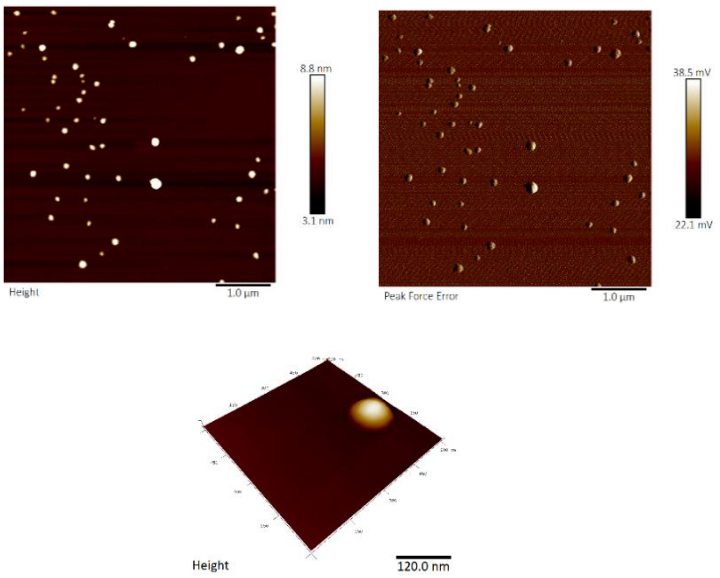

F**igure G.10**. AFM images of the dispersed MNGs.

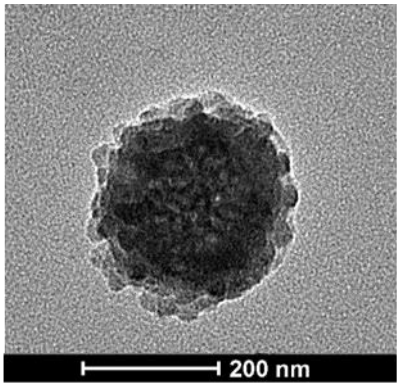

Figure G. 11. TEM image of a 200 nm MNG.

Once the different variables that can affect MNPs and MNGs (MEMO, HEMA) have been studied, and having verified that the size, polydispersity and shape of the nanogels are as desired, the next step would be to carry out the MNGs-LALF contact. This, is planned to be carried out at later step, hence only the synthesis and characterization has been be detailed in this section.

List of scientific contributions

Publications in peer-reviewed journals

1. **A. Basauri**, M. Fallanza, L. Giner-Robles, R. Fernandez-Lopez, G. Moncalián, F. de la Cruz, I. Ortiz. Integrated strategy for the separation of endotoxins from biofluids. LPS capture on newly synthesized protein Separaton and Purification Technology, 25(2021),117689.https://doi.org/10.1016/j.seppur.2020.117689.

2. **A. Basauri**, C. González-Fernández, M. Fallanza, E. Bringas, R. Fernandez-Lopez, L. Giner, G. Moncalián, F. de la Cruz, I. Ortiz. Biochemical interactions between LPS and LPS-binding molecules. Critical Reviews in Biotechnology, 40 (2020) 292–305. https://doi.org/10.1080/07388551.2019.1709797.

3. C. González-Fernández, J. Gómez-Pastora, **A. Basauri**, M. Fallanza, E. Bringas, J.J. Chalmers, I. Ortiz. Continuous-flow separation of magnetic particles from biofluids: How does the microdevice geometry determine the separation performance? Sensors (Switzerland), 20 (2020), 1–20, 3030. https://doi.org/10.3390/s20113030.

4. **A. Basauri**, J. Gómez-Pastora, M. Fallanza, E. Bringas, I. Ortiz. Predictive model for the design of reactive micro-separations. Separation and Purification Technology, 209 (2019), 900-907. https://doi.org/10.1016/j.seppur.2018.09.028.

Publications in book chapters

1. **A. Basauri**, J. Gómez-Pastora, M. Fallanza, E. Bringas, I. Ortiz. Computational analysis of facilitated transport in a microfluidic device, Computer Aided in Chemical Engineering, 40 (2017), 1189-1194. https://doi.org/10.1016/B978-0-444-63965-3.50200-2.

Contributions to international conferences

1. C. González-Fernández, J. Gómez-Pastora, **A. Basauri**, M. Fallanza, E. Bringas, I. Ortiz. Intensified microfluidic separations under magnetic field. International Symposium on Catalysis in Multiphase Reactors and Multifunctional Reactors (CAMURE-11 & ISMR-10), Milan, Italy. March 2021. Oral presentation.

2. C. González-Fernández, **A. Basauri**, M. Fallanza, E. Bringas, I. Ortiz. Contribution to the design of novel tailor-made magnetic biomaterials for blood detoxification through molecular dynamics simulations. XXXVII Congreso Anual de la Sociedad Española de Ingeniería Biomédica (CASEIB2019), Santander, Spain. November 2019. Oral presentation.

3. **A. Basauri**, L. Giner, M. Fallanza, G. Moncalián, F. de la Cruz, I. Ortiz. Design of high-performance micro-devices for endotoxins removal from biological fluids. Protein-lipid A binding step. European Congress of Applied Biotechnology (ECAB), Florence, Italy. September 2019. Oral presentation.

4. **A. Basauri**, L. Giner, M. Fallanza, G. Moncalián, F. de la Cruz, I. Ortiz. Micro-separators design for lipopolysaccharides selective sequestration**.** 3rd ANQUE-ICCE International Congress of Chemical Engineering, Santander, Spain. June 2019. Oral presentation.

5. **A. Basauri**, J. Gómez-Pastora, M. Fallanza, E. Bringas, I. Ortiz. Mass transfer performance under different flow pattern systems in micro-extractors. 5th European Conference on Microfluidics – µFlu18, Strasbourg, France. March 2018. Oral presentation.

6. **A. Basauri**, J. Gómez-Pastora, M. Fallanza, E. Bringas, I. Ortiz. CFD analysis of interfacial mass transfer in micro-solvent extraction processes. The 21st International Solvent Extraction Conference, Miyazaki, Japan. November 2017. Poster communication.

7. **A. Basauri**, J. Gómez-Pastora, M. Fallanza, E. Bringas, I. Ortiz. Computational and experimental techniques to describe a microextraction process with selective solvents. 10th World Congress of Chemical Engineering, Barcelona, Spain. October 2017. Oral presentation.

8. J. Gómez-Pastora, **A. Basauri**, M. Fallanza, E. Bringas, I. Ortiz. Contribution to the design of magnetic blood cleansing microdevices. 10th World Congress of Chemical Engineering, Barcelona, Spain. October 2017. Oral presentation.

9. **A. Basauri**, J. Gómez-Pastora, M. Fallanza, E. Bringas, I. Ortiz. Computational analysis of facilitated transport in a microfluidic device. 27th European Symposium on Computer-Aided Process Engineering (ESCAPE-27), Barcelona, Spain. October 2017. Poster communication.

10. J. Gómez-Pastora, **A. Basauri**, M. Fallanza, E. Bringas, I. Ortiz. Computational Analysis of a Two-Phase Continuous-Flow Magnetophoretic Microsystem for Particle Separation from Biological Fluids. 27th European Symposium on Computer-Aided Process Engineering (ESCAPE-27), Barcelona, Spain. October 2017. Oral presentation.

11. **A. Basauri**, J. Gómez-Pastora, M. Fallanza, E. Bringas, I. Ortiz. Computational analysis of a microsolvent extraction process. VIII International Conference on Computational Methods for Coupled Problems in Science and Engineering, Rhode, Greece. June 2017. Oral presentation.

12. **A. Basauri**, J. Gómez-Pastora, M. Fallanza, E. Bringas, I. Ortiz. CFD analysis of facilitated transport in microextraction processes. 20th annual Nanotech 2017 Conference & ExpoNanotech, Washington, EEUU. May 2017. Poster communication.